AD-A038 073 APPLIED HYDRO-ACOUSTICS RESEARCH INC ROCKVILLE MD F/G 17/1

HANDBOOK OF ARRAY DESIGN TECHNOLOGY. VOLUME I.(U)

JUN 76 N00039-76-C-0015

UNCLASSIFIED NL

1 OF 3

ADA038073

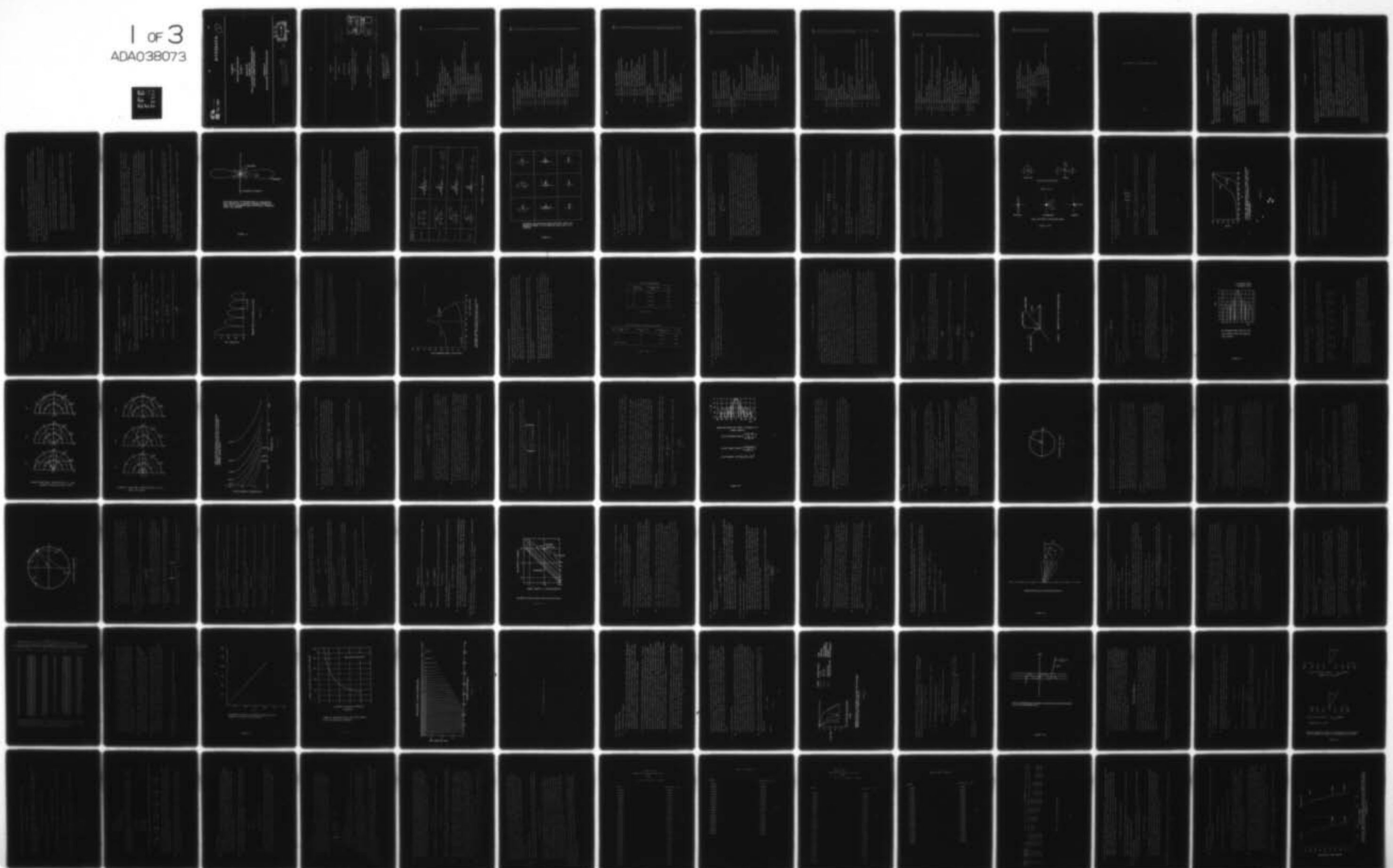

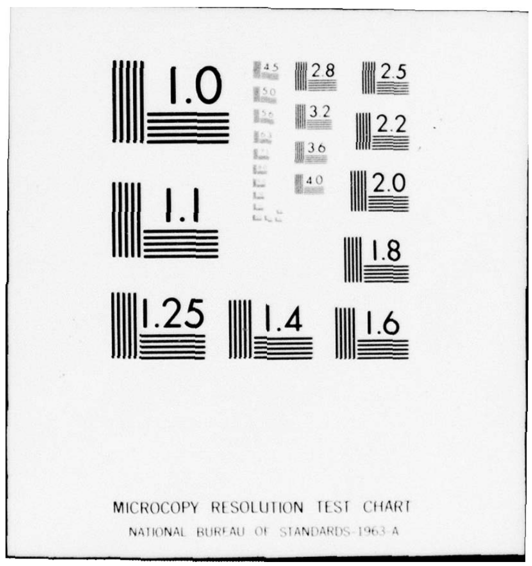
1.0
1.1
1.25
1.4
1.6
1.8
2.0
2.2
2.5
2.8
3.2
3.6
4.0
MICROCOPY RESOLUTION TEST CHART
NATIONAL BUREAU OF STANDARDS-1963-A

1

HANDBOOK
OF
ARRAY DESIGN TECHNOLOGY

VOLUME I

JUNE 30, 1976

PREPARED FOR
NAVAL ELECTRONIC SYSTEMS COMMAND, CODE 320
CONTRACT NUMBER N0003976C0015

PREPARED BY
APPLIED HYDRO-ACOUSTICS RESEARCH, INC.

HANDBOOK
OF
ARRAY DESIGN TECHNOLOGY.
VOLUME I.

(6)

(11) 30 Jun 76

(12) 262p.

JUNE 30,1976

PREPARED FOR

NAVAL ELECTRONIC SYSTEMS COMMAND, CODE 320

CONTRACT NUMBER N00039-76-C-0015

(15)

PREPARED BY

APPLIED HYDRO-ACOUSTICS RESEARCH, INC.

Table of Contents

Page

Page

Page

THIS PAGE LEFT INTENTIONALLY BLANK

1.0 INTRODUCTION

This array design technology handbook is the first in a series of handbooks funded by the Naval Electronic Systems Command, Code 320. The handbook series is to serve as a technology guide to program managers in the following areas:

Sensor/Arrays;

Hydrophone Sensors; and

Active Systems.

A vugraph-like format has been utilized in order to make the handbook useful to program managers. The technology is summarized in short pithy statements, presented in graphic format and followed by textural material for amplification and clarification. In many cases, tabular data is used to show pertinent results or trends. Emphasis is placed on surveillance array systems which have two major purposes:

Transduction of acoustic pressure waves properly summed to form shaped beams,

Provision of high spatial resolution and large signal-to-noise gains for further spectral processing.

This handbook concentrates on the formation of M beams from N independent sensors or hydrophone groups and deals with temporal processing only to the extent of the gains, losses and constraints which it impcses on the array design. The telemetry system and ocean engineering are treated from a similar point of view.

2.0 SUMMARY

In addition to an introduction and summary, Volume 1 of this handbook consists of the following chapters or sections:

Chapter 3, APERTURE THEORY, concentrates on the concept of continuous line antennas. These permit the expression of fundamental relationships as Fourier Transform pairs (i.e. far-field patterns and aperture distributions, etc.) and the use of standard mathematical relationships in Fourier Transform Theory. Thus, it is possible to introduce in a simple manner the concepts of directivity, beampatterns, sidelobe weighting and beam scanning, etc.

Chapter 4, DISCRETE ELEMENT ARRAYS, introduces the concept of a line array of point receiving sensors. Key performance equations are given which relate beampatterns, beamwidth, shading for sidelobe control, scanning and sector coverage in multi-beam systems, and various ideal performance relationships.

Chapter 5, ARRAY PERFORMANCE, discusses a number of real world constraints on array performance. These include system electrical and self noise, vibration induced noise, performance as a function of depth, multipath structure, performance with system errors, amplitude and phase fluctuations, performance in directional noise fields and the constraints imposed by related technologies.

VOLUME 2 consists of Chapter 6 which describes the dominant characteristics of certain current and projected surveillance array systems. Chapter 6 is presented separately because it includes classified information.

3.0 APERTURE THEORY

- In this section we shall provide a somewhat cursory discussion of aperture theory as it relates to linear antennas. Linear antennas obey the laws of superposition and reciprocity. By the latter we mean that the spatial pattern of the antenna is independent of whether it is radiating into or receiving from space.
- The discussions herein will deal entirely with line sources and some of the different current amplitude and phase distributions that can be used with them. Planar or other geometrical extensions of the line source will not be dealt with until discrete element arrays are considered (i.e. Section 4.0).

Continuous line sources have the following significant features:

The far-field amplitude (beam) patterns are simply related to the aperture distribution function through the Fourier Transform.

Important antenna parameters such as directivity, beamwidth, sidelobe level, shading etc., can be easily derived from integral formulas and presented in graphical as well as tabular formats.

Concepts developed from the line antenna are fundamental to an understanding of discrete element arrays.

3.1 Amplitude Patterns

3.1.1 Fourier Transform Pairs

- Associated with any antenna is a function $F(u)$ which describes the spatial distribution of the radiated field strength produced by the antenna. The quantity u is related to some coordinate, generally an angle. This function, called the amplitude pattern, can be used to obtain the beampattern of the antenna.

- Another important quantity in antenna theory is the aperture distribution $g(p)$ which describes the excitation amplitude over the extent of the antenna aperture. The quantity p represents a dimension along the antenna. The aperture distribution is important since it also affects the spatial distribution of radiated energy. In fact, the far-field* amplitude pattern $F(u)$ and the aperture distribution $g(p)$ are Fourier transforms of each other.

- For a continuous line source of length L this transform relationship can be written as

$$F(u) = \frac{1}{2\pi} \int_{-\pi}^{\pi} g(p)\exp(ipu)\, dp,$$

where the normalized variables $u = (L/\lambda)\sin\theta$ and $p = 2\pi x/L$ $(-L/2 \le x \le L/2)$ are used. The angle θ is the azimuthal angle measured from array broadside (See Fig. 3-1).

- The (power) beampattern $b(\theta)$ of an antenna is obtained by taking the square of $F(u)$ and normalizing the result to unity at its maximum.

---

* By far-field we mean at distances large compared to L^2/λ where L is the aperture dimension and λ is the wavelength.

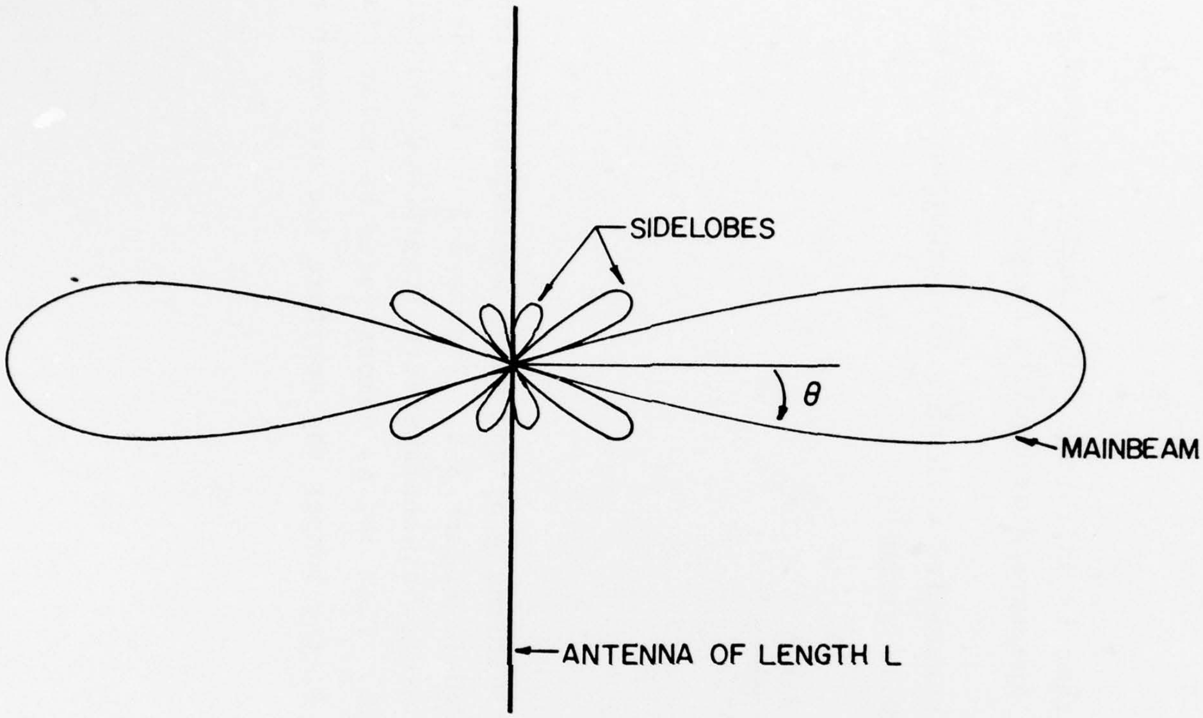

CROSS SECTION OF THE BEAMPATTERN OF A CONTINUOUS LINE ANTENNA WITH A UNIFORM APERTURE DISTRIBUTION. NOTE THAT THE BEAMPATTERN IS ROTATIONALLY SYMMETRIC ABOUT THE ANTENNA.

FIGURE 3-1

3.1.2 Examples of Fourier Transform Pairs

3.1.2.1 Uniform Line Source

- A continuous line source of length L that is uniformly (constantly) excited across its aperture can be represented by an aperture distribution, $g(p)=1$.

- The far-field amplitude pattern $F(u)$ associated with this distribution can be obtained from the transform equation and is given by

$$F(u) = \frac{\sin \pi u}{\pi u} = \frac{\sin(\frac{\pi L}{\lambda} \sin\theta)}{\frac{\pi L}{\lambda} \sin\theta} ,$$

  where θ is shown in Figure 3-1.

3.1.2.2 Other Examples

- Additional examples of aperture distributions $g(p)$ and their corresponding far-field amplitude patterns $F(u)$ are given in Figure 3-2. Figure 3-3 is included to demonstrate the reciprocal relationship between aperture length and the main pattern width or beamwidth, $b(\theta)=F^2(\theta)$. That is, as demonstrated by polar diagrams of the beams or plots of $b(\theta)$ versus θ, the longer the aperture the narrower the beamwidth and vice-versa.

Aperture Dist.	= g(x)	F(u)
Constant	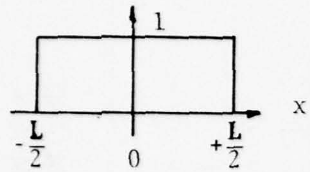	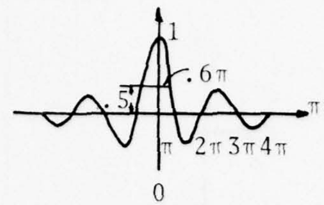 $F(u)=\frac{\sin \pi u}{\pi u}$
Triangular	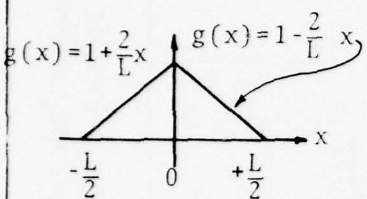	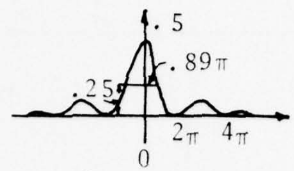 $F(u)=\frac{1-\cos \pi u}{(\pi u)^2}=\frac{1}{2}\left(\frac{\sin \frac{\pi u}{2}}{\frac{\pi u}{2}}\right)^2$
Cosine	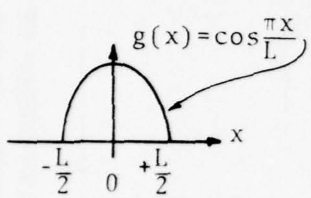	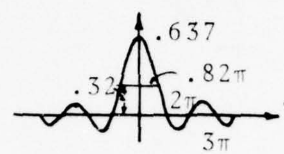 $F(u)=\frac{\pi}{2}\frac{\cos \pi u}{\left(\frac{\pi}{2}\right)^2-(\pi u)^2}$
Cosine Squared	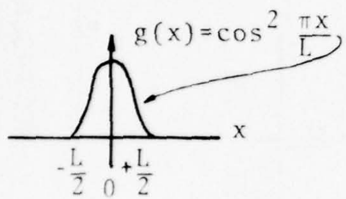	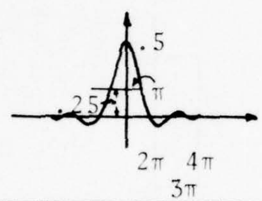 $F(u)=\frac{1}{2}\frac{\sin \pi u}{\pi u}\frac{\pi^2}{\pi^2-(\pi u)^2}$

FIGURE 3-2 FOURIER TRANSFORMS

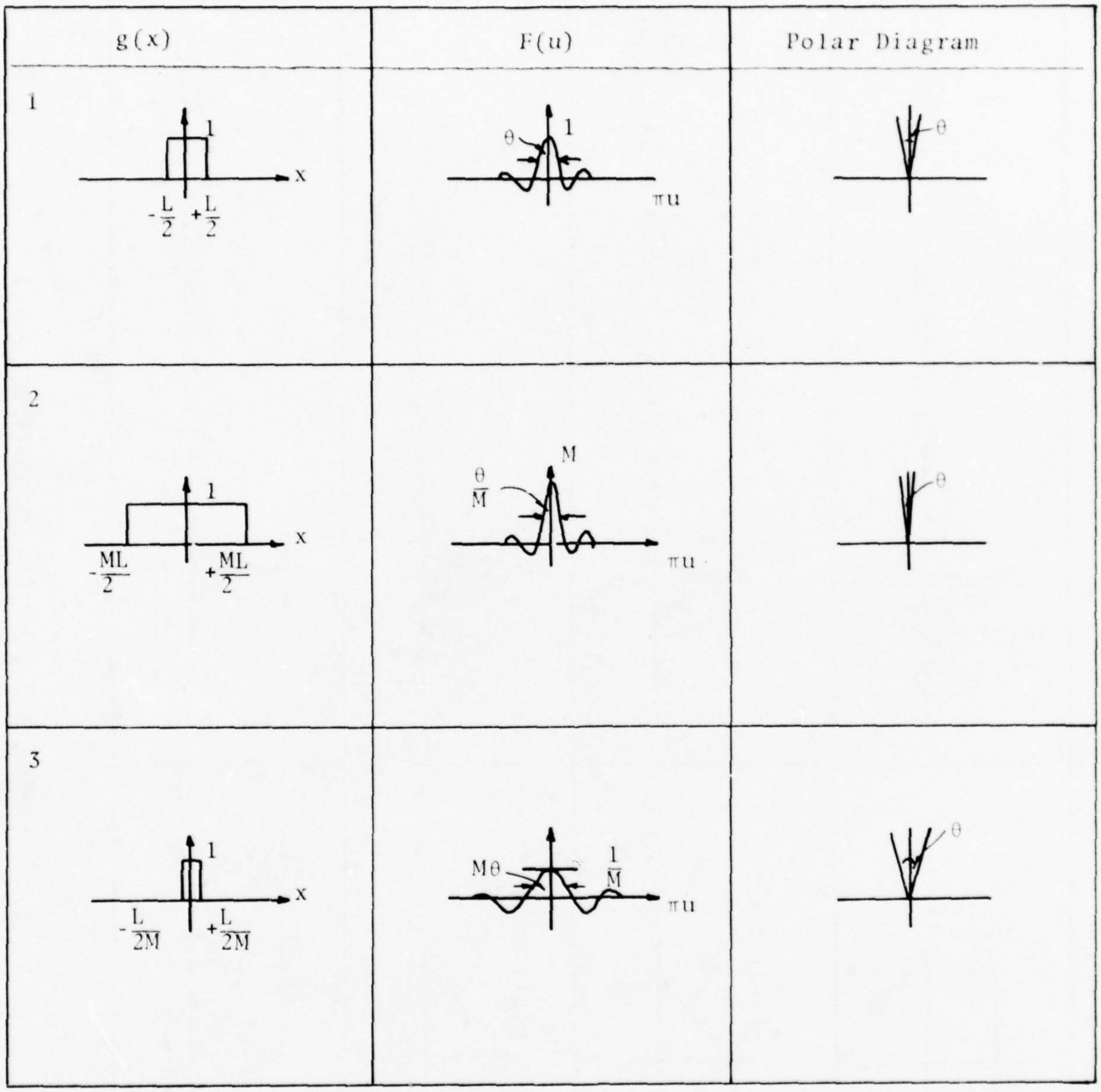

RECIPROCAL RELATIONSHIP BETWEEN APERTURE LENGTH AND BEAMWIDTH WHERE L IS THE APERTURE LENGTH AND M IS A CONSTANT.

FIGURE 3-3

3.2 Line Source Directivity

3.2.1 Definition

- The ability of an antenna to receive energy from or to concentrate radiated* energy into some volume of space, can be characterized by a quantity termed the directivity.

- Directivity is defined as the ratio of power per unit solid angle radiated in the direction of the maximum of the amplitude pattern to the average radiated power per unit solid angle.

- Using spherical coordinates, and for a beam pattern $b(\theta,\phi)=F^2(\theta,\phi)$ normalized to unity at its maximum $(F^2_{max}(\theta_o,\phi_o)$, the directivity D can be written as**

$$D = \frac{4\pi}{\int_o^{2\pi}\int_{-\pi/2}^{\pi/2} F^2(\theta,\phi)\cos\theta d\theta d\phi} .$$

---

* Recall that we shall discuss only antennas that obey the reciprocity law as described in Section 3.0.

** Note that if θ is measured from broadside, the term $\cos\theta$ will appear in the integrand as shown. If θ is measured from the line of the array, a $\sin\theta$ will appear.

If the beampattern $b(\theta,\phi)$ has rotational symmetry and is non-directional in the plane in which ϕ is measured, as in the case with a line source (See Fig. 3-1), then this expression further simplifies to

$$D = \frac{2}{\int_{-\pi/2}^{\pi/2} F^2(\theta)\cos\theta d\theta} .$$

- Directivity is usually given in terms of the directivity index or D.I. and quoted in decibels above that of an isotropic radiator whose directivity is unity or zero dB (i.e. D.I. = 10 log D/1 = 10 log D). Actually, the directivity or D.I. of an antenna is a measure of the amount of discrimination that it can achieve against noise and in favor of the signal by virtue of its beampattern. The receiving D.I., for example, can be given in terms of the increased signal-to-noise ratio at the output of an antenna over that which would be observed with an omnidirectional receiver. This increase, however, *depends upon the* directional characteristics of both the signal and noise fields. When used, the term Directivity Index or D.I. implies the existence of a unidirectional signal in isotropic noise. For signal and noise fields with other directional characteristics, a quantity called Array Gain is used (See Section 4.0).

3.2.2 Example Line Source Directivities

3.2.2.1 Uniform Line Source

- The beampattern of a uniformly excited line source of length L is given by

$$b(\theta) = F^2(\theta) = \left[\frac{\sin\pi u}{\pi u}\right]^2 ,$$

where $u = (L\sin\theta)/\lambda$. Using this expression, the directivity D of this uniform line source (for $L >> \lambda$) becomes

$$D = 2L/\lambda .$$

For a uniform phase distribution over the aperture, the uniform amplitude distribution yields the highest directivity ($2L/\lambda$) of all possible amplitude distributions over the aperture.

3.2.2.2 Scanned Line Source

- If a line source is given a uniform amplitude and a linear progressive phase distribution, then the radiation will add in phase in a direction normal to the phase front (See the angle θ_o in Fig. 3-4). The beampattern $b(\theta)=F^2(\theta)$, also given in Figure 3-4, is disk-shaped and rotationally symmetric about the line axis. As the beam is scanned, the disk folds forward to make a hollow cone until it reaches endfire where it becomes a pencil beam.

- At broadside the line source produces directivity in only one plane whereas at endfire it produces directivity in two planes. The directivity D can be calculated

from the definition in Section 3.2.1 which, for long line sources (i.e. $kL=2\pi L/\lambda>>1$), gives

$$D = 2L/\lambda$$

at broadside and for most of the scan range (See Fig. 3-5). At endfire, the directivity becomes

$$D = 4L/\lambda.$$

- Figure 3-5 is a graph of the scanned line source directivity versus scan angle. The quantity G or the gain factor is defined as the ratio D/D_o where D_o is the directivity of the unscanned uniform amplitude distribution ($D_o = 2L/\lambda$).

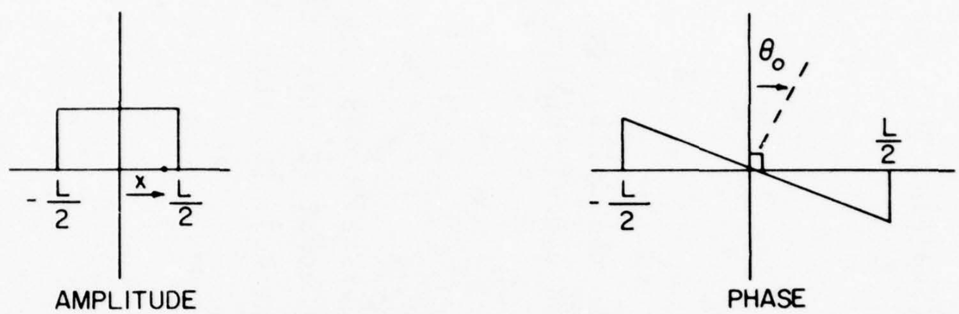

LINE APERTURE PHASE SHIFT

FIGURE 3-4 (a)

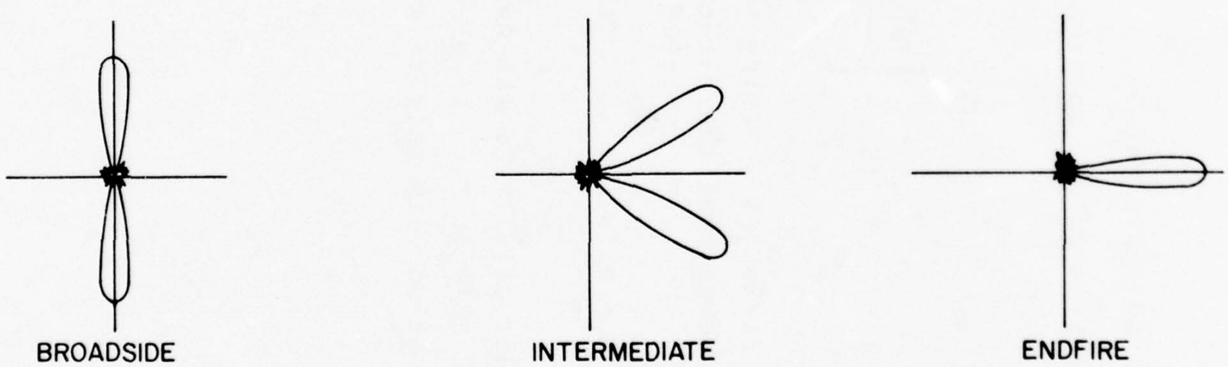

CROSS SECTIONS OF LINE SOURCE BEAMS

FIGURE 3-4 (b)

3.2.2.3 Triangular Amplitude Distribution

- The uniform phase triangular amplitude distribution (See Fig. 3-2) has a beam pattern given by

$$b(\theta) = 4F^2(\theta) = \left[\frac{\sin\frac{\pi u}{2}}{\frac{\pi u}{2}}\right]^4 ,$$

where again, $u = (L\sin\theta)/\lambda$. Using this expression in the definition in Section 3.2.1, it can be shown that the directivity D for such a distribution becomes

$$D = 0.75\ D_o, \qquad (L >> \lambda)$$

where D_o is the directivity of the uniform amplitude distribution ($D_o = 2L/\lambda$). The gain factor $G \equiv D/D_o$, which is always less than or equal to unity for any amplitude distribution with uniform phase, becomes $G = 0.75$ for this particular case.

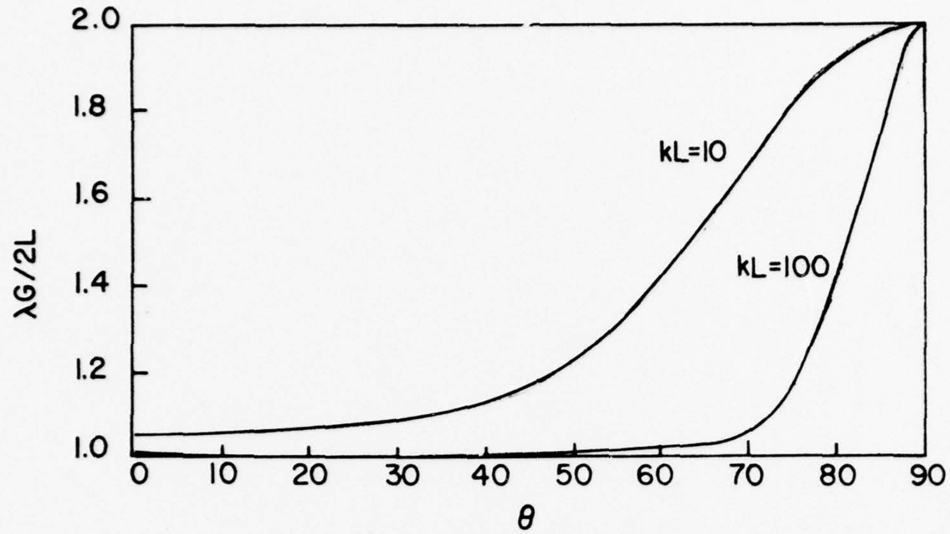

SCANNED LINE SOURCE DIRECTIVITY D VERSUS SCAN ANGLE θ. G IS THE GAIN FACTOR D/D_0, WHERE $D_0=2L/\lambda$ AND $k=2\pi/\lambda$ IS THE WAVENUMBER.

FIGURE 3-5

3.2.2.4 Amplitude Distributions of the $\cos^n p/2$ Type

- The directivities or gain factors of some of the different ($n=1,2,\ldots$) $\cos^n p/2$ amplitude distributions (See Fig. 3-2) can be calculated in the same manner as above.

- The resulting gain factors ($G=D/D_o$) for some of these amplitude distributions are given as follows for the specified value of n and for $L \gg \lambda$.

n	0	1	2	3	4
G	1.0	.810	.667	.575	.515

3.3 Beampatterns Of Line Sources

3.3.1 Uniform Line Source

- The beampattern (Section 3.2.2.1) of a uniformly excited continuous line source of length L is given by

$$b(\theta) = \left[\frac{\sin \pi u}{\pi u}\right]^2 ,$$

where $u = (L/\lambda)\sin\theta$. The main features of this pattern (See Fig. 3-6) are given below and include:

The total beamwidth null-to-null is approximately

$$BW_\infty = 2\lambda/L.$$

The total half-power or -3dB beamwidth is

$$BW_3 = .886\lambda/L(\text{Rad}) = 50.4\lambda/L(\text{deg}).$$

Sidelobes occur at angles θ such that $\pi u = \tan \pi u$ for which the first few roots are $\pi u = 4.49, 7.73$ and 10.90.

Sidelobe levels decrease with increasing $u = (L/\lambda)\sin\theta$. The first sidelobe is -13.2dB below the main beam maximum (0dB).

The nulls in the pattern occur for $u = (L/\lambda)\sin\theta = n$, where
$n = \pm 1, \pm 2, \ldots$.

3.3.2 Scanned Line Source

- The beampattern of a scanned line source of length L is given by

$$b(\theta) = \left[\frac{\sin\pi u}{\pi u}\right]^2,$$

where now,

$$u = \frac{L}{\lambda}(\sin\theta - \sin\theta_o).$$

The angle θ_o is the scan or steered angle measured from broadside. The main features of this pattern (See Fig. 3-7) are given below and include:

The total half-power or 3dB down beamwidth is given by

$$BW_3 = \arcsin\left(\frac{0.443\lambda}{L} + \sin\theta_o\right) + \arcsin\left(\frac{0.443\lambda}{L} - \sin\theta_o\right).$$

At broadside ($\theta_o = 0^o$), and for long sources ($L \gg \lambda$) this reduces to

$$BW_3 = \frac{0.886\lambda}{L} \quad \text{(Rad.)}.$$

At endfire ($\theta_o = 90^o$) and for long sources ($L \gg \lambda$) this reduces to

$$BW_3 = 2\left[\frac{0.886\lambda}{L}\right]^{1/2} \quad \text{(Rad.)}$$

The endfire beam is broader than the broadside beam by a factor of

$$2.14\sqrt{L/\lambda}$$

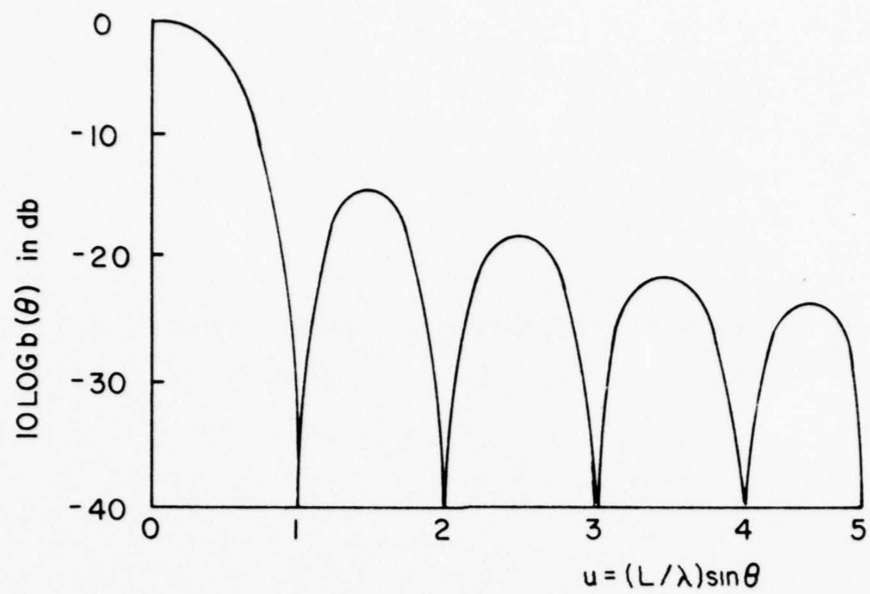

BEAMPATTERN OF A UNIFORM LINE SOURCE

FIGURE 3-6

3.3.3 Cosine Distributions ($\cos^n p/2$)*

- The $g(p) = \cos^n p/2$ family constitutes a tapered distribution which can be used when sidelobes of the uniform distribution ($g(p) = 1$) are too high. For the cases given in Table 3-1(a), the distributions are assumed to be zero at the line source end (i.e., there is no pedestal).

- The results given in Table 3-1(a) show that as the value of n increases, the gain factor G decreases. This means that the directivity D for these distributions is lower than that (D_o) of the uniform amplitude distribution.

* Recall that $p = 2\pi x/L$, where ($-L/2 \le x \le L/2$) and L is the aperture length.

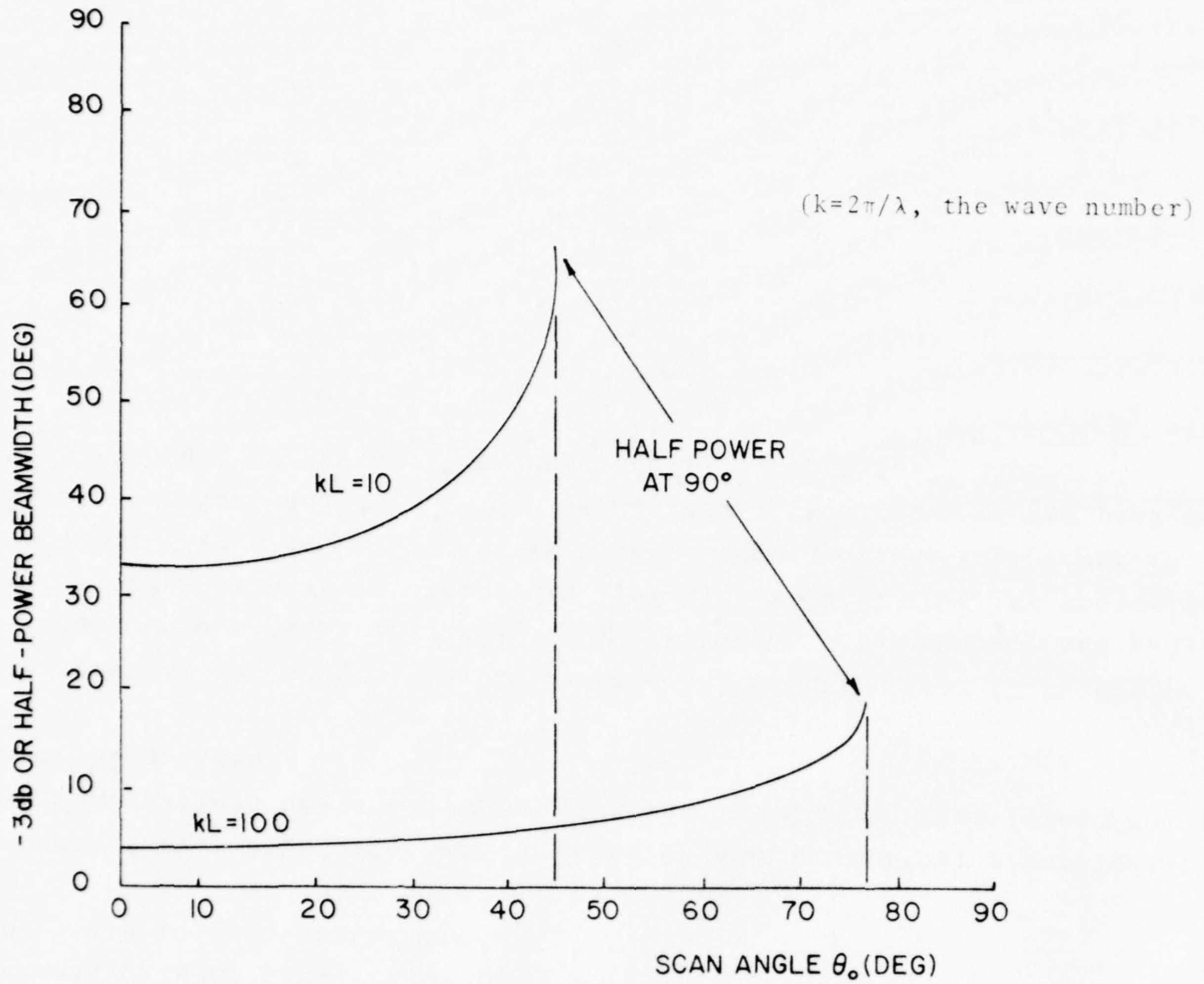

LINE SOURCE BEAMWIDTH VERSUS SCAN ANGLE (THE GRAPHS STOP WHEN THE 3 db DOWN POINT REACHES ENDFIRE).

FIGURE 3-7

3.3.4 Cosine-On-Pedestal Distributions

- A modification to the foregoing cosine aperture distributions involves adding a constant value to them so that the illuminations at the line source ends are not zero. These so-called cosine-on-pedestal distributions have both practical and economic origins since it is quite difficult to illuminate an antenna with a taper that falls to zero at the ends.

- The effect of the pedestal can be found by adding together a particular cosine amplitude pattern and the pattern of a uniform distribution ($\sin\pi u/\pi u$) to obtain the total pattern.

- Detailed data for several cosine-on-pedestal distributions (i.e. $\cos(p/2)$ with different edge tapers) are given in Table 3-1(b). In general, the pedestal provides a somewhat narrower beamwidth (and higher gain) than the cosine distribution alone, but also somewhat higher sidelobes. The aperture edge taper is a measure of relative pedestal height. It can be defined as the ratio of the peak amplitude (in dB) to that of the uniform amplitude (i.e., pedestal) alone.

$Cos^n p/2$ DISTRIBUTION

n	Sidelobe Level (dB)	Beamwidth, BW_3 (Rad)	$G = \frac{D}{D_o}$
0	13.2	$0.88\lambda/L$	1.00
1	23	$1.2\lambda/L$	0.81
2	32	$1.45\lambda/L$	0.67
3	40	$1.66\lambda/L$	0.58

TABLE 3-1(a)

VALUES FOR COSINE-ON-PEDESTAL PATTERNS

Aperture Edge Taper (dB)	Sidelobe Level (dB)	Beamwidth, BW_3 (Rad)	$G = \frac{D}{D_o}$
10	20	$1.06\lambda/L$	0.90
15	22	$1.13\lambda/L$	0.84
∞ (cosine alone)	23	$1.20\lambda/L$	0.81

TABLE 3-1(b)

3.3.5 Other Distributions

- Other distributions or shading functions such as Dolph-Chebyshev Taylor etc., are also important. These shall be treated in greater detail in Section 4.0 where they are best applied to discrete line arrays.

4.0 DISCRETE ELEMENT ARRAYS

- We shall begin the discussion of discrete element arrays by obtaining the beampattern for a two-hydrophone array which will then be generalized to a line array with an arbitrary number of elements. Planar arrays will be considered later in a separate section. As in the foregoing treatment of continuous line sources, the distribution needed across a line array to achieve a desired far-field radiation pattern may be determined from Fourier-transform theory. Also, the uniform amplitude distribution again results in maximum directivity and relatively large sidelobes whereas a tapered distribution results in lower sidelobes at the expense of reduced directivity (i.e. the so-called waterbed effect). The relative phases between the array elements determine the position of the main beam. If the phases are fixed, so is the beampattern. The beam can be scanned either by moving the array structure or by varying the relative phase between array elements. The line array generates a fan beam when the phase relationships are such that the radiation is perpendicular to the array. When the radiation is at some other angle, the fan beam pattern will close to form a conically-shaped beam. (See Fig. 3-4b).

- It is assumed in the following sections, unless noted otherwise, that the array elements are all isotropic point sources radiating uniformly in all directions. That is, the dimensions of the individual elements are assumed to be small compared with the wavelength of sound at the frequencies of interest and also compared with the separation distance between the elements. This minimizes the far-field effects of the individual element geometries and also any effects stemming from mutual element coupling. The array will generally be considered as a receiving array for convenience but, employing the reciprocity principle, any results will apply equally well to a transmitting array.

4.1 Geometrical Considerations

- With reference to Figure 4-1, the acoustic pressures due to the plane wave arriving at hydrophones A and B can be written as

$$p_A = p_o \sin\omega t$$

and

$$p_B = p_o \sin(\omega t - \frac{2\pi d \sin\theta}{\lambda}),$$

where λ is the wavelength of the sound wave, θ its angular direction relative to the array normal and d, the hydrophone spacing. Since the voltage response of any array is proportional to the sum of the acoustic pressures at each element, it can be shown for unit element response that the array response V will be

$$V = \frac{\sin 2u}{\sin u} \quad ,$$

where $u = (\pi d \sin\theta)/\lambda$. The beampattern, defined as the square of this function normalized to unity at $\theta = 0$, is

$$b(\theta) = \left[\frac{\sin 2u}{2 \sin u}\right]^2 .$$

- Generalization of the two-hydrophone case to a linear array with N hydrophones gives the voltage response

$$V = \frac{\sin Nu}{\sin u} ,$$

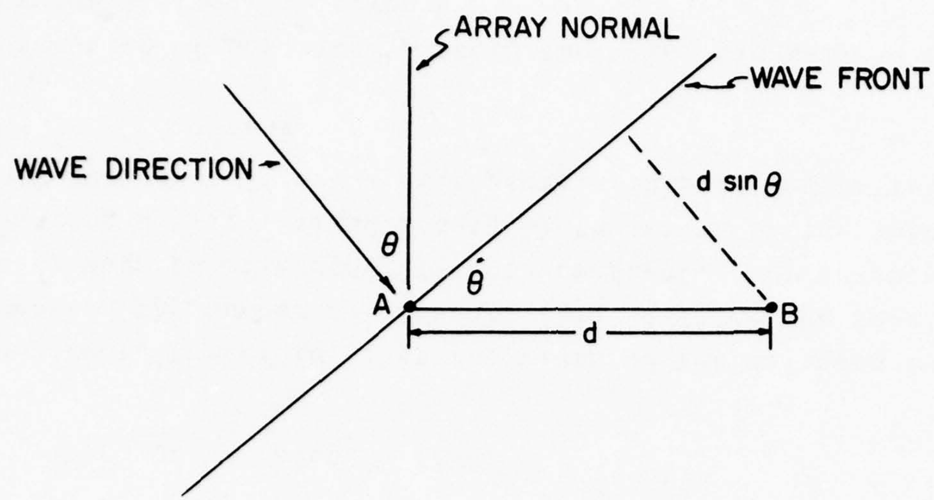

FIGURE 4-1 GEOMETRY FOR A TWO HYDROPHONE ARRAY

and the (normalized) beampattern

$$b(\theta) = \left[\frac{\sin Nu}{N \sin u}\right]^2$$

4.2 Broadside Beampattern

4.2.1 Mainbeam

- For an N-element line array, the half-width θ_o of the main beam corresponds to the first zero in the expression for the voltage response which is given by $Nu = \pi$. That is,

$$u = \frac{\pi}{N} = \frac{\pi d}{\lambda} \sin\theta_o$$

$$\text{or,} \qquad \sin\theta_o = \lambda/Nd.$$

It is apparent, therefore, that the width of the mainbeam $2\theta_o$ can only be reduced by increasing the number of elements (Fig. 4-2) or the spacing between elements d (Fig. 4-3) when the frequency is held constant. For an array with N elements at fixed spacing d (i.e., fixed length,L) the width of the main beam decreases as frequency increases (i.e., λ decreases). This is demonstrated in Figure 4-4 and Figure 4-5.

- For a broadside or unscanned pattern the main beam axis is at $\theta = 0$ and its level, due to normalization, is given by

$$10 \log b(\theta=0) = 0\text{dB}.$$

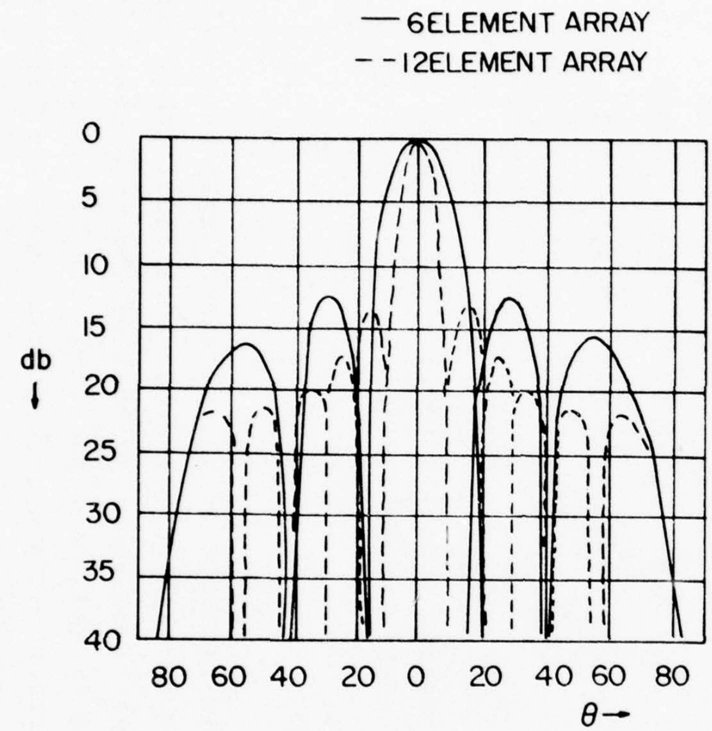

THE BEAMPATTERNS $b(\theta)$ FOR TWO (N=6ELEMENT AND N=12ELEMENT) LINE ARRAYS.

FIGURE 4-2

Moreover, if the element spacing is $d = \lambda/2$ and for small θ, the half-power or 3dB down beamwidth is approximately given by

$$BW_3 = \frac{101.8^\circ}{N} ,$$

where N is the number of array elements. An indication of the validity of this approximation is contained in Table 4-1 where both the accurate half-power widths and those computed from this expression are given.

N	2	3	4	5	6	12	50
$101.8^\circ/N$	50.9	33.9	25.4	20.4	16.97	8.48	2.036
BW_3	60.0	36.3	26.3	20.8	17.19	8.50	2.039

TABLE 4-1 Approximating the half-power (3dB down) width of an N-element line array

4.2.2 Grating Lobes and Spacing

- Whenever the spacing d between the elements of an unscanned array becomes equal to or greater than λ, where λ is the (design) wavelength, additional lobes can appear in the radiation pattern with amplitudes equal to that of the main beam (Fig. 4-3). These lobes are called grating lobes and their positions can be found from the beam-pattern function $b(\theta)$ and the definition of u. They occur whenever both the numerator and denominator in $b(\theta)$ are zero, or when

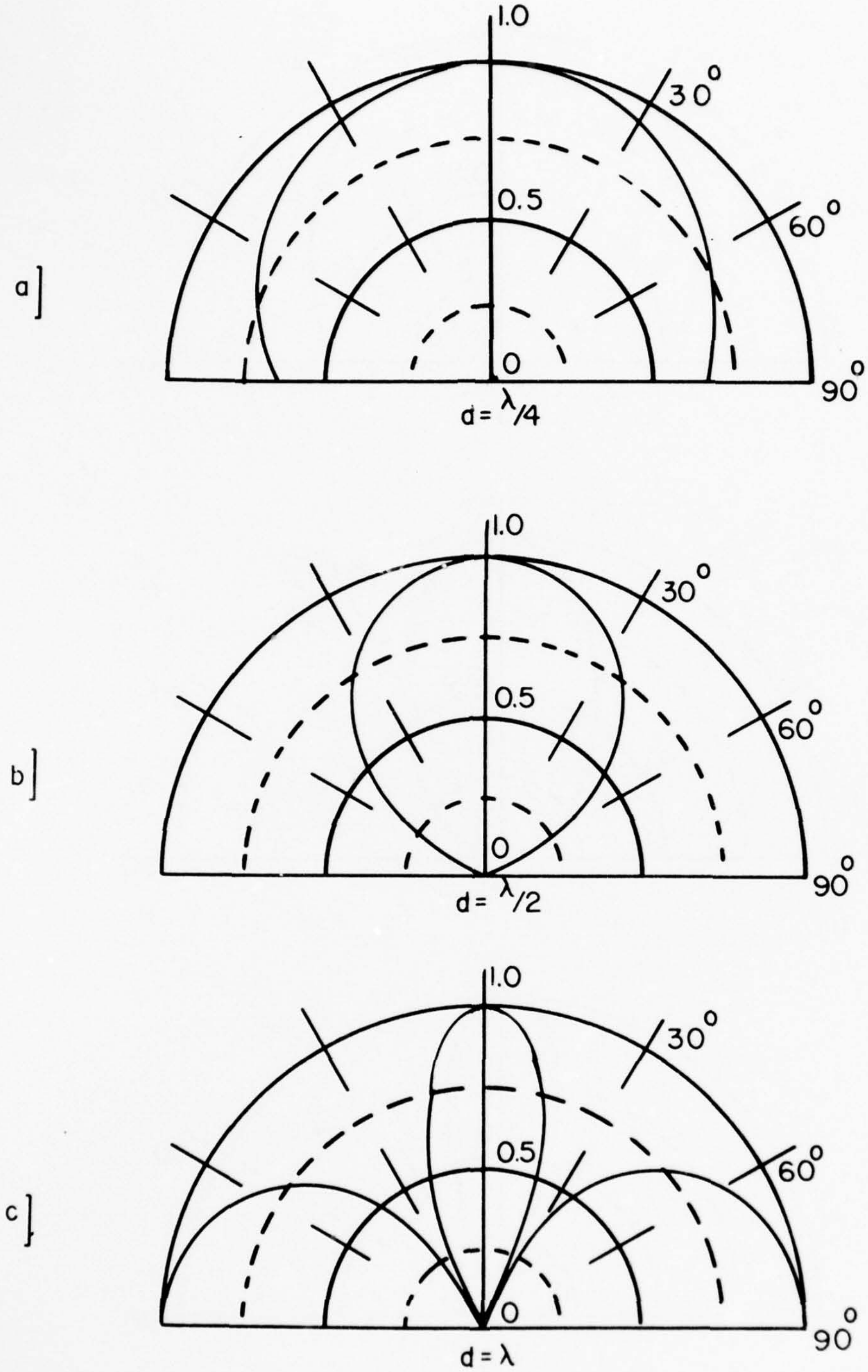

FIGURE 4-3 DIRECTIONAL CHARACTERISTICS OF TWO ISOTROPIC SOURCES A DISTANCE d APART.

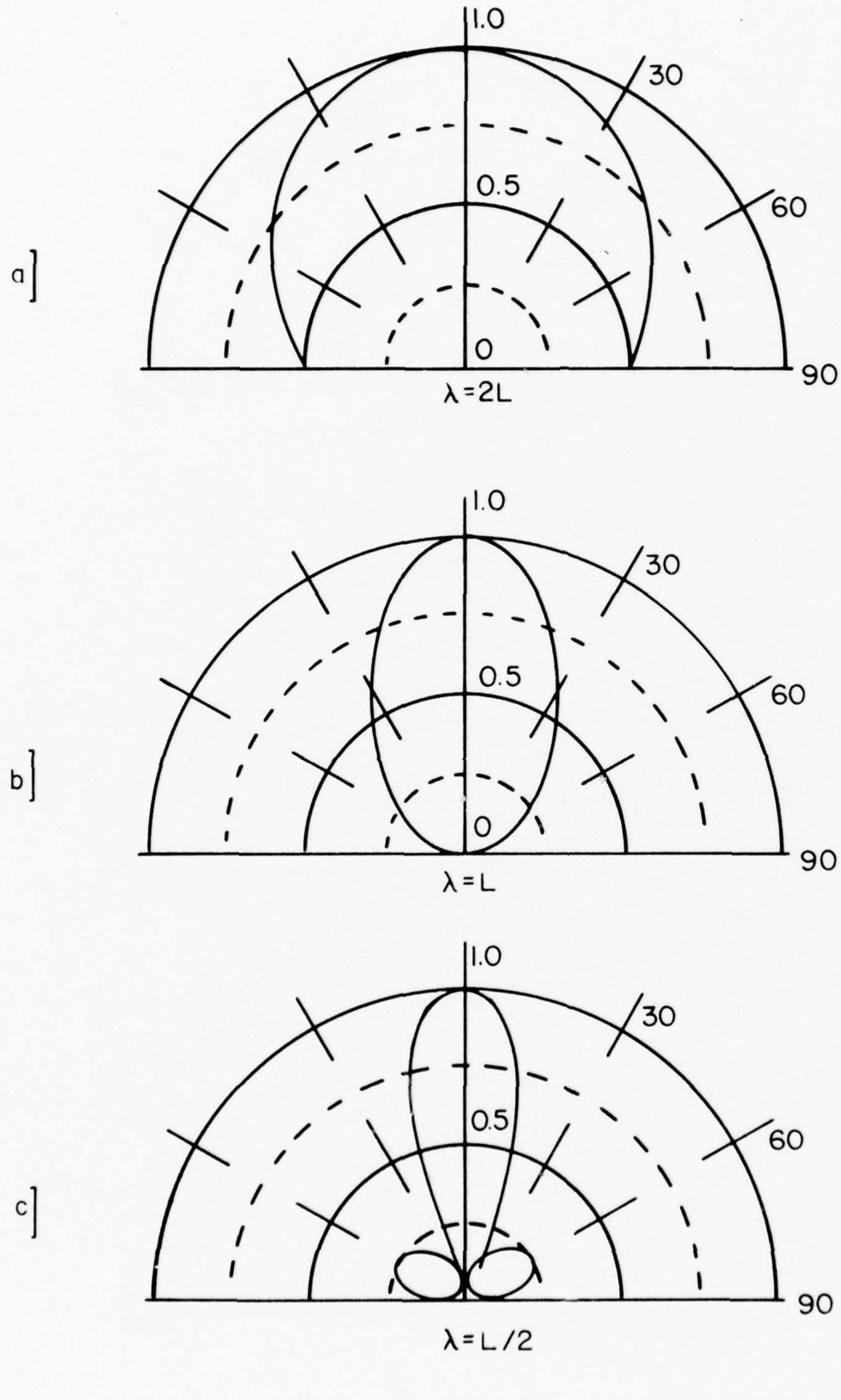

FIGURE 4-4 DIRECTIONAL CHARACTERISTICS OF A LINE ARRAY OF LENGTH L

ARRAY APERTURE REQUIRED TO ACHIEVE A GIVEN BROADSIDE BEAMWIDTH AT A GIVEN FREQUENCY FOR AN UNSHADED UNIFORMLY SPACED ARRAY

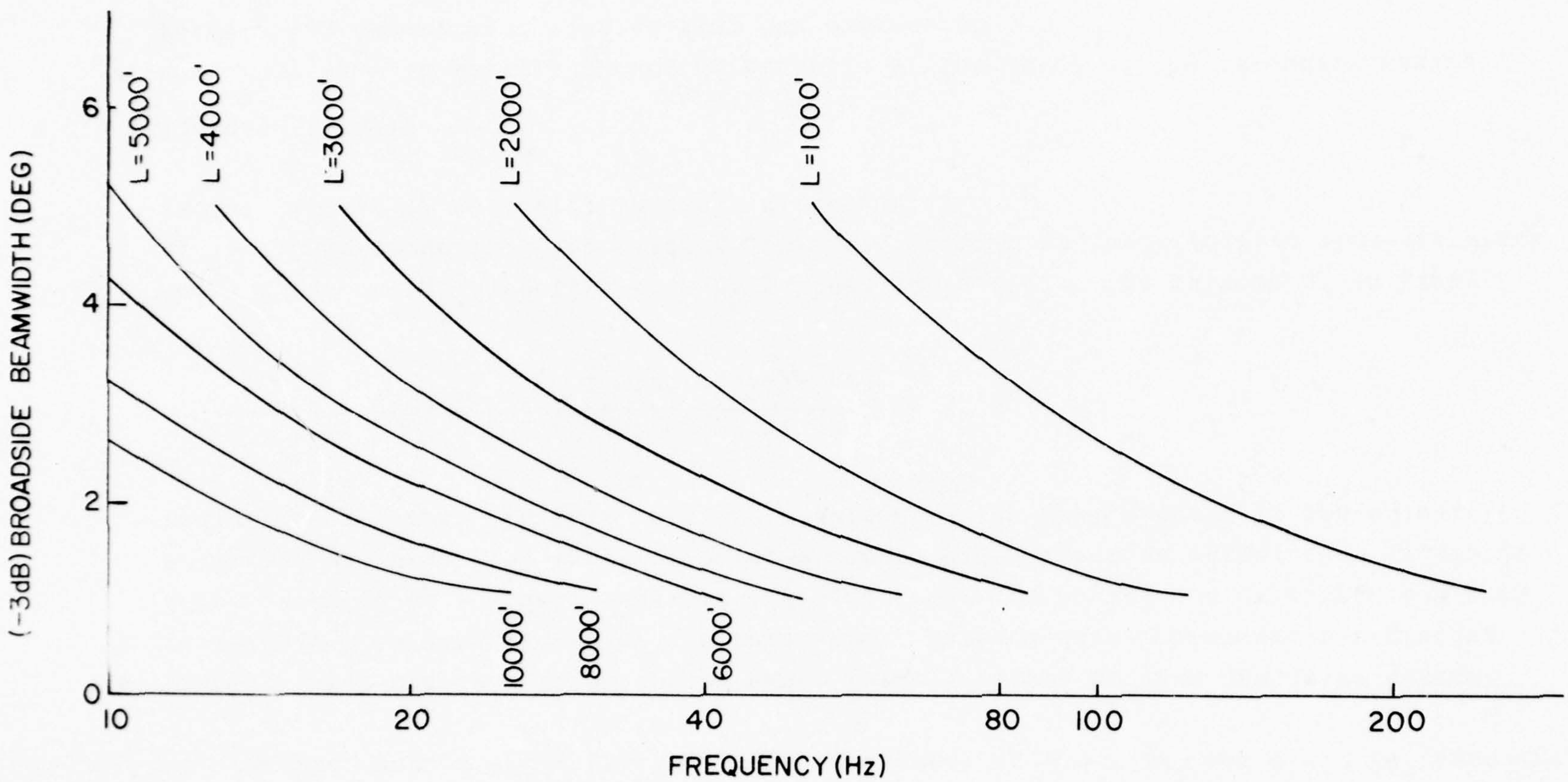

FIGURE 4-5

$$\pi(d/\lambda)\ \sin\theta = \pm\ \pi, \pm 2\pi,\ \ldots\ .$$

For example, when $d = 2\lambda$, grating lobes will occur at $\theta = \pm\ 30^{o}$ and $\theta = \pm\ 90^{o}$ (endfire).

- Grating lobes can lead to confusion since targets viewed by them cannot be distinguished from targets viewed by the main beam. In some cases, however, the grating lobes produced by a widely separated ($d>\lambda/2$) array can be reduced or eliminated over a limited azimuthal (θ) range by using elements with directive rather than isotropic radiation patterns. In this case the resultant array beam pattern is approximately

$$b(\theta) = b_e(\theta)\ \frac{\sin^2[N\pi(d/\lambda)\sin\theta]}{N^2\sin^2[\pi(d/\lambda)\sin\theta]} = b_e(\theta)\ b_a(\theta)\ ,$$

where $b_e(\theta)$ is the directive element pattern and $b_a(\theta)$ is the pattern of an array of isotropic elements. The grating lobes are reduced by the directive elements which radiate little or no energy in their direction.

4.2.3 Sidelobes & Nulls

- For an array with a large number of elements N, the level of the secondary maxima (sidelobes) can be approximated from the expression·

$$u = \left[(2k+1)/2\right]\pi/N \qquad k = 1, \pm\ 2, \pm\ 3\ldots\ .$$

Moreover, the angular positions of the sidelobe axes can also be determined from this expression and the definition $u = \pi(d/\lambda)\sin\theta$. For example, for large N, the level of the first sidelobe $b(\theta_1)$ is obtained from the beampattern function $b(\theta)$ with $u = 3\pi/2N$, or

$$b(\theta_1) = \left[\frac{\sin(3\pi/2)}{N(3\pi/2N)}\right]^2 = \left(\frac{2}{3\pi}\right)^2$$

for which $10 \log b(\theta_1) = -13.5$ dB. Continuing for $u = 5\pi/2N$ (i.e., the second sidelobe) for which we obtain a level of -17.9 dB, $u = 7\pi/2N$, etc., it is apparent that the sidelobes decrease in level as θ increases from broadside ($\theta=0$) to endfire ($\theta=\pm 90^{o}$). For the case of half-wavelength element spacing ($d = \lambda/2$), the level of the last sidelobe is approximately $1/N^2$ ($-20 \log N$). The total number of sidelobes produced by an N-element line array of length L is given by $(N-1)d/\lambda = L/\lambda$.

- In some cases it is of interest to know not only the orientation of the sidelobe maxima but also the location of the intervening nulls. By employing a phasor description of the beampattern, one can determine the azimuthal position of the nulls. When the array length L is much greater than the wavelength ($L>>\lambda$), the first null occurs at $\theta_1 = \pm\lambda/L$ radians array from the main beam axis at broadside ($\theta=0$). The second null, or the one between the first and second sidelobes, occurs at $\theta_2 = \pm 2\lambda/L$ and succeeding nulls at $\theta_n = \pm n\lambda/L$ ($n = 3,4...$).

4.2.4 Directivity

- The beampattern $b(\theta)$ of a uniformly illuminated array with elements spaced $\lambda/2$ apart is similar to the pattern produced by a uniformly illuminated continuous line source

(See Section 3.2). It has rotational symmetry and is nondirectional in the plane in which ϕ is measured (i.e., the plane orthogonal to the θ-plane and the array). For example, see Figure 3-1.

- Inserting the beampattern function $b(\theta)$ of a uniformly illuminated N-element line array with equal element spacing d, into the expression for the directivity D of a line source (Section 3.2), we can calculate the directivity D of this array, or

$$D.I. \equiv 10 \log D = 10 \log \left\{ \frac{N}{1 + \frac{2}{N} \sum_{n=1}^{N-1} \frac{(N-n)\sin(2n\pi d/\lambda)}{2n\pi d/\lambda}} \right\}$$

For the particular case of half-wavelength spacing ($d=\lambda/2$), the D.I. becomes

$$D.I. = 10 \log N.$$

- Note that the length of an N-element line array can be written as $L = (N-1)d$ which, for $d = \lambda/2$, leads to the expression

$$N = \frac{2L}{\lambda} + 1.$$

Thus, for long arrays ($L \gg \lambda$), the D.I. can be written as

$$D.I. = 10 \log N \simeq 10 \log 2L/\lambda,$$

which is the same as that of a continuous line source of length L.

4.2.5 Nonuniform Amplitude Distributions

Gabled Array

- One characteristic of the uniform array, where the elements all have the same amplitude and phase, is the relatively large height of the first sidelobe. Array element distributions can be formulated, however, so that the sidelobes are as small as desired.

- Consider, for example, an array where all elements are in phase but where the amplitudes decrease uniformly from the central element to the ends. This is a special case of the so-called gabled illumination and its beampattern will be the square of the beampattern of a uniform array. Thus, the first sidelobe will have a height of only 1/4% of the main beam height (unity) instead of the 5% (i.e., 0.045) height for the uniform array. All other sidelobes will be similarly reduced but the main beam will be somewhat broader than its uniform counterpart. The half-power (3 dB) width of the gabled array is approximately $145^{\circ}/N$ compared to $102^{\circ}/N$ for the uniform array (See Table 4-1). An example beampattern of a gabled array is given in Figure 4-6.

Binomial Array

- Another example of a nonuniform amplitude distribution is the binomial array where the array elements are weighted according to the coefficients $\binom{n}{m}$ in the binomial expansion

$$(a+b)^n = \sum_{m=0}^{n} \binom{n}{m} a^{n-m} b^m ,$$

where $n = (N-1)$ and N is the number of elements in the array. The coefficients $\binom{n}{m}$ are given by

$$\binom{n}{m} = \frac{n!}{m!\,(n-m)!}$$

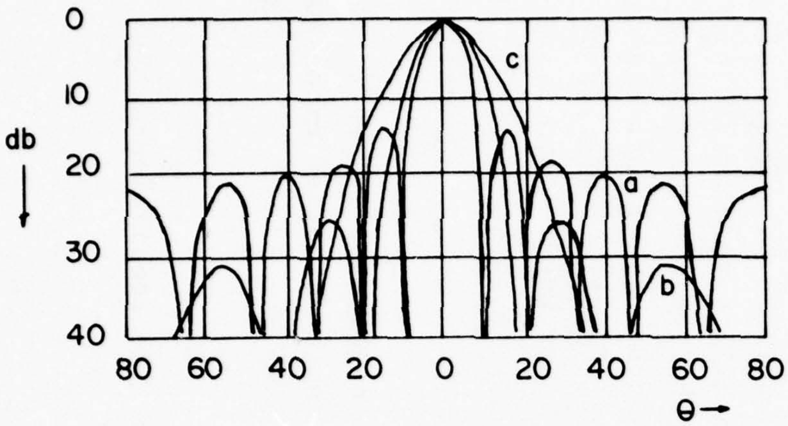

BEAM PATTERNS FOR THREE 11-ELEMENT $\lambda/2$ SPACED ARRAYS

(a) THE UNIFORM ARRAY $\left[\dfrac{\sin\left(\frac{11}{2}\pi\sin\theta\right)}{11\sin\left(\frac{\pi}{2}\sin\theta\right)}\right]^2$

(b) THE GABLED ARRAY $\left[\dfrac{\sin(3\pi\sin\theta)}{6\sin\left(\frac{\pi}{2}\sin\theta\right)}\right]^4$

(c) THE BINOMIAL ARRAY $\left[\cos\left(\frac{\pi}{2}\sin\theta\right)\right]^{10}$

FIGURE 4-6

which, for a six-element array, indicates relative element amplitudes proportional to 1,5,10,10,5,1. The important characterisitcs of a binomial array is that it has no sidelobes. It is not used very much in practice, however, because of its relatively wide beamwidth and the large individual element amplitudes required across the array, especially when the number of elements is large. An example beampattern of a binomial array is given in Figure 4-6.

Other Distributions

- Other nonuniform amplitude distributions such as cosine or cosine-on-pedestal will not be reviewed here since they will be discussed in detail in the subsequent section entitled "Shading of Arrays". It should be emphasized, however, that of all amplitude distributions on half-wavelength ($d = \lambda/2$) spaced arrays for which the elements have the same phase, the uniformly illuminated array provides the maximum directivity.

4.3 Theorems of Schelkunoff

- Although this subject is treated very briefly here and may be somewhat obscure, it is nevertheless presented as an introduction to a viable analysis technique.

4.3.1 Theorems

Theorem I

- One well known method for analyzing the beampatterns of arrays associates a polynomial of degree (N-1) with an N-element line array. This is essentially Schelkunoff's first theorem which states that every line array with equal element spacing can be represented by a polynomial* in the complex number z, or

$$F(z) = a_o+a_1z+a_2z^2+\ldots a_{N-1}z^{N-1},$$

where the weighting coefficients a_i express the amplitude and phase of the i^{th} element relative to some reference element.

- The beampattern $b(\theta)$ of an array may be completely analyzed in terms of the properties of this polynomial. In fact, the unnormalized pattern $b(\theta)$ can be written as

$$b(\theta) = |f(z)|^2.$$

- The independent variable z is a complex number which can be expressed as $z=\exp[i\psi]$, where $i = \sqrt{-1}$. The variable ψ is defined as $\psi=2\pi(d/\lambda)\sin\theta-\alpha$, where d is the element spacing, θ the direction from array broadside and α the progressive phase delay. Expressed in this way, one can see that the variable z will always have some value on the circumference of the unit circle with ψ the associated angle as shown in Figure 4-7. As θ decreases from $\theta=\pi/2$ (which is along the array)

---

*In a manner analogous to that of Sections 4.1 and 4.6.1.3, each term of the polynomial represents the response of an element in the array. It should be apparent, therefore, that the polynomial is just another way of expressing the (voltage) response or field strength of the whole array.

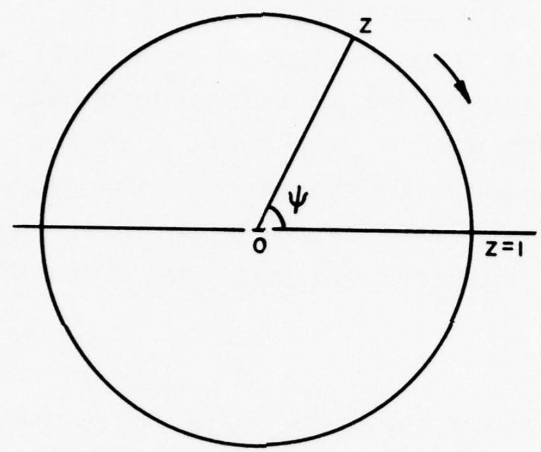

SCHELKUNOFF UNIT CIRCLE

FIGURE 4-7

to $\theta=-\pi/2$(also along the array), ψ decreases and z moves in the clockwise direction. The range R of ψ as θ changes from $\pi/2$ to $-\pi/2$ is given by $R=4\pi d/\lambda$.

- From the expression for R, when $d = \lambda/2$ the range R of ψ will be 2π. That is, z will describe one complete cycle on the unit circle which maps, by a one-to-one correspondence, to the points on the surface of the beam pattern $b(\theta)$. If $d<\lambda/2$, z will traverse less than one complete turn on the unit circle and if $d>\lambda/2$ it will traverse more than one complete turn. In the latter case, since the beampattern is a periodic function of ψ (or θ), some lobes will be repeated. In fact, if $d = \lambda$, two complete patterns including two main beams will occur for one complete cycle of z.

Theorem II

- The second or product theorem stems from the fact that the product of a polynomial is also a polynomial. It essentially states that there exists a line array with a beampattern equal to the product of the beampatterns of any two line arrays. This process may be repeated so that a line array may be constructed with a beampattern equal to the product of the beampatterns of any number of line arrays. The theorem may also be extended, as in many sonar texts, where it is stated that if the elements of an array are directive, the resultant pattern $b_R(\theta)$ of the array is the product of the element pattern $b_E(\theta)$ and the pattern $b_o(\theta)$ derived as if the elements were all omnidirectional, or

$$b_R(\theta) = b_E(\theta)\ b_o(\theta) \ .$$

Theorem III

- By the fundamental theorem of algebra a polynomial $f(z)$ of degree $(N-1)$ has $(N-1)$ zeros and can be factored into a multiple product of $(N-1)$ binomials

$$f(z) = (z-t_1)\,(z-t_2)\,\ldots\,(z-t_{N-1})\ .$$

Note that the zeros t_i represent the null points of the array beampattern since for z equal to any t_i, $f(z)$ and therefore $b(\theta)$ will be zero. This leads to the third and final theorem which states essentially that the beampattern of a line array of N-elements is the product of the beampatterns of $(N-1)$ couplets or two-hydrophone arrays.

4.3.2 Geometrical Interpretations

- The theorems lend themselves to a geometric interpretation since the pattern of each couplet $(z-t_i)$ can be represented by a line drawn between the points t_i and z on the unit circle (Fig. 4-8). Thus, if we have an $N=5$ element array as demonstrated in Figure 4-8 then, for a given z and ψ (corresponding to a given direction θ), the magnitude of $b(\theta)$ will be proportional to the product of the four distances $D_1, \ldots D_4$. As z ranges over the unit circle, these four distances change giving a variation in the magnitude of $b(\theta)$ as ψ (i.e., θ) is varied. When z coincides with a root or zero (i.e., t_i), then one of the four distances will be zero giving a null$(b(\theta) = 0)$ in the product or beampattern.

- Figure 4-8 is actually the Schelkunoff unit circle representation for a uniformly (i.e., all coefficients, $a_i = 1$) excited equispaced linear array with $N=5$ elements.

In this case the array polynomial becomes

$$f(z) = 1+z+z^2+z^3+z^4 = (z^5-1)/(z-1),$$

and
$$b(\theta) = \left|\frac{z^5-1}{z-1}\right|^2 .$$

The nulls of the pattern are given by the (N-1) = 4 roots of the polynomial which correspond to the four ψ values

$$\psi_m = \frac{2m\pi}{5} , \qquad m = 1,2,3.4.$$

These roots lie on the unit circle and, along with the $\psi = 0$ value ($\theta=0$) which corresponds to the principal maximum or mainbeam axis, divide this circle into $N = 5$ equal parts.

- In Figure 4-8, the range of z between the roots 4 and 1 corresponds to the main beam and the range of z between the roots 1 and 2, the roots 2 and 3 and the roots 3 and 4 corresponds to the sidelobes. Positioning these roots, by adjusting the polynomial coefficients, or the ratio d/λ, effects the sidelobe levels. By clustering the roots closer together, in the region of $z = -1$ ($\psi = 180^{o}$), the sidelobes can be reduced relative to the mainbeam. This, however, increases the separation between roots 1 and 4 and broadens the main beam.

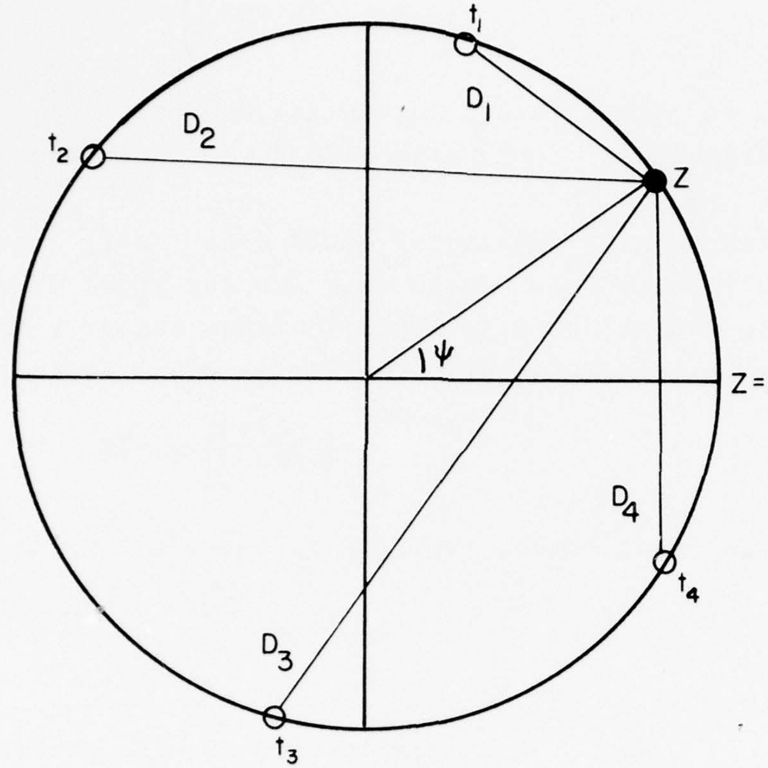

SCHELKUNOFF BEAMPATTERN

FIGURE 4-8

- In terms of the Schelkunoff unit circle, the pattern synthesis problem is really a question of where to place the roots of the polynomial. If it is desired to produce a pattern with a main beam and well defined nulls and sidelobes, then the question is limited to where to place the roots <u>on</u> the unit circle. However, if a pattern of some particular shape is desired which is free from nulls, then the roots must be placed <u>off</u> the unit circle.

4.4 Scanned Arrays

4.4.1 Main Beam and Other Major Lobes

- We saw in Section 4.0 that the (broadside) beampattern for an unscanned array was given by

$$b(\theta) = \left[\frac{\sin Nu}{N\sin u}\right]^2$$

where $u = (\pi d\sin\theta)/\lambda$. Here, θ is an angle measured from array broadside, d is the element spacing, λ is the wavelength and N is the number of elements in the array. This expression is valid for any line array whose element current amplitudes are equal and in phase (i.e., zero phase difference between array elements).

- If we now introduce a uniform progressive phase to the array elements while maintaining equal amplitudes, the expression for the $b(\theta)$ will be modified somewhat since u now becomes

$$u = \left\{\left[(\pi d\sin\theta)/\lambda\right]-\alpha/2\right\}$$

where α is a constant called the phase-shift factor. This factor can be used to position the main beam in space. If α is varied, the beam will scan.

- When $u = m\pi$, it can be shown that the beampattern $b(\theta)$ has an absolute maximum or major lobe for every θ satisfying

$$\sin\theta = \frac{\lambda}{\pi d}\,(m\pi + \alpha/2) \qquad m = 0,\ \pm 1,\ \pm 2,\ \ldots\ .$$

The position θ_o of the axis of the first ($m = 0$) major lobe or main beam is given by

$$kd\sin\theta_o = \alpha,$$

where $k = 2\pi/\lambda$ is the wave number. The angle θ_o is also called the scan angle or scan position.

- Other major lobes can also occur. For example, the conditions $m = \pm 1$ indicate major lobes at the locations θ' given by

$$kd\sin\theta' = \alpha \pm 2\pi$$

which, since $kd\sin\theta_o = \alpha$, can be related to the location of the main beam θ_o by

$$\sin\theta' = \sin\theta_o \pm \lambda/d.$$

If the location of the main beam is at $\theta_o = 0^\circ$ (i.e., broadside) then the other major (i.e., grating) lobes will occur at angles given by

$$\sin\theta' = \pm\lambda/d.$$

- Note that for $d<\lambda$, no second major lobe can form when the main beam is at broadside.

- If the position of the main beam is to remain arbitrary and it is desired to prevent the appearance of a second major lobe, then the element spacing d must be chosen so that

$$|\sin\theta_o| + (\lambda/d) > 1$$

and

$$|\sin\theta_o| - (\lambda/d) < -1.$$

It should be apparent, from the general expression for $\sin\theta'$ above, that no second major lobe can occur under these conditions. The second of these conditions is the more stringent and can be rewritten as

$$\frac{d}{\lambda} < (1 + |\sin\theta_o|)^{-1}$$

Thus, if the main beam is scanned close to endfire (i.e., $\theta_o \simeq \pm\ \pi/2$), the elements must be spaced less than a half-wavelength apart (i.e., $d/\lambda < 1/2$) if a second main beam is to be prevented.

4.4.2 Beamwidths and Nulls

- When $u = m\pi/N$, it can be shown that $b(\theta)$ has a null for every θ satisfying

$$\sin\theta = \frac{\lambda}{\pi d}\left(\frac{m\pi}{N} + \frac{\alpha}{2}\right) \qquad m = \pm 1, \pm 2, \ldots \ .$$

Thus, the positions θ_1 and θ_2 of the first nulls on either side of the main beam axis or scan angle θ_o are given (i.e., for $m=\pm 1$) by

$$N(kd\sin\theta_1 - \alpha) = 2\pi$$

and

$$N(kd\sin\theta_2-\alpha) = -2\pi$$

Since $kd\sin\theta_o = \alpha$ as shown above (Section 4.4.1) and $Nd \simeq L$, the array length, these expressions reduce to

$$\sin\theta_1 - \sin\theta_o = \lambda/L$$

and

$$\sin\theta_2 - \sin\theta_o = -\lambda/L.$$

Moreover, for $L >> \lambda$ and letting $\theta_1 = \theta_o + \Delta\theta$ and $\theta_2 = \theta_o - \Delta\theta$, it can be shown that *

$$\Delta\theta \simeq (\lambda/L)\sec\theta_o$$

or, that the angular spacing between the nulls on each side of the main beam (or the main beamwidth itself) is

$$BW_\infty = 2\Delta\theta \simeq 2(\lambda/L)\sec\theta_o.$$

- Expressions have also been developed which give the half-power or -3 dB beamwidth for a line array as a function of array length L, the wavelength λ and the scan position θ_o. These are given graphically in Figure 4-9. Approximations to these expressions for those cases where $L >> \lambda$ are

---

* Note that in some texts, $\Delta\theta$ is proportional to $\csc\theta_o$. In those texts, θ_o is measured from the line of the array and not from broadside as is the case herein.

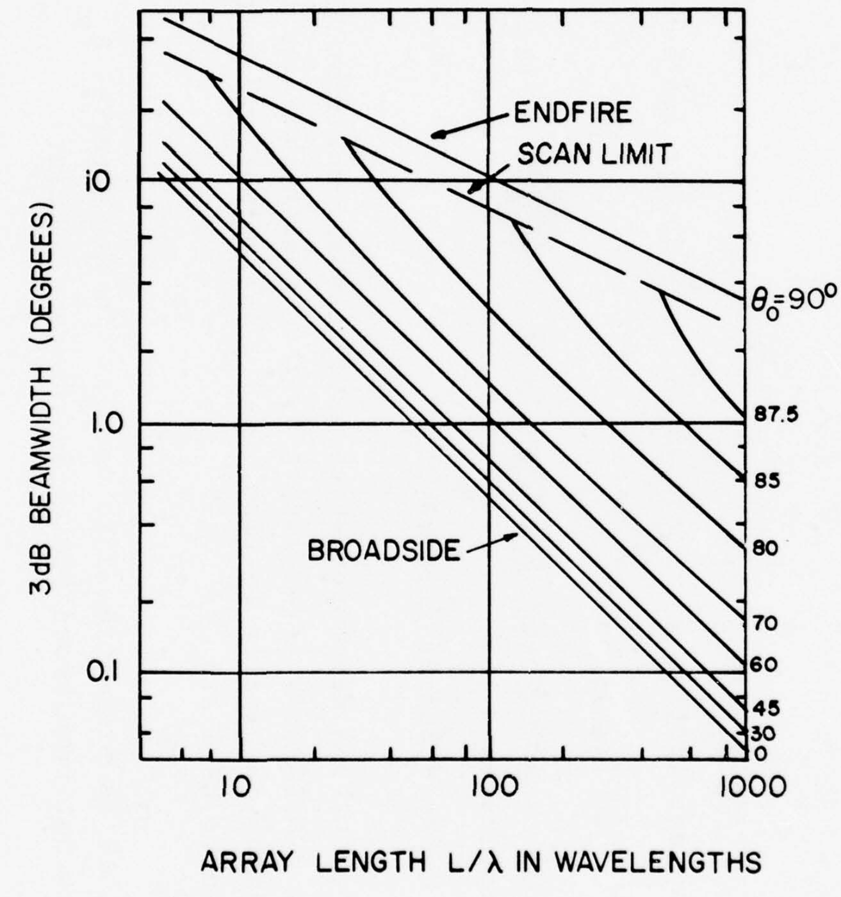

BEAMWIDTH VERSUS ARRAY LENGTH AND SCAN ANGLE

FIGURE 4-9

$$BW_3 = 0.886\ (\lambda/L)\sec\theta_o \quad \text{(at or near broadside, in Radians)}$$

$$BW_3 = 2[0.886\ (\lambda/L)]^{1/2} \quad \text{(at endfire, in Radians)}$$

Actually, when $L>5\lambda$ (at least), the first of these approximations is in error by less than 4% when the beam is scanned to within two beamwidths of endfire. The second approximation, for $L>5\lambda$, is in error by less than 1%.

4.4.3 Beam Broadening and Directivity

- The above expressions for BW_∞ and BW_3 show that the beam broadens as it is scanned from broadside toward endfire and that the broadening is proportional to the term $\sec\theta_o$. This is an approximate result which is valid for beam positions θ_o near broadside. Although the effect of scanning is to broaden the beamwidth in the plane of the scan, this does not mean that the broadside directivity (See Section 4.2.4) will decrease proportionately.

- As the conical beam of a line array is scanned toward endfire, the cone tends to occupy a smaller solid angle in space. This will just cancel the beam broadening effect on the directivity which remains essentially independent of the scan angle. However, when the beam actually reaches endfire and becomes a pencil beam, the directivity will double (i.e. a 3 dB increase in D.I. will occur) provided that the array element spacing d is slightly less than half-wavelength which is usually the case. It should be noted that this doubling of the directivity at endfire will not occur if the array element spacing d is half-wavelength or greater since, under these conditions, a second equivalent main (i.e. grating) lobe will appear at reverse endfire.

4.4.4 Sidelobes

- The positions θ of the sidelobes or secondary maxima are approximately given by the following expression

$$\sin\theta = \frac{\lambda}{2\pi d}\left[\frac{(2m+1)\pi}{N} + \alpha\right] \qquad m = 1, \pm 2, \pm 3, \ldots$$

for an array with a large number of elements, N. It is also apparent, after comparing this expression with its counterpart for an unscanned array, (Section 4.2.3) that scanning does not affect the sidelobe levels, at least not to a first approximation. The level of the first sidelobe remains approximately -13.5 dB down from the main beam level whether the array is scanned or not.

4.5 Sector Coverage in Multibeam Arrays

4.5.1 Crossover and Steering Angles

- When line arrays are used for listening, it is frequently desirable to form beams that are simultaneously steered at certain angles so that sound arrivals over a broad angular sector may be detected. This requires that the beams overlap in order that a certain minimum response be maintained. Thus, questions arise as to how many beams are needed to cover a given angular sector and what steering angles will produce this family of beams.

- It has already been shown that the beampattern for a line array of N uniformly spaced point sources (or receivers) is given by

$$b(u) = \left[\frac{\sin Nu}{N\sin u}\right]^2 ,$$

where u can be expressed as

$$u = (\pi d/\lambda)\ (\sin\theta - \sin\phi).$$

Here again, d is the interelement spacing, λ is the wavelength of sound, θ is the angle to the point of interest measured from array broadside and ϕ (formerly, θ_o) is the beam steering angle which is also measured from broadside.

- The requirement here is to steer beams in the directions ϕ_n so that they overlap at values θ_n on a polar plot (Fig. 4-10). The crossover points or θ_n values are determined in such a fashion that the array response is never less than some set value (say 10 log b(u) = -3dB) in the sector being covered. The basic sector to be considered here for full coverage is $0^o \leq \theta \leq 90^o$. The coverage in all other quadrants can be obtained from symmetry.

- In the expression for the beampattern function, it is apparent that b(u) is an even function of u which means that it is symmetric (or unaffected) with respect to an interchange of θ and ϕ. This fact not only simplifies the problem but also assures that the results obtained for positive angles ϕ_n and θ_n are equally valid for negative angles.

- The first or broadside beam is not steered which means that $\phi_o = 0$. From the expression for u, we get

$$u_o = (\pi d/\lambda)\sin\theta_o$$

or,

$$\theta_o = \sin^{-1} u_o \lambda/\pi d.$$

The angle θ_o is the first crossover angle and corresponds to the smallest θ_n for which the beampattern takes on the stipulated minimum response $b(u_o)$.

- In order to obtain the first steering angle ϕ_1, recall that $\sin\theta$ and $\sin\phi$ can be interchanged in the expression for u and then match the first off-broadside beam (u_1) to the broadside beam (u_o) at the crossover angle θ_o, or

$$u_1 = \frac{\pi d}{\lambda} (\sin\phi_1 - \sin\theta_o) = u_o = \frac{\pi d}{\lambda} \sin\theta_o \ .$$

This expression reduces to $\sin\phi_1 = 2 \sin\theta_o$, or

$$\phi_1 = \sin^{-1} (2\sin\theta_o)$$

for the first steering angle.

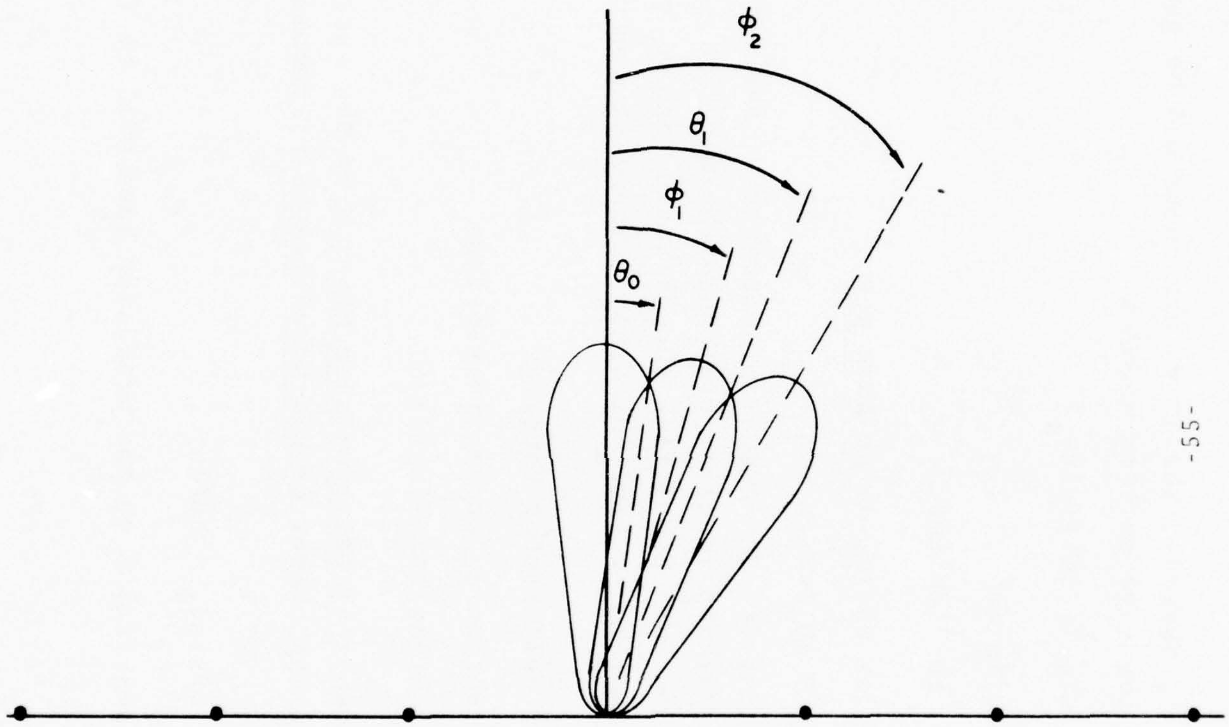

BEAMSTEERING (ϕ_n) AND CROSSOVER (θ_n) ANGLES

FIGURE 4-10

- Although it is not completely obvious, the above procedure can be generalized so that the solution to the sector coverage problem becomes

$$\theta_n = \sin^{-1}[(2n+1)\sin\theta_o]$$

for the n beam crossover angles and

$$\phi_n = \sin^{-1}[2n\sin\theta_o]$$

for the n beam steering angles where, as we have seen,

$$\sin\theta_o = \lambda u_o/\pi d \ .$$

For a given array with spacing d/λ and number of elements N, the value of $\sin\theta_o$ can be calculated from the beampattern function $b(u)$ once the *minimum response* $b(u_o)$ has been selected. The procedure for calculating successive θ_n and ϕ_n values across the sector is halted as soon as either a $\sin\theta_n$ or $\sin\phi_n$ value equals unity.

4.5.2 Number of Beams Required for *Full Sector Coverage*

- Since the n^{th} beamsteer direction ϕ_n occurs just before

$$\sin\phi_n = 2n\sin\theta_o = n\sin\phi_1 > 1 \ ,$$

it can be shown that the number of off-broadside beams M in the sector 0^o to 90^o will be $M = 1/\sin\phi_1$. Thus, the number of off-broadside beams required for full 360^o coverage is

$$2M = 2/\sin\phi_1 = \pi d/\lambda u_o \ ,$$

and the total number of beams including the broadside beam will be (2M+1).

- Table 4-2 provides a list of u_o/π values versus N, the number of array elements, for a range of N from 8 to 80. The minimum response or u_o/π entries correspond to the half-power point ($10 \log b(u_o) = 3$dB) on the main beam. These entries were computed for $d/\lambda = 1$. To correct them for any d/λ value, divide the entry by the value of d/λ. For the same conditions, Table 4-2 also provides a comparison of M, the number of off-broadside beams versus N, the number of array elements.

- When M is not an integer (which is usually the case) the M^{th} beamsteer direction ϕ_M will occur prior to 90^o, a condition which results in an endfire beam with a dimple at 90^o. In order to avoid this dimple and steer the M^{th} beam exactly at endfire, the above procedure can be modified somewhat by setting the first beamsteer direction at ϕ_1 so that

$$\sin\phi_1 = 2\sin\theta_o = 1/[M],$$

where the brackets [] indicate the largest integer in M. Using this expression (i.e., $1/2[M]$) for $\sin\theta_o$ in

$$\sin\phi_n = 2n\sin\theta_o ,$$

it is apparent that an integral number of beams will result with no dimple although a slightly lower crossover level will occur. For large N and M, however, this difference level will be negligible.

- It was shown earlier (Section 4.2.1) that the half-power (-3dB) broadside or near broadside beamwidth of an N-element half wavelength spaced array is approximately

$$BW_3 = 1.772/(N-1),$$

in radians. If the crossover point is selected so that $\theta_o = BW_3/2$, then we have the approximate relationship

$$M = \frac{2(N-1)}{1.772}$$

which is applicable near broadside. In other words, the number of beams required for full quadrant coverage is rougly equal to the number of array elements. This expression is plotted in Figure 4-11 and is significant from a systems engineering view point in that the number of beams and sensors must all be accomodated by signal processing and display subsystems.

- As we shall see shortly, the shading of arrays will not only reduce the sidelobe level, but it will also broaden the main beam. The procedure given above can still be applied to obtain full sector coverage but the number of beams will be reduced due to the broadening factor, f. This can be demonstrated by rewriting the above approximation for M as

$$M \approx \frac{2(N-1)}{1.772\ f}$$

For example, a 50 wavelength ($L/\lambda = 50$) array with half-wavelength element spacing has a beamwidth of about 1^o and approximately $N \approx 100$ elements. Here,

$$M \approx \frac{2(N-1)}{1.772} = 112$$

TABLE 4-2

Minimum Response or u_0/π Values Corresponding to the Half-power (10 log $b(u_0)$=-3dB)Point in the Beampattern Versus N,the Number of Elements

N	u_0/π	M	N	u_0/π	M
8	0.556E-01	8.98	45	0.983E-02	50.86
9	0.494E-01	10.12	46	0.961E-02	51.99
10	0.444E-01	11.26	47	0.941E-02	53.12
11	0.403E-01	12.39	48	0.921E-02	54.25
12	0.369E-01	13.53	49	0.902E-02	55.38
13	0.341E-01	14.66	50	0.884E-02	56.51
14	0.316E-01	15.79	51	0.867E-02	57.65
15	0.295E-01	16.93	52	0.850E-02	58.78
16	0.276E-01	18.06	53	0.834E-02	59.91
17	0.260E-01	19.19	54	0.819E-02	61.04
18	0.246E-01	20.32	55	0.804E-02	62.17
19	0.233E-01	21.46	56	0.789E-02	63.30
20	0.221E-01	22.59	57	0.775E-02	64.43
21	0.210E-01	23.72	58	0.762E-02	65.56
22	0.201E-01	24.85	59	0.749E-02	66.69
23	0.192E-01	25.98	60	0.737E-02	67.82
24	0.184E-01	27.11	61	0.725E-02	68.95
25	0.177E-01	28.24	62	0.713E-02	70.08
26	0.170E-01	29.38	63	0.702E-02	71.21
27	0.163E-01	30.51	64	0.691E-02	72.35
28	0.158E-01	31.64	65	0.680E-02	73.48
29	0.152E-01	32.77	66	0.670E-02	74.61
30	0.147E-01	33.90	67	0.660E-02	75.74
31	0.142E-01	35.03	68	0.650E-02	76.87
32	0.138E-01	31.66	69	0.641E-02	78.00
33	0.134E-01	37.29	70	0.631E-02	79.13
34	0.130E-01	38.43	71	0.622E-02	80.26
35	0.126E-01	39.55	72	0.614E-02	81.39
36	0.122E-01	40.68	73	0.605E-02	82.52
37	0.119E-01	41.81	74	0.597E-02	83.65
38	0.116E-01	42.94	75	0.589E-02	84.78
39	0.113E-01	44.08	76	0.581E-02	85.91
40	0.110E-01	45.21	77	0.574E-02	87.04
41	0.107E-01	46.34	78	0.567E-02	88.17
42	0.105E-01	47.47	79	0.559E-02	89.31
43	0.102E-01	48.60	80	0.552E-02	90.43
44	0.100E-01	49.73			

All entries correspond to $d/\lambda=1$ but can be adjusted for any d/λ value by dividing the entry by d/λ. A comparison of N versus M, the number of off-broadside beams in one quadrant is also provided.

with no shading (i.e., $f=1$). If this same array is shaded to -40 dB sidelobes using Taylor shading (instead of only -13.5 dB sidelobes with no shading) then $f = 1.4$. In this case, the number of beams becomes $M \approx 80$, a reduction of about 32 beams. Thus, in order to discriminate against signals in off-axis directions, the sidelobes must be reduced. This has a deleterious effect on beamwidth but is an advantage to the overall system because there are fewer beams which require sophisticated signal processing and display hardware.

- A useful performance graph is given in Figure 4-12 which shows the number of unshaded beams (2M+1) necessary for complete 360° coverage, given the value of the unshaded broadside beamwidth in degrees. It is apparent that as the broadside beamwidth approaches 1° the number of beams approaches 100 and is increasing rapidly.

- Figure 4-13 is another practical graph giving the beam response versus angle for a Taylor* shaded 100 element array. Note that the beam crossover point is not at -3dB but rather more like -3.5dB. Thus, there are even fewer beams than one might expect if one accounts only for the beam broadening factor due to shading. Note also that there is no dimple in the endfire beam but that it points directly at 90° from broadside.

---

* Taylor shading is a particular form of element amplitude shading which is discussed in detail in Sections 4.6.1.5, 4.6.2.3 and 4.6.3.3.

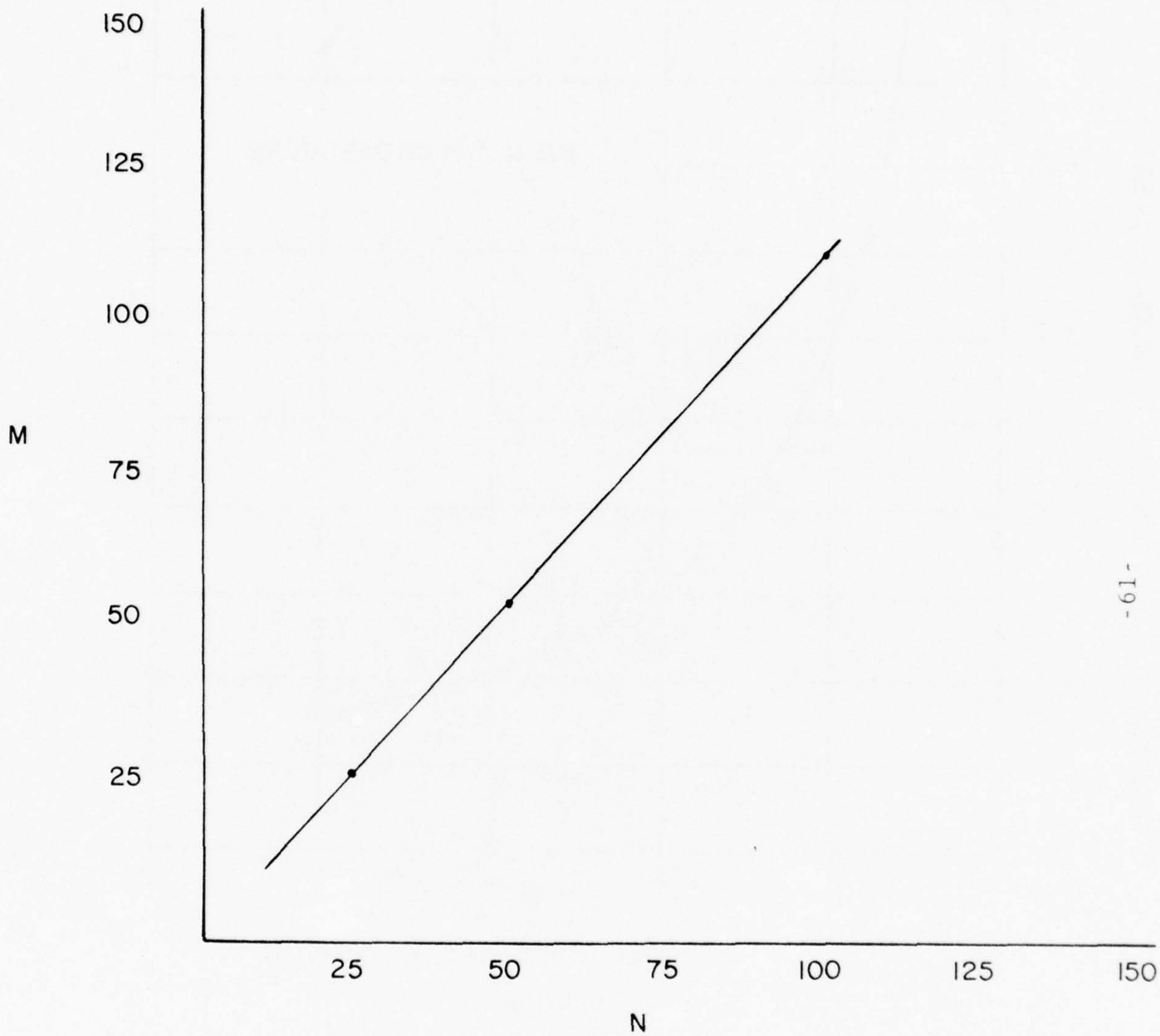

RELATIONSHIP BETWEEN THE NUMBER OF BEAMS M AND THE NUMBER OF ELEMENTS N IN A LINE ARRAY

FIGURE 4-11

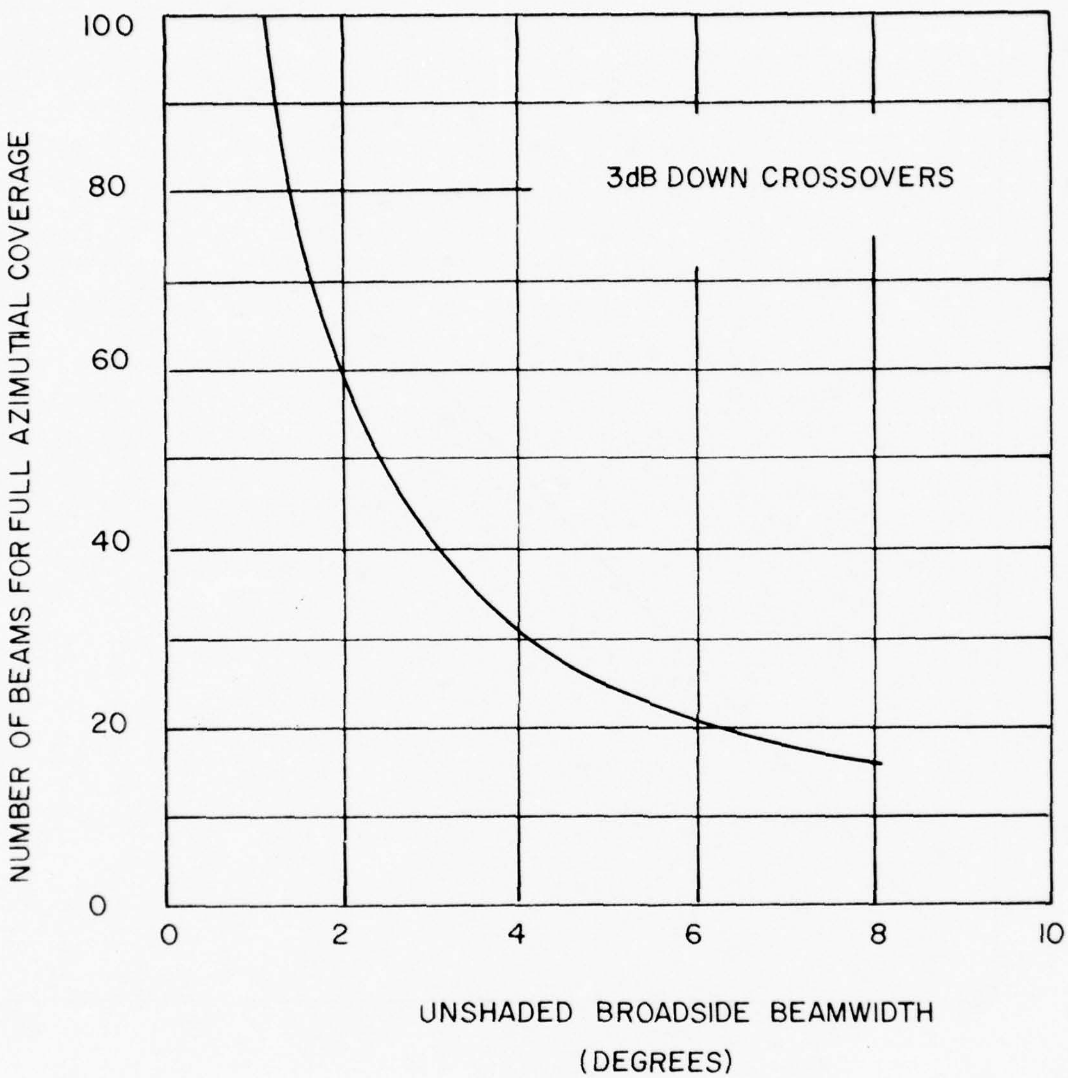

NUMBER OF BEAMS NECESSARY FOR 360° COVERAGE
GIVEN THE BROADSIDE BEAMWIDTH

FIGURE 4-12

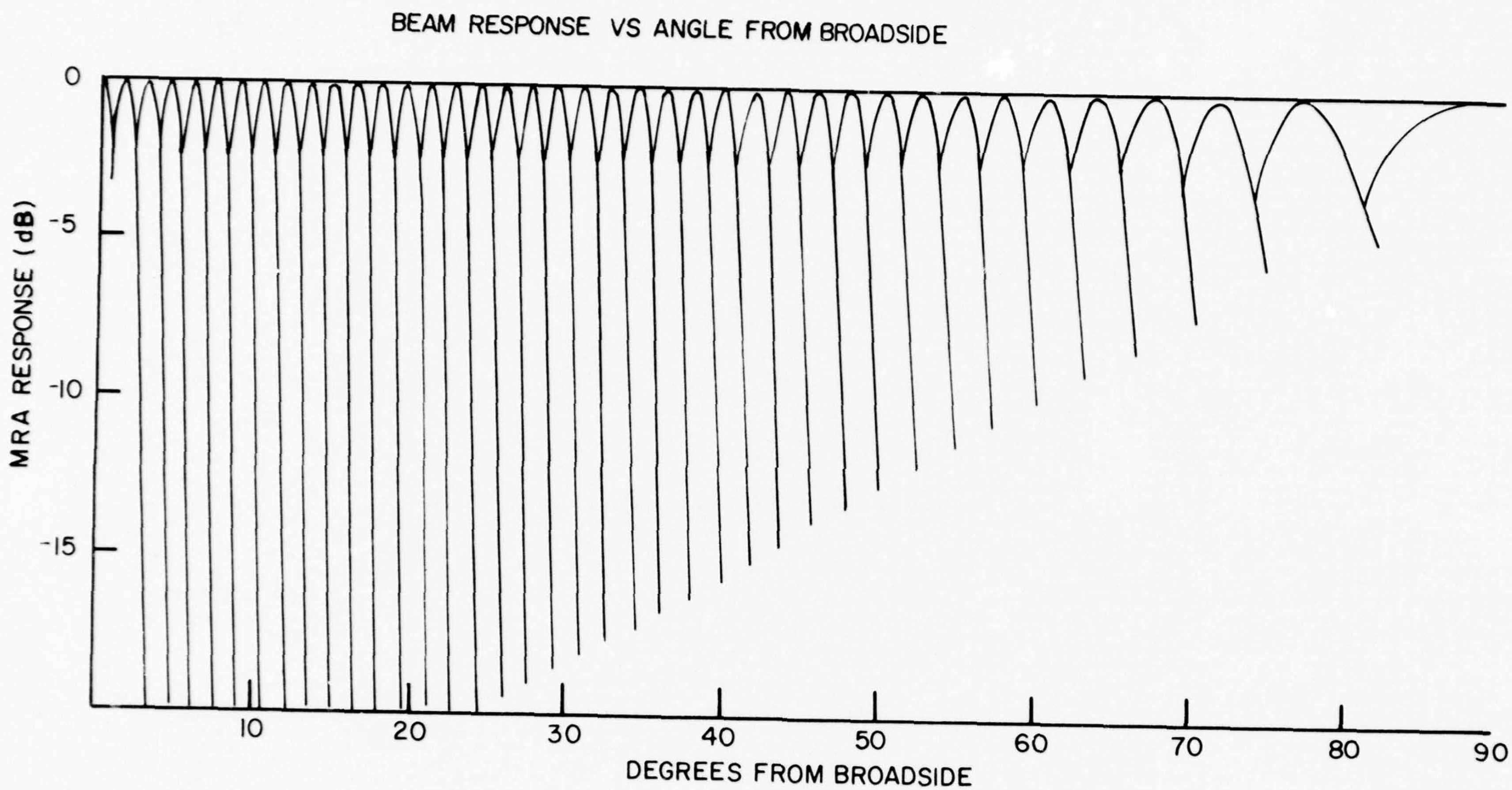
BEAM RESPONSE VS ANGLE FROM BROADSIDE
MRA RESPONSE (dB)
0
-5
-10
-15
10
20
30
40
50
60
70
80
90
DEGREES FROM BROADSIDE

FIGURE 4-13

THIS PAGE INTENTIONALLY LEFT BLANK.

4.6 Shading of Arrays

4.6.1 Amplitude Shading

4.6.1.1 Definition and Examples

- In this section we shall discuss only the amplitude shading of arrays although phase shading is also employed in underwater sound. With phase shading the spacing of the array elements is frequently varied or made nonuniform in order to obtain the desired beampattern. This will be discussed in a subsequent section as will super-directivity or supergain which is a more extreme form of shading.

- Several examples of array amplitude shading have already been given. In Section 4.2.5, we discussed the beampattern of an array whose elements were all in phase but whose amplitudes of excitation decreased uniformly from the central element to the ends. We also discussed a form of amplitude shading (binomial distribution) which resulted in a beampattern that had no sidelobes. The amplitude shading of an array is generally accomplished by adjusting the individual element sensitivities. Nearly always, the sensitivities are tapered from a high value at the central element to lower values at the ends. In this way, the level of the sidelobes are reduced although, as we have seen, the main beam will broaden. It will soon become apparent that the price paid for sidelobe reduction is beambroadening.

- The effects of adjusting the amplitude response or sensitivities of array elements is demonstrated in Figure 4-14 where the beampatterns of a six-element array, shaded in different ways, are shown. For comparison purposes, the beampattern of the unshaded array whose shading or element response formula is (1,1,1,1,1,1) is also shown. It is apparent that the effect of tapering from the array center outward

(0,0,1,1,0,0) is to widen the main beam and to reduce the sidelobes. The effect of the reverse tapering (1,0,0,0,0,1), which is not shown, is to narrow the main beam and increase the sidelobes. Binomial shading, with sensitivities proportional to the coefficients in a binomial expansion (0.1,0.5,1,1,0.5,0.1) provides the narrowest main beam for the condition of zero sidelobes. Dolph-Chebyshev shading (0.30, 0.69, 1,1, 0.69, 0.30) yields the narrowest main beam for a given or preassigned sidelobe level.

4.6.1.2 Dolph-Chebyshev Shading

- It was shown earlier that with a uniform amplitude distribution the sidelobes become successively lower as one considers angles further removed from the main beam. However, if all regions of space outside the main beam are equally important in which to have sidelobe reduction, then it follows that an improved shading technique should be one where all sidelobes have the same height. Dolph developed such a technique, using Chebyshev polynomials, which also optimizes beampatterns *so that (a), for any* specified sidelobe level the narrowest possible main beam is achieved; or (b), for any specified main beam width, the lowest possible sidelobe level is achieved.

- Dolph was aware of Schelkunoff's formulation of arrays as polynomials (See Section 4.3) and he also noticed the interesting properties of Chebyshev polynomials. The expression

$$T_n(z) = \cos nu ,$$

where

$$z = \cos u,$$

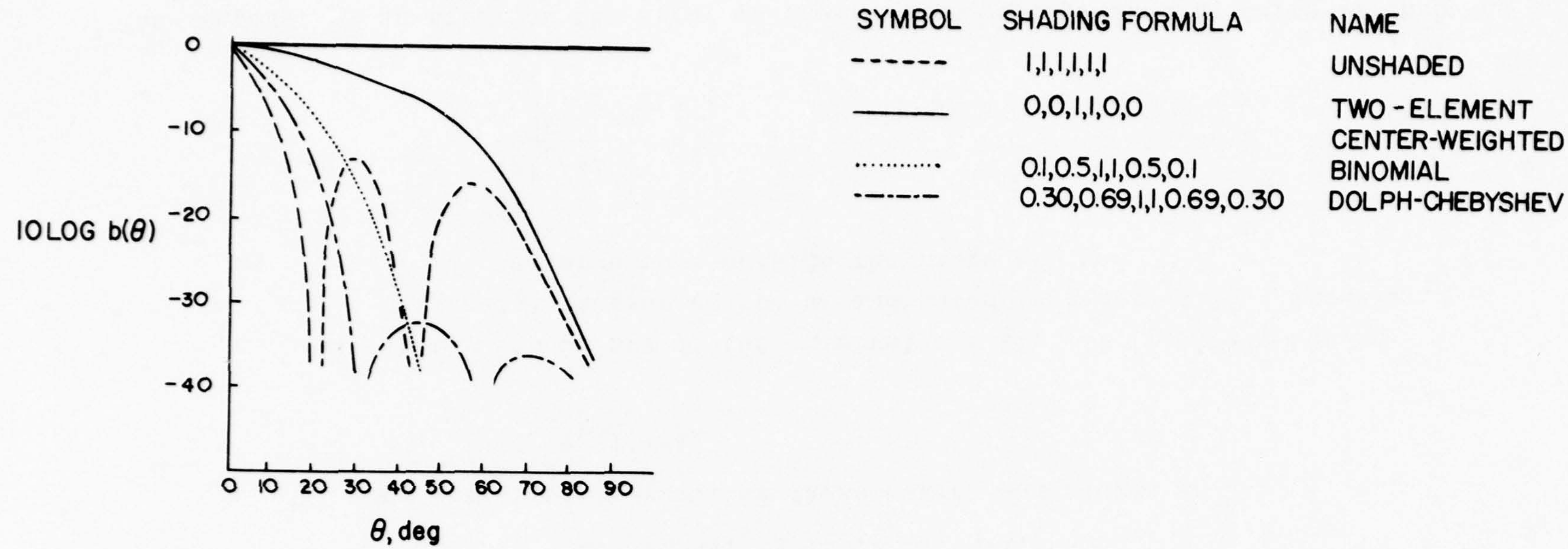

BEAM PATTERN OF A SIX-ELEMENT LINE ARRAY WITH HALF-WAVE SPACING AND DIFFERENT SHADING FORMULAE.

FIGURE 4-14

uniquely defines polynomials of the n^{th} degree which are known as Chebyshev polynomials; $T_o = 1$, $T_1 = z$, $T_2 = (2z^2-1)$, $T_3 = (4z^3-3z)$, $\ldots T_n(z)$. All Chebyshev polynomials have the following important properties:

(1) $T_n(z) = (1/2z)\,[T_{n+1}(z) + T_{n-1}(z)]$,

(2) The n roots of $T_n(z)$ are real and lie between -1 and +1,

(3) Maxima and minima occur alternately at

$$z_k = \cos(k\pi/n), \quad k=1,2,3 \ldots n-1,$$

and the absolute value of these maxima and minima is

$$|T_n(z_k)| = 1,$$

(4) At the end points of the interval $z = \pm 1$, $|T_n(\pm 1)| = 1$, but no horizontal tangent exists as indicated in Figure 4-15. Actually, $|T_n| > 1$ for arguments outside the range ± 1, and

$$\left|\frac{dT_n(z)}{dz}\right|_{z = \pm 1} = n^2 \quad .$$

The response of an array or the array polynomial may be expressed in terms of Chebyshev polynomials.

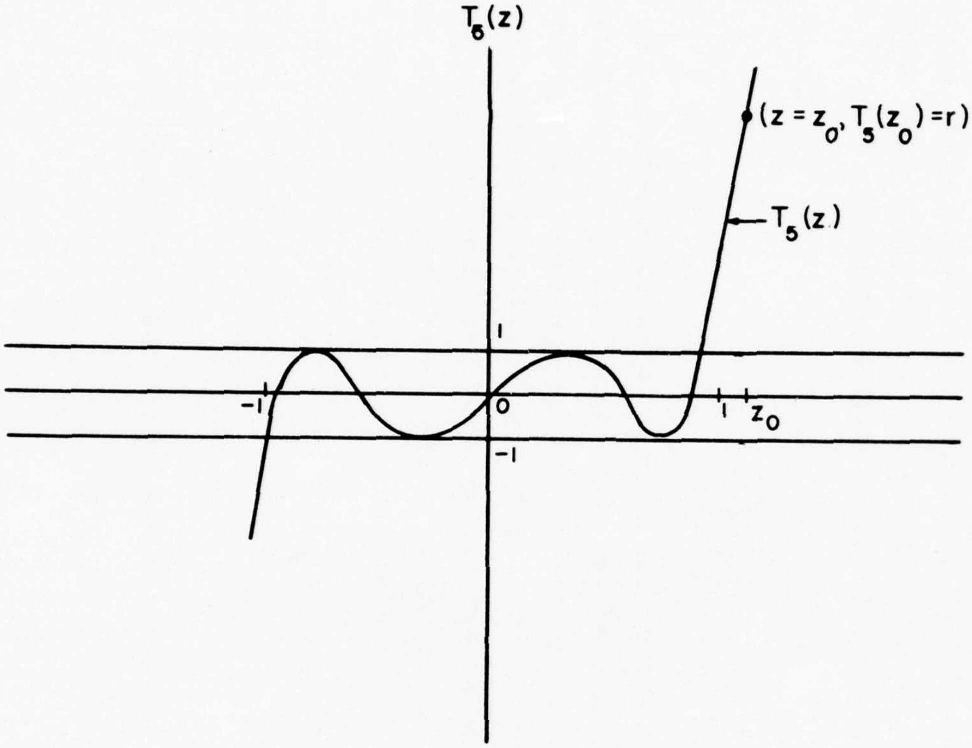

FIFTH TSCHEBYSCHEF POLYNOMIAL SHOWING RELATIONSHIP BETWEEN THE RATIO r AND PARAMETER z_0

FIGURE 4-15

- In the Dolph-Chebyshev method, the response or polynomial of an N-element array is set equal to the Chebyshev polynomial of like degree (i.e. N-1) so that the array coefficients (coefficients of z) can be equated to the corresponding coefficients of the Chebyshev polynomial. In this way, the proper amplitude shading of the elements can be obtained in order to produce the desired far-field amplitude pattern. First, however, the main beam amplitude is selected which corresponds to the value of $T_n(z_o)$ where $z_o > 1$ (See Fig. 4-15). The minor lobe amplitude(s) are numerically equal to the interior ($-1<z<1$) maxima or minima (i.e., $|T_n(z_k)|$) of $T_n(z)$*. The amplitude ratio

$$\frac{\text{Main beam amplitude}}{\text{Minor lobe amplitude}} = r,$$

which can be made as large as desired, can then be used to determine the value of z_o. That is, $T_n(z_o) = r$ can be solved for z_o. Only when z_o is known can the coefficients of the array response or polynomial be equated to the proper Chebyshev-polynomial. The reason for this is that it is necessary to introduce a scale change from z to zz_o in the independent variable of the Chebyshev polynomial, since z itself cannot exceed unity (i.e. $z \equiv \cos nu$). The coefficients of z in the array response are then equated with the coefficients of zz_o in the Chebyshev polynomial, $T_n(zz_o)$.

* Note, that this means that all minor lobe levels are equal and correspond to the value of unity since $|T_n(z_k)| = 1$.

4.6.1.3 Example of Dolph-Chebyshev Shading

- A Dolph-Chebyshev shaded aperture distribution, for a given number of array elements, is completely specified by the design sidelobe (power) level, 20 log r.

- To illustrate the Dolph-Chebyshev method of shading, consider the design of a six-element array (N-1=5) and require that the minor lobe (power) level be 30 dB below the main beam level. Thus, taking 20 log of the main to minor lobe amplitudes ratio r, we get

$$20 \log r = 30$$

or,

$$r = 31.6.$$

The value of z_o can then be determined from

$$T_5(z_o) = r,$$

which is a fifth degree polynomial in z_o. Dolph, however, has shown that z_o can be calculated more easily for large values of r (which is usually the case) from the approximate expression

$$z_o = (1/2)\ [2(r)^{1/n} + 1/(2r)^{1/n}],$$

where n = N-1.

Thus, for the present case of n=5 and r=31.6, we find that

$$z_o = 1.35.$$

The final step is to calculate the amplitude shading coefficients. We shall first,

a

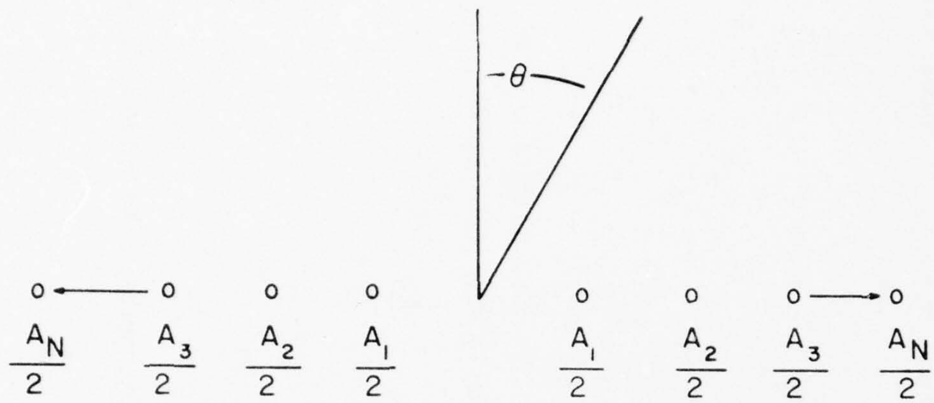

$$V = A_1 \cos u + A_2 \cos 3u + A_3 \cos 5u + \cdots A_{(N/2)} \cos (N-1)u$$

WHERE $u = (\pi d/\lambda)\sin\theta$

b

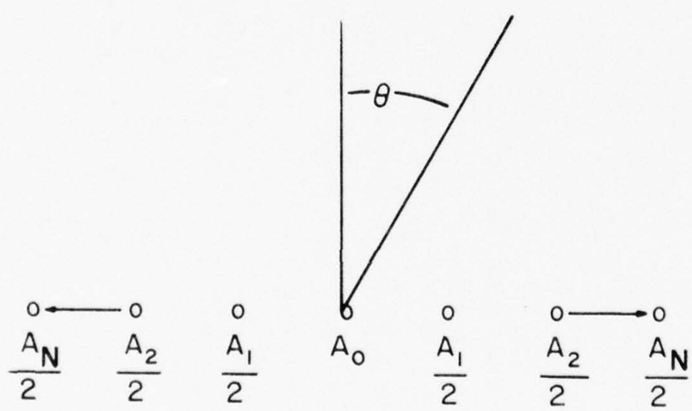

$$V = A_0 + A_1 \cos 2u + A_2 \cos 4u \cdots A_{(N-1)/2} \cos (N-1)u$$

WHERE $u = (\pi d/\lambda)\sin\theta$

SYMBOLS FOR EQUALLY SPACED LINE ARRAYS OF POINT ELEMENTS
a) EVEN NUMBER OF ELEMENTS b) ODD NUMBER OF ELEMENTS.

FIGURE 4-16

however, express the response of the six-element array in the form

$$V=A_1\cos u+A_2\cos 3u+A_3\cos 5u \ ,$$

where $u = \pi(d/\lambda)\sin\theta$, d is the element spacing and θ is the azimuthal angle measured from array broadside (See Fig. 4-16). Substituting z for cosu in the response V yields the array polynomial

$$V = f(z) = A_1 z+A_2(4z^3-3z)+A_3(16z^5-20z^3+5z)$$

or, collecting terms in like powers of z,

$$V = f(z) = 16A_3 z^5+(4A_2-20A_3)z^3+(A_1-3A_2+5A_3)z.$$

The Chebyshev polynomial of the fifth (n=5) degree written in terms of the variable $z_o z$ is

$$T_5(z_o z) = 16z_o^5 z^5-20z_o^3 z^3+5z_o z.$$

Thus, equating the coefficients of like powers in this expression to those in the last expression for the array polynomial f(z) gives

$$16A_3 = 16z_o^5$$
$$4A_2-20A_3 =-20z_o^3$$
$$A_1-3A_2+5A_3 = 5z_o$$

or,

$$A_3 = z_o^5$$

$$A_2 = 5z_o^5 - 5z_o^3$$

$$A_1 = 10z_o^5 - 15z_o^3 + 5z_o \ .$$

Since z_o was found to be $z_o = 1.35$, then $A_3 = 4.66$, $A_2 = 10.70$ and $A_1 = 15.60$. Expressing these weighting coefficients in normalized form by dividing all three by $A_1 = 15.60$ we get

$$A_1 = 1.000$$

$$A_2 = 0.685$$

$$A_3 = 0.298.$$

Thus, shading a six-element array so that the weighting coefficients have the values

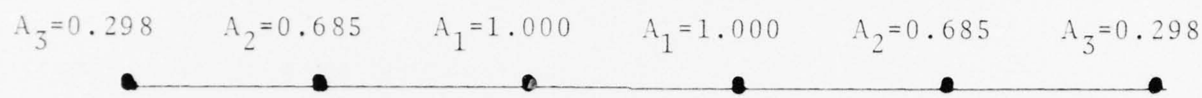

achieves the narrowest possible main beam for the specified sidelobe level of 30 dB below the main beam level. By inserting these coefficient values into the array polynomial (or voltage response, etc.) given above, one can calculate the resulting beam pattern $b(\theta) = |f(z)|^2 = |V|^2$.

- Two other examples of the weighting coefficients required for two specified side-lobe levels of a Dolph-Chebyshev shaded, N=100 element array are given in Table 4-3 of section 4.6.1.5.

4.6.1.4 Binomial Shading

- It is of value to examine the Chebyshev shading coefficients obtained above at two extremes. The first extreme is of no great interest but occurs as z_o approaches unity resulting, as expected, in a main beam whose level is equal to the sidelobe level. In this case, the Chebyshev coefficients reduce to $A_3=1$ and $A_2=A_1=0$ or (1,0,0,0,0,1) which, as we saw in Section 4.6.1.1, is just the two-element end-weighted or reverse tapered array.

- The second and more interesting extreme occurs as z_o approaches infinity and is most conveniently examined by first normalizing the coefficient expressions in the previous section by the coefficient A_3 so that

$$A_3/A_3=1,$$

$$A_2/A_3=5-5/z_o^2,$$

and,

$$A_1/A_3=10-15/z_o^2+5/z_o^4 .$$

As z_o approaches infinity, these normalized Chebyshev coefficients take on the values 1, 5, 10 (i.e., 1, 5, 10, 10, 5, 1). As we saw previously (Fig. 4-14), these are just the binomial shading coefficients for which the beampattern has no sidelobes. Thus, binomial shading can be considered a special case of Dolph-Chebyshev shading.

4.6.1.5 Taylor Shading

- It has been shown that as the number of elements N in a Dolph-Chebyshev array is increased, the beampattern becomes very sensitive to small changes in the end element excitations. This establishes a practical upper limit to the number of elements that can be used in a Dolph-Chebyshev array and therefore a lower limit (See also Section 4.6.2.3) to the main beamwidth. As the number of elements approaches infinity, the voltage response of a Dolph-Chebyshev array becomes

$$V(\theta) = \begin{cases} \cos\pi(u^2-A^2)^{1/2} & A^2<u^2 \\ \cosh\pi(A^2-u^2)^{1/2} & A^2>u^2 \end{cases}$$

where, $u = (L/\lambda)\sin\theta$,

L = the array length,

θ = angle measured from the array normal, and

A is a constant related to the sidelobe level 20 log r(Section 4.6.1.3) by $\cosh\pi A=r$.

The main lobe of this pattern occurs in the region $u^2<A^2$ and an infinite number of equal sidelobes appear in the region $u^2>A^2$. Unfortunately, this ideal* pattern is not physically realizable because the required aperture distribution contains infinite peaks at the end elements of the array.

---

*The term "ideal" is apparently used in the literature in the same sense that the term "optimum" is used. That is, the Dolph-Chebyshev pattern is "optimum" or "ideal" in that it offers the narrowest main beamwidth of all constant phase aperture distributions with sidelobes at or below some specified level.

- Taylor showed that it is possible to approximate this ideal pattern with a physically realizable aperture distribution. The beam pattern produced by this Taylor distribution has uniform sidelobes like the Dolph-Chebyshev pattern but only in the vicinity of the main beam. Unlike the Dolph-Chebyshev pattern, however, the sidelobes of the Taylor pattern decrease outside of some specified angular region. For long arrays ($L/\lambda \gg 1$), the region in which the sidelobe level is uniform is given by

$$|(L/\lambda)\sin\theta| < \bar{n}$$

and the region where the sidelobe level decreases with increasing θ is given by

$$|(L/\lambda)\sin\theta| > \bar{n} ,$$

where $\bar{n}$ is a finite integer. Thus, $\pm\,\bar{n}$ divides the Taylor beam pattern into a region including the main beam surrounded by uniform sidelobes and a decaying sidelobe region.

- The Taylor aperture distribution for a given number of array elements N in a long array is specified by the design sidelobe (power) level 20 log r (or A, through the relation $\cosh \pi A = r$) and the value of $\bar{n}$. Two examples of the amplitude weighting coefficients required for $\bar{n}=10$ with the two sidelobe levels of 35 and 40 dB are given in Table 4-3. The coefficients are only given for half the elements in an N=100 element array (beginning with the center elements) since, similar to Dolph-Chebyshev shading, Taylor shading is symmetric. The Dolph-Chebyshev weighting coefficients, which are specified by the sidelobe level only, are also given. Similar comparisons are provided for an N=50 element array in Figure 4-17(a) on page 86.

- In selecting a value of $\bar{n}$ for Taylor shading, values that are too small must be avoided. For a design sidelobe level of 25 dB, $\bar{n}$ must be at least 3 and for a design sidelobe

level of 40 dB, $\bar{n}$ must be at least 6. The larger the value of $\bar{n}$ the narrower the beam. But, if $\bar{n}$ is too large the same difficulties will arise as with Dolph-Chebyshev shading since, for high values of $\bar{n}$, Taylor aperture distributions will also peak at the ends of the aperture. For a given design sidelobe level, Table 4-4 can be used as a guide in the selection of $\bar{n}$. As we shall see shortly (Section 4.6.2.3), the values of the parameter σ in Table 4-4 directly affect the main beamwidth of the Taylor pattern.

4.6.1.6 Cosine-On-Pedestal Shading

Another form of shading that can drastically reduce sidelobes is cosine-on-pedestal shading where the weighting coefficient of the m^{th} array element has the general form

$$A_m = 1 + 2(a_1/a_o)\cos(2\pi m/2M+1) .$$

Here, $N=2M+1$ is the total number of array elements and m takes on the values $-M$ through M. It should be apparent from this expression that cosine-on-pedestal refers to the superposition of a cosine element excitation pattern onto a uniform pattern. The parameter a_1 can be adjusted over the span $0 \le 2a_1 \le a_o$* which extends from the case of uniform element excitation (i.e. $a_1=0$) to that of a severe taper (i.e. $2a_1=a_o$) from the array center outwards such that the excitation at the end elements A_M and A_{-M} drops to zero. In order to see the latter case more clearly, note that when $m=M$ in the expression for A_m, the argument of the cosine approaches π (and $\cos\pi=-1$) for large element numbers M.

---

*The parameters a_o and a_1 actually arise by representing the current amplitude I_m in the m^{th} element of the array by the first two terms of a Fourier series expansion whose respective amplitudes are a_o and $2a_1$. The element weighting coefficient a_m is then just the normalized current amplitude, $a_m = I_m/a_o$.

TABLE 4-3(a)

Amplitude Shading Coefficients

N=100

S.L.L.=-20 log r = -35 dB

DOLPH	TAYLOR ($\bar{n}$ = 10)
1.00000	1.00000
.99864	.99867
.99594	.99598
.99189	.99186
.98651	.98628
.97981	.97920
.97183	.97065
.96259	.96070
.95211	.94945
.94043	.93700
.92760	.92346
.91364	.90886
.89861	.89322
.88255	.87652
.86552	.85874
.84756	.83987
.82874	.81998
.80911	.79917
.78874	.77759
.76768	.75540
.74601	.73276
.72378	.70975
.70106	.68639
.67792	.66265
.65443	.63848
.63065	.61385
.60665	.58881
.58249	.56347
.55825	.53805
.53398	.51279

TABLE 4-3(a)(Con't.)

DOLPH	TAYLOR ($\bar{n}$ = 10)
.50975	.48793
.48562	.46359
.46166	.43979
.43791	.41639
.41445	.39316
.39131	.36984
.36856	.34629
.34623	.32259
.32439	.29907
.30306	.27636
.28230	.25529
.26211	.23677
.24258	.22159
.22368	.21024
.20549	.20280
.18798	.19890
.17124	.19772
.15519	.19823
.13998	.19933
.62212	20013

TABLE 4-3(b)

Amplitude Shading Coefficients

N=100

S.L.L. = -20 log r = -40 dB

DOLPH	TAYLOR ($\bar{n}$ = 10)
1.00000	1.00000
.99842	.99838
.99525	.99513
.99053	.99023
.98425	.98368
.97645	.97548
.96717	.96568
.95642	.95432
.94426	.94148
.93074	.92724
.91590	.91168
.89980	.89487
.88250	.87685
.86408	.85767
.84459	.83737
.82411	.81600
.80272	.79365
.78049	.77040
.75751	.74640
.73385	.72176
.70961	.69661
.68486	.67106
.65969	.64517
.63418	.61899
.60843	.59255
.58250	.56592
.55650	.53915
.53048	.51236

TABLE 4-3(b) (Cont'd.)

DOLPH	TAYLOR ($\bar{n}$ = 10)
.50455	.48567
.47877	.45926
.45323	.43327
.42797	.40780
.40309	.38292
.37864	.35860
.35469	.33479
.33129	.31142
.30849	.28844
.28634	.26590
.26490	.24393
.24418	.22282
.22425	.20292
.20510	.18467
.18680	.16845
.16933	.15457
.15275	.14319
.13702	.13431
.12220	.12776
.10823	.12325
.09520	.12047
.33631	.11916

Sidelobe Level (dB)	Sidelobe Amplitude Ratio (r)	B_o (rad)	A^2	σ Values							
				$\bar{n} = 3$	$\bar{n} = 4$	$\bar{n} = 5$	$\bar{n} = 6$	$\bar{n} = 7$	$\bar{n} = 8$	$\bar{n} = 9$	$\bar{n} = 10$
20	10.00	0.893	0.9077	1.1213	1.1027	1.0870	1.0749				
25	17.78	0.978	1.2917	1.0924	1.0869	1.0772	1.0683	1.0608	1.0546		
30	31.62	1.057	1.7422		1.0693	1.0661	1.0607	1.0553	1.0505	1.0462	1.0426
35	56.23	1.131	2.2597			1.0538	1.0523	1.0492	1.0458	1.0426	1.0397
40	100.0	1.200	2.8442				1.0429	1.0424	1.0406	1.0385	1.0364

TABLE 4-4 TAYLOR SHADING PARAMETERS

- The sidelobes of the radiation pattern resulting from a cosine-on-pedestal excitation becomes successively lower as one departs in either direction from the main beam. However, if the sidelobe level (S.L.) is defined as the ratio of the height of the largest sidelobe to that of the main beam, then it can be shown that for the range $0 \leq 2a_1/a_o \leq 0.83$, the sidelobe level (S.L.) is approximately

$$S.L(dB) \simeq -[13+15(2a_1/a_o)+22(2a_1/a_o)^2] .$$

Note that for the case of uniform excitation ($a_1=0$), this expression reduces to the expected value of approximately -13 dB.

4.6.2 Beamwidths and Beam Broadening Factors

4.6.2.1 Uniform Shading

- We saw in Section 4.4.2 that the half power or -3 dB down beamwidth for an unshaded line array of length L is given approximately (for $L \gg \lambda$) by

$$BW_3 = 0.886\ (\lambda/L)\sec\theta_o .$$

In this expression, θ_o is the scanning angle which is measured from array broadside* and the expression is quite accurate for scanning to within two beamwidths of end-fire ($\theta_o = \pm\pi/2$). Although the term $\sec\theta_o$ represents a broadening of the beam as it is scanned from broadside to endfire, there is , of course, no connection between this broadening and any shading of array elements.

* Note that if θ_o were measured from the line of the array, the $\sec\theta_o$ term would be a $\csc\theta_o$.

4.6.2.2 Dolph-Chebyshev Shading

- The half-power or -3 dB down beamwidth of a Chebyshev shaded line array of length L is given approximately by

$$BW_3 = [0.886(\lambda/L)\sec\theta_o]f$$

where the beam broadening factor* f, in this case, is

$$f = 1+0.636\{(2/r)\cosh[(\text{arccosh}\,r)^2-\pi^2]^{1/2}\}^2.$$

The parameter r in this expression for f was discussed earlier (Section 4.6.1.2) and is the main beam to sidelobe voltage or amplitude ratio. For example, if we require the minor-lobe level to be 30 dB below the major-lobe level, then 20 log r = 30 dB. The beam broadening factor f versus sidelobe level for Chebyshev shading is plotted in Figure 4-17(b).

- It is apparent from Figure 4-17(b) that, for a given amount of beam broadening, a Chebyshev distribution is capable of providing a lower sidelobe level than a cosine-on-pedestal distribution. Moreover, for a line array of any length, with the main beam pointing in any direction, the correct beamwidth for a Chebyshev pattern can be determined by reading the beamwidth from Figure 4-9 (Section 4.4.2) and then multiplying by the appropriate f value obtained from Figure 4-17(b). The same procedure can also be applied to find the correct beamwidth for a Taylor or a cosine-on-pedestal distribution as discussed in the following two sections.

---

* f can be considered as the ratio of the beamwidth BW_3 of a shaded array to that of the equivalent unshaded (i.e. uniformly illuminated) array.

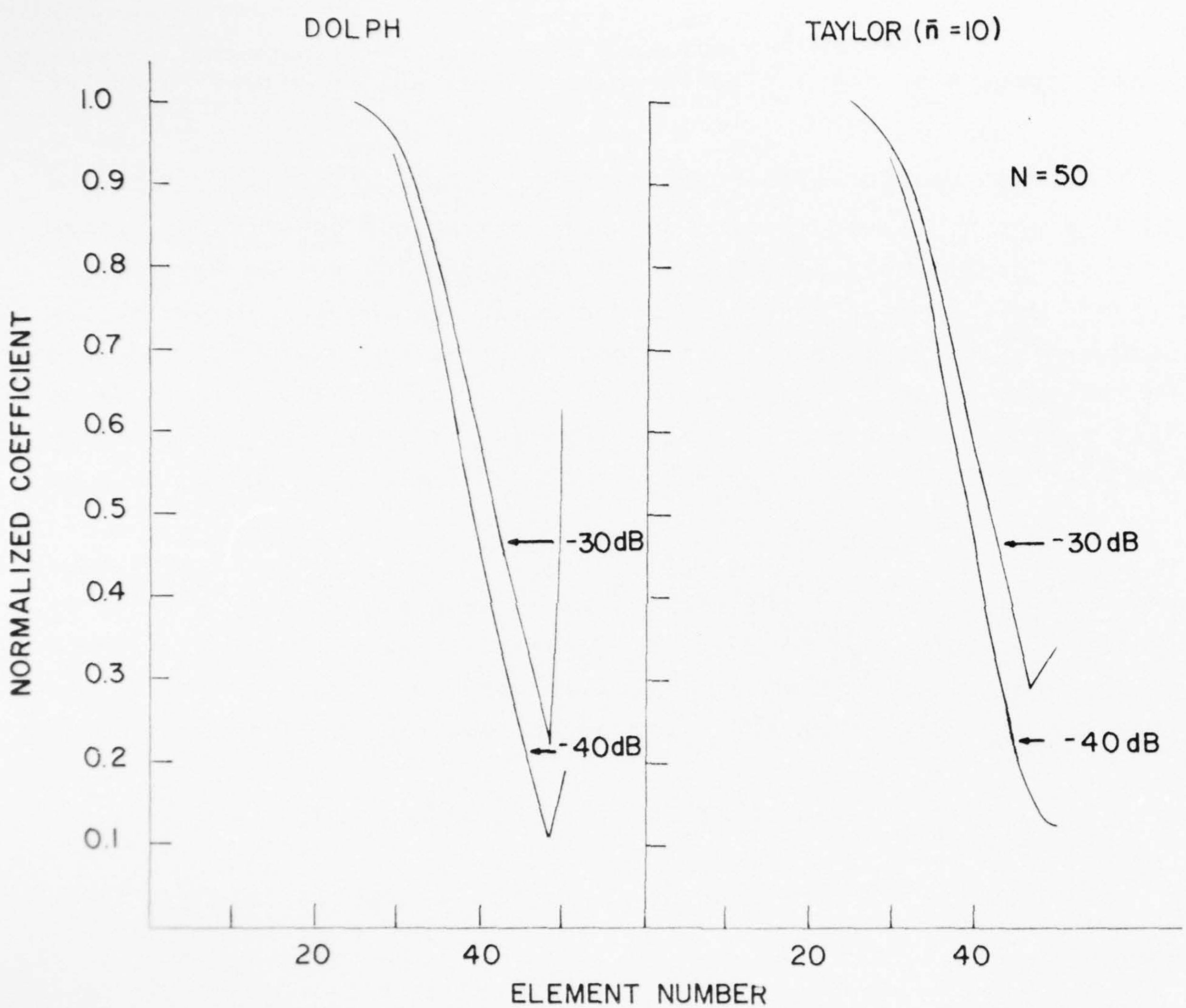

NORMALIZED AMPLITUDE COEFFICIENTS FOR AN N=50 ELEMENT ARRAY WITH DOLPH-CHEBYSHEV AND TAYLOR SHADING. THE SIDELOBE LEVELS ARE SPECIFIED.

FIGURE 4-17(a)

AD-A038 073 APPLIED HYDRO-ACOUSTICS RESEARCH INC ROCKVILLE MD F/G 17/1

HANDBOOK OF ARRAY DESIGN TECHNOLOGY. VOLUME I.(U)

JUN 76 N00039-76-C-0015

UNCLASSIFIED NL

2 OF 3

ADA038073

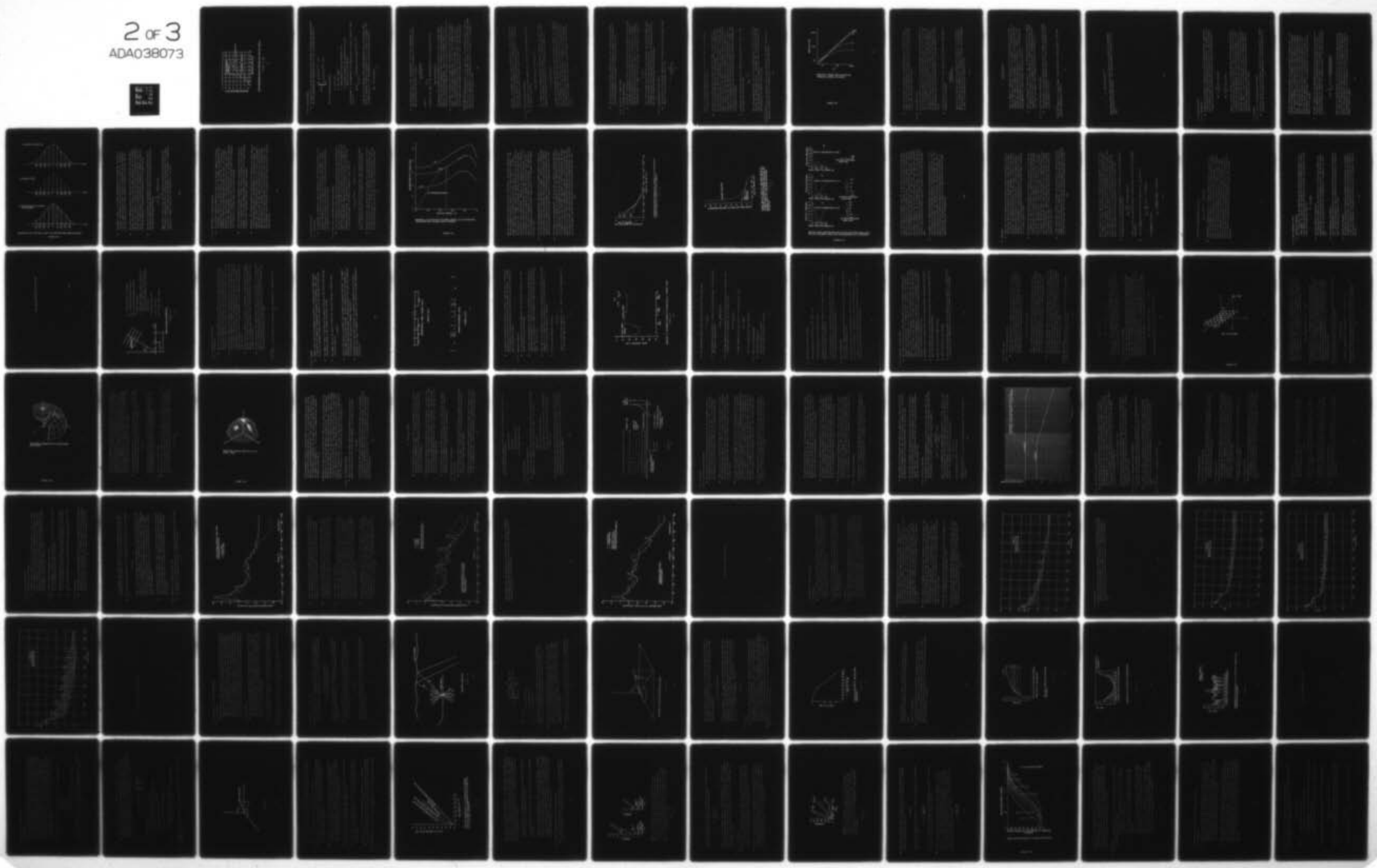

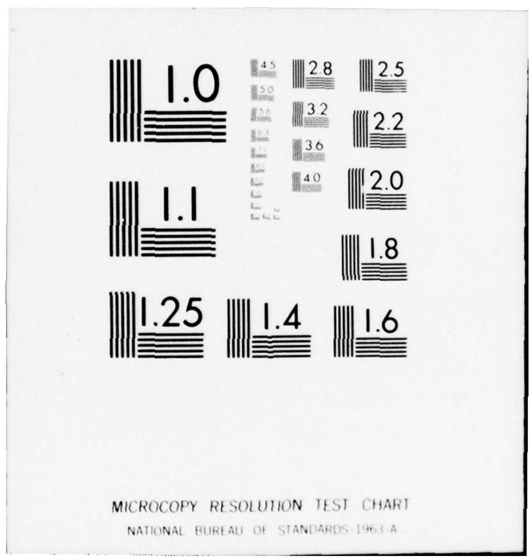
1.0
1.1
1.25
1.4
1.6
1.8
2.0
2.2
2.5
2.8
3.2
3.6
4.0
4.5
5.0
5.6
MICROCOPY RESOLUTION TEST CHART
NATIONAL BUREAU OF STANDARDS-1963-A

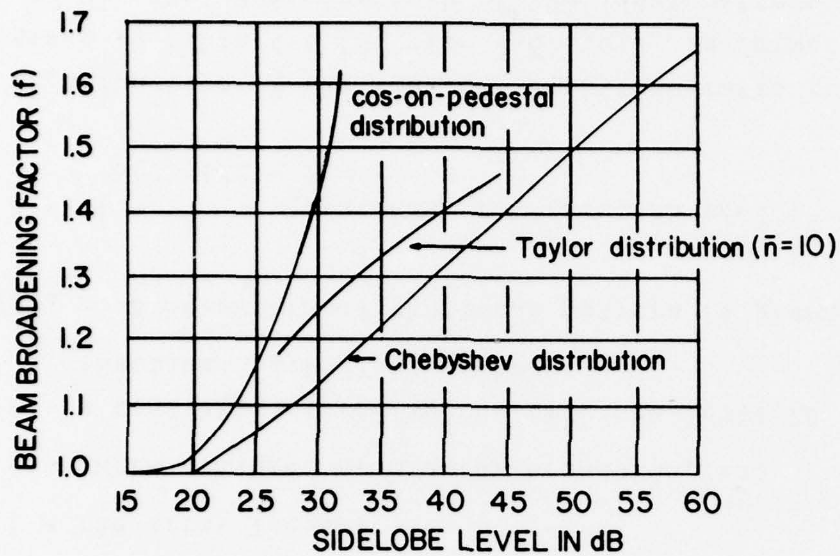

BEAM BROADENING VERSUS SIDELOBE LEVEL FOR LINE ARRAYS

FIGURE 4-17 (b)

4.6.2.3 Taylor Shading

- In section 4.6.1.5 we discussed the Taylor aperture distribution for approximating the ideal Dolph-Chebyshev beampattern which is given (in normalized form) by

$$b(\theta)=\begin{cases}\frac{1}{r^2}\cos^2\pi(u^2-A^2)^{1/2} & A^2<u^2\\ \frac{1}{r^2}\cosh^2\pi(A^2-u^2)^{1/2} & A^2>u^2\end{cases}.$$

Here, as indicated previously,

$u = (L/\lambda)\sin\theta$,

L = the array length,

θ = angle measured from array broadside, and

A = a constant related to the sidelobe level 20 log r (Section 4.6.1.3) by $\cosh\pi A=r$.

The half-power or -3dB beamwidth of the ideal pattern is given in terms of u (and not θ) by

$$B_o=2u\Big|_{b(\theta)=1/2}=\frac{2}{\pi}\left[(\operatorname{arccosh} r)^2-(\operatorname{arccosh} r/\sqrt{2})^2\right]^{1/2}.$$

Values for B_o as a function of the sidelobe amplitude ratio r or sidelobe level, 20 log r, are given in Table 4-4 (Section 4.6.1.6). In terms of the angle θ (See the definition of u), the -3dB beamwidth of the ideal pattern is given by

$$BW_3= 2\arcsin(\lambda B_o/2L).$$

- For long arrays ($L/\lambda >> 1$) the -3dB beamwidth B of the Taylor approximate (i.e., Taylor shaded) pattern will, in terms of the quantity u, be broader than that of the ideal pattern by the factor σ, where

$$\sigma = \frac{\bar{n}}{[A^2+(\bar{n}-1/2)^2]^{1/2}}.$$

  That is,

$$B \simeq \sigma B_o.$$

  In terms of the angle θ, the -3dB beamwidth of the Taylor pattern will be

$$BW_3 = 2\arcsin(\lambda\sigma B_o/2L).$$

  The quantity $\bar{n}$ has already been defined in Section 4.6.1.5 as an integer whose value divides the Taylor beampattern into a region of uniform sidelobes and main beam and a decaying sidelobe region. Values for the broadening factor* σ as a function of the design sidelobe level and $\bar{n}$ are given in Table 4-4 (Section 4.6.1.5).

- As indicated in Section 4.6.1.5, the Taylor distribution is specified by two parameters. They are the design sidelobe level, 20 log r, and the integer $\bar{n}$ defined above. The selected value of $\bar{n}$ should not be too small (i.e., use the values listed in Table 4-4 of Section 4.6.1.5). On the other hand, $\bar{n}$ does not have to be very large in order to make the broadening factor σ only a few percent greater

---

* Note that the broadening factor σ is not equivalent to the broadening factor f used in Sections 4.6.2.2 or 4.6.2.4. It can be shown, however, in the case of long Taylor shaded arrays that the approximation $f=\sigma B_o/0.886$ (see Table 4-4), where B_o is in radians, is quite accurate (see Figure 4-17(b)).

than unity. For example, given a design sidelobe level of 25 dB, a Taylor distribution with $\bar{n}=5$ gives a beamwidth only about 7.7% greater than the optimum produced by the ideal but unattainable Dolph-Chebyshev distribution. A value of $\bar{n}=8$ gives a beamwidth of about 5.5% greater than the optimum.

4.6.2.4 Cosine-On-Pedestal Shading

- The half-power or 3 dB down beamwidth for a cosine-on-pedestal shaded line array of length L is given by

$$BW_3=0.886(\lambda/L)\sec\theta_o[1+0.636(2a_1/a_o)^2].$$

This expression is an approximation for long arrays scanned not too close to endfire. The parameters a_1 and a_o, where $0\leq 2a_1\leq a_o$, are related to the array element excitation distribution (Section 4.6.1.4). The quantity in brackets, or

$$f = [1+0.636(2a_1/a_o)^2],$$

is called the beam broadening factor for cosine-on-pedestal shading. It is apparent that when $a_1=0$, f becomes unity and the beamwidth BW_3 reduces to that of a uniform (i.e., *no shading*) array. However, when severe shading is used to achieve drastic sidelobe reduction, as with the case $2a_1=a_o$ for example, it is apparent that the main beamwidth BW_3 will broaden significantly. A graph of the beam broadening factor f versus sidelobe level for cosine-on-pedestal shading is given in Figure 4-17 (b).

- For a line array of any length scanned not too close to endfire, the beamwidth of a cosine-on-pedestal pattern can be determined by reading it from Figure 4-9 and then multiplying by the appropriate f value obtained from 4-17(b).

4.6.3 Directivity of Shaded Arrays

4.6.3.1 Uniformly Shaded Arrays

- Directivity is defined as ratio of the power per unit solid angle in the direction of the main beam maximum to the average total power of the array. A general expression for directivity is given in Section 3.2. In Section 4.2.4 we showed that the directivity D or the directivity index (D.I. = 10 log D) of a uniformly illuminated array of length L with half-wavelength element spacing is given by

$$D = 2L/\lambda .$$

This is the maximum directivity that can be obtained from a half-wavelength spaced line array of length L and uniform progressive phase. In other words, for half-wavelength spacing, uniform amplitude shading provides the maximum directivity of any type of amplitude shading applied with uniform phase.

4.6.3.2 Dolph-Chebyshev Shaded Arrays

- The directivity of a Chebyshev shaded array of length L and half-wavelength element spacing is given approximately for $(L>>\lambda)$ by

$$D = \frac{2r^2}{1+(r^2-1)\,f(\lambda/L)} .$$

Here, f is the beam broadening factor (Section 4.6.2.3) and r is the main beam to sidelobe voltage or amplitude ratio.

- Directivity was defined above in terms of the total power of an array which is the sum of the main beam power and the sidelobe power.* For modest length arrays the main beam power will dominate. However, for those patterns in which the sidelobe levels are all equal (i.e., Dolph-Chebyshev), an increase in the array length beyond a certain point will not result in a corresponding increase in the main beam power. Rather, a limit will eventually be reached as the array length (L/λ) is increased, beyond which any additional power will be directed primarily into the constant level sidelobes and the directivity will remain essentially constant. Such a directivity limit does not occur with uniform or cosine-on-pedestal shading where the sidelobes are tapered.

- To determine the directivity limit for a Chebyshev shaded array, we let $L \to \infty$ in the above expression for D which gives

$$D_{max} = 2r^2 .$$

Thus, the maximum directivity (as $L \to \infty$) of a Chebyshev array is 3 dB (i.e. 10 log 2) more than the sidelobe level 20 log r. This means that if one desires a long line array with uniform sidelobes and a directivity of 63 dB, it will be necessary for the sidelobes to be down by at least 60 dB.

---

* Recall that we are discussing only linear arrays herein where the spatial pattern is independent of whether the array is radiating into or receiving from space.

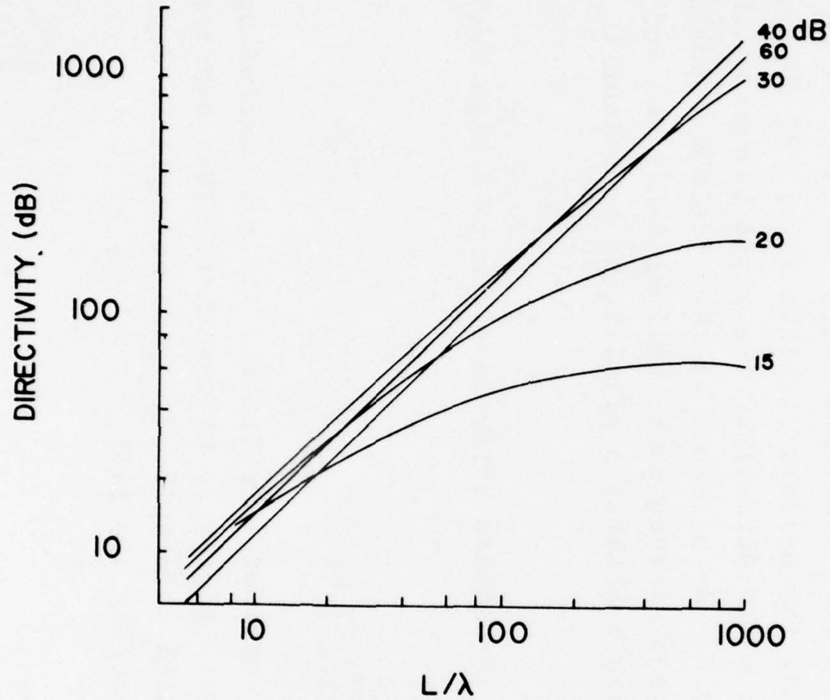

DIRECTIVITY VERSUS ARRAY LENGTH FOR CHEBYSHEV SHADED LINE ARRAYS.

FIGURE 4-18

- As the array length is increased, the maximum directivity is approached rather quickly at first, but any additional directivity is very costly in terms of array length. This can be seen from Figure 4-18 which is a plot of the expression for D given above for several sidelobe levels.

4.6.3.3 Taylor Shaded Arrays

- As we saw in Section 4.6.1.5, the Taylor "approximate" aperture distribution (i.e. Taylor shaded array) does not yield uniform sidelobes only. In fact, it is specified by two parameters, the first being the uniform sidelobe level, 20 log r, and the second being $\bar{n}$, a finite integer which determines the angle beyond which the sidelobes will taper with increasing θ. As a result of the sidelobe tapering, the problem of a directivity limit as discussed above will be minimized and long narrow-beamwidth arrays will be possible without a significant reduction in directivity.

- The directivity of a long ($L \gg \lambda$) Taylor shaded array is given to a high degree of accuracy by the expression

$$D = \frac{(4L/\lambda)r^2}{1.93\ Ar^2 + 2(\bar{n}-1)}$$

where all terms have been previously defined (See Section 4.6.1.5) including, A, which is related to the sidelobe level, 20 log r, by $\cosh \pi A = r$. This expression for the directivity should be used with care however, since no explicit dependance is shown on the broadening factor (Section 4.6.2.3),

$$\sigma = \frac{\bar{n}}{[A^2+(\bar{n}-1/2)^2]^{1/2}} \quad .$$

Thus, it appears as though the directivity D will be maximized for a fixed array length by minimizing the value of $\bar{n}$ which is not correct. It is true that, as $\bar{n}$ is decreased, the number of tapered sidelobes is increased which decreases the total sidelobe power somewhat thereby increasing the directivity . However, σ is no longer approximately unity for small values of $\bar{n}$. Thus, as $\bar{n}$ is decreased, the main beamwidth will increase thereby decreasing directivity.

- Tables are available* which give $\bar{n} = \bar{n}_{max}$ for which the directivity D is a maximum. As a general rule, however, it turns out that the larger the value of $\bar{n}$ for a given sidelobe level (20 log r), the greater the directivity. Regarding the selection of $\bar{n}$ values, the reader is also referred to Sections 4.6.1.5 and 4.6.2.3.

4.6.3.4 Cosine-On-Pedestal Shaded Arrays

- The directivity of a cosine-on-pedestal shaded array of length L and half-wavelength element spacing is again most conveniently given in terms of the parameters a_o and a_1 (See Section 4.6.1.6), or

---

* See, for example, R.C. Hansen (1960b), "Gain Limitations of Large Antennas", IRE Trans. Antennas Propagation 8, 490-495.

$$D = (2L/\lambda)[1+2(a_1/a_o)^2]^{-1} .$$

Since the practical range of a_1/a_o extends from zero to one-half, the corresponding directivity D extends from $2L/\lambda$ (i.e. uniform shading) to two-thirds of this value.

4.7 Pattern Synthesis

4.7.1 Introduction

- In general, the problem of synthesizing a desired radiation pattern is equivalent to the problem of finding a particular aperture distribution. For example, as we saw in Section 3.0, the far-field amplitude pattern $F(u)$ of an antenna of length L is given by the Fourier transform of the antenna aperture distribution $g(p)$, or

$$F(u) = \frac{1}{2\pi} \int_{-\infty}^{\infty} g(p)\ \exp(ipu)\,dp$$

$$g(p) = \int_{-\infty}^{\infty} F(u)\exp(-ipu)\,du\ ,$$

where $u = L/\lambda \sin\theta$, $p = 2\pi x/L$, θ is an angle measured from the antenna normal and x is measured along the antenna $(-L/2 \leq x \leq L/2)$. Thus, for a desired $F(u)$, we need to determine the corresponding $g(p)$ over some finite aperture length, L. Moreover, just as the Fourier integral can be used to synthesize the pattern of a continuous aperture, the Fourier series can be used to synthesize the pattern of a discrete array. In fact, the distributions derived for continuous apertures may be used to approximate discreet aperture distributions when the number of elements of the discrete array is large.

4.7.2 Methods

4.7.2.1 $\sin\pi u/\pi u$ (or Woodward-Lawson) Method

- The Fourier method is only one technique available for pattern synthesis. Another and perhaps the best known method for approximating a desired array pattern $F(u)$

involves reconstructing the pattern from a finite number of sampled values. The principle is analagous to one used in information theory where a time waveform $f(t)$ of limited bandwidth is reconstructed from a finite number of its sampled values. That is, the function $f(t)$ containing no frequencies higher than B Hz can be reconstructed from its values at a series of points spaced $1/2B$ seconds apart. The analogous process for the far-field amplitude pattern $F(\theta)$ of an array with a finite aperture length L is to reconstruct it from a series of values spaced λ/L radians apart. The n sampled values can be denoted by $F(n\lambda/L)$ where n is an integer.

As shown in Figure 4-19, an approximate far-field pattern $F_A(\theta)$ can be constructed from the sampled values $F(n\lambda/L)$ by superimposing another pattern of the form $\sin\pi u/\pi u$ on each of the sampled values, where u is now given by $u=(L/\lambda)(\sin\theta-n\lambda/L)$. The function $\sin\pi u/\pi u$ is called the "composing function". The result can be written as

$$F_A(\theta) = \sum_{n=-N}^{N} F(n\lambda/L) \frac{\sin\pi[(L/\lambda)(\sin\theta-n\lambda/L)]}{\pi(L/\lambda)(\sin\theta-n\lambda/L)}$$

where N will be defined shortly. In other words, the far-field amplitude pattern of a finite aperture can be constructed from a sum of $\sin\pi u/\pi u$ composing functions each spaced λ/L radians apart (Fig. 4-19(c)) and each weighted by the sample value $F(n\lambda/L)$. The approximate or reconstructed pattern $F_A(\theta)$ will fit or be matched to the desired pattern $F(\theta)$ at a finite number $(2N+1)$ of points equal to the total number of required samples.

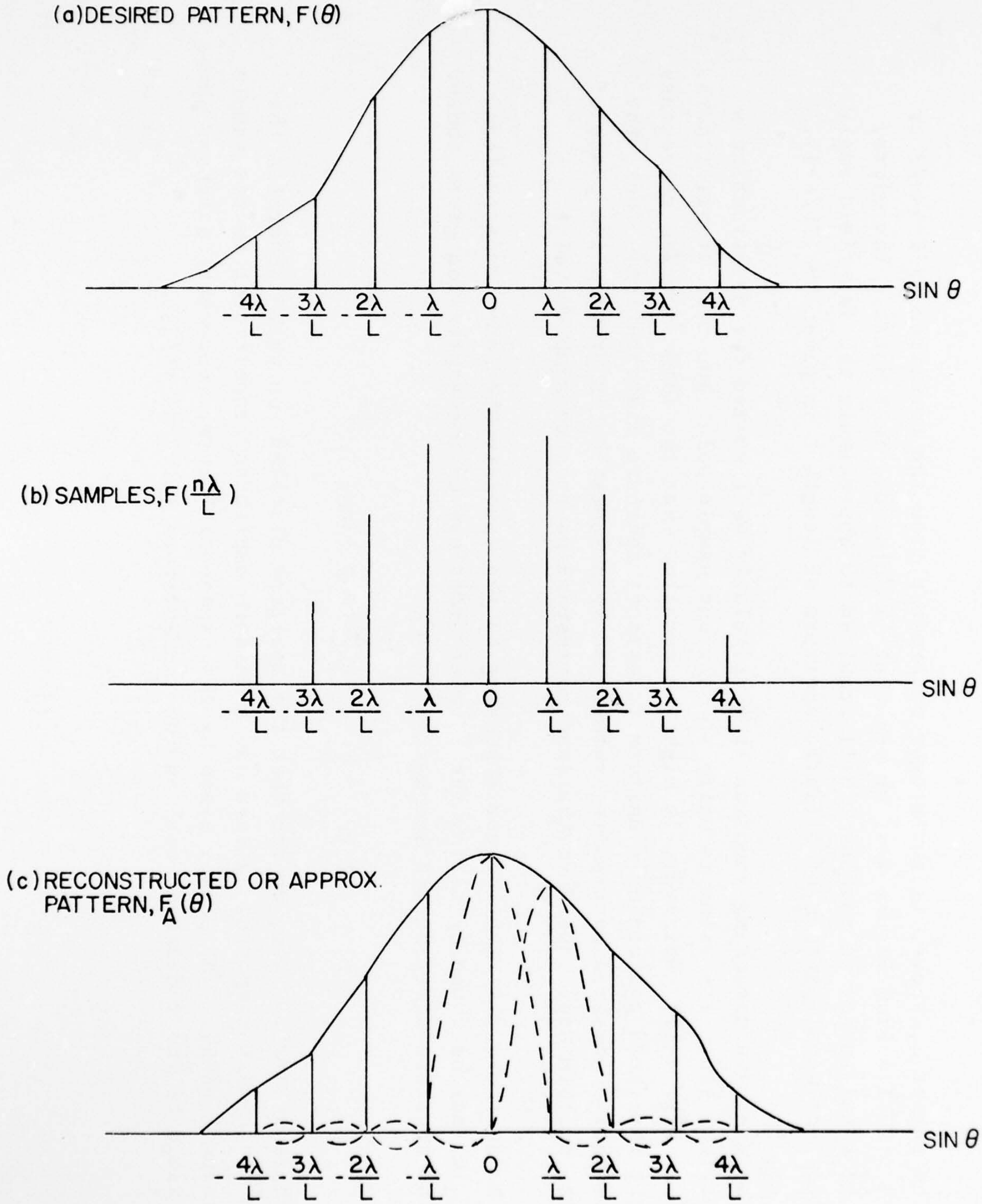

CONSTRUCTION OF A FAR-FIELD AMPLITUDE PATTERN FROM SAMPLED VALUES.

FIGURE 4-19

- The number N, above, is an integer determined from the condition $-\pi/2<\theta<\pi/2$ or $-1\leq\sin\theta\leq 1$. From Figure 4-19 we see that $|N\lambda/L|\leq 1$ or, that $N\leq L/\lambda$. Therefore, the total number of samples $(2N+1)$ required to approximate the far-field amplitude (or beam) pattern of a finite aperture of length L is given by $(2L/\lambda+1)$.

- The $\sin\pi u/\pi u$ composing function is particularly well suited for constructing a pattern since its value is unity at only one sample point but zero at all others. (See Fig. 4-19) Moreover, it might be recalled that the form $\sin\pi u/\pi u$ represents the far-field pattern of a uniform (constant) aperture distribution. Thus, the overall or desired pattern is synthesized by a summation in progressive phase of the uniform amplitude distributions corresponding to each sampled value.

- The aperture distribution corresponding to the reconstructed amplitude pattern $F_A(\theta)$ may be found by taking the Fourier transform of the expression given above. The aperture distribution becomes

$$g\,(p) = \sum_{n=-N}^{N} F\left(\frac{n\lambda}{L}\right)\exp(-inp)\ ,$$

where $p=2\pi x/L$. Thus, we see that the aperture distribution which generates the n^{th} $\sin\pi u/\pi u$ composing pattern has a uniform amplitude proportional to the sample value $F(n\lambda/L)$. The phase, given by the exponential term, represents a linear phase change of $\pm n\pi$ radians at each end of the aperture (i.e. at $\pm L/2$).

4.7.2.2 Other Methods of Pattern Synthesis

- The $\sin\pi u/\pi u$ synthesis method given above is the one most frequently discussed in textbooks. There are, of course, others. For example, one approach has been suggested which involves raising the pattern function $F(\theta)$ of a line array of equispaced elements to some integral power greater than unity. The resulting expression is then identified as the pattern function of a larger line array with the same element spacing. Proceeding this way, one can determine an aperture distribution for a large array so that its pattern displays some of the characteristic features of a smaller array, such as fewer sidelobes.

- Still other methods of pattern synthesis involve expanding the pattern function in terms of spatial harmonics or the use of Green's functions or even linear programming. Even the array shading methods discussed earlier such as Dolph-Chebyshev or Taylor can be considered as pattern synthesis techniques.

- Generally, each synthesis method is considered to be optimum in the sense that its resulting pattern approximates a desired pattern in some particular manner. For example, the Fourier integral method (See Section 4.7.1) is said to approximate a desired pattern so that the mean square difference between the desired and the approximate pattern is a minimum. The $\sin\pi u/\pi u$ method gives a radiation pattern that exactly fits the desired pattern at a finite number $(2N+1)$ of points. The Dolph-Chebyshev method synthesizes the narrowest main beam for a given or specified side-lobe level.

4.8 Maximum Directivity

4.8.1 Introduction

- In attempting to synthesize a desired beampattern, the question frequently arises as to how one can obtain the maximum directivity for a given number of array elements. Moreover, it is also important to know what sacrifices or tradeoffs are necessary to achieve such a directivity. We shall discuss these questions as they relate to line arrays in this section.

4.8.2 Directivity, Interelement Spacing and Shading

- As has been mentioned several times previously, maximum directivity is achieved in the case of integral half-wavelength element spacing when the relative excitation or weighting coefficient A_m of the m^{th} array element is a constant and independent of m. That is, uniform amplitude shading yields the maximum directivity for integral half-wavelength element spacing. The directivity D (or D.I. = 10 log D) in this case is well known and equal to the number of elements N in the array, or

$$D.I._{max} = 10 \log N. \qquad d/\lambda = n/2, \quad n = 1, 2, \ldots$$

  It is important to note here that for spacing other than integral half-wavelength spacing, maximum directivity is not obtained with uniform amplitude shading.

- Maximum directivity index versus element spacing (d/λ) curves are given in Figure 4-20 for N=3,5 and 7 element arrays. In addition, the dashed curve gives the directivity index versus d/λ for the N=5 case with uniform excitation. Note that the individual maximum directivity curves in Figure 4-20 were not obtained for

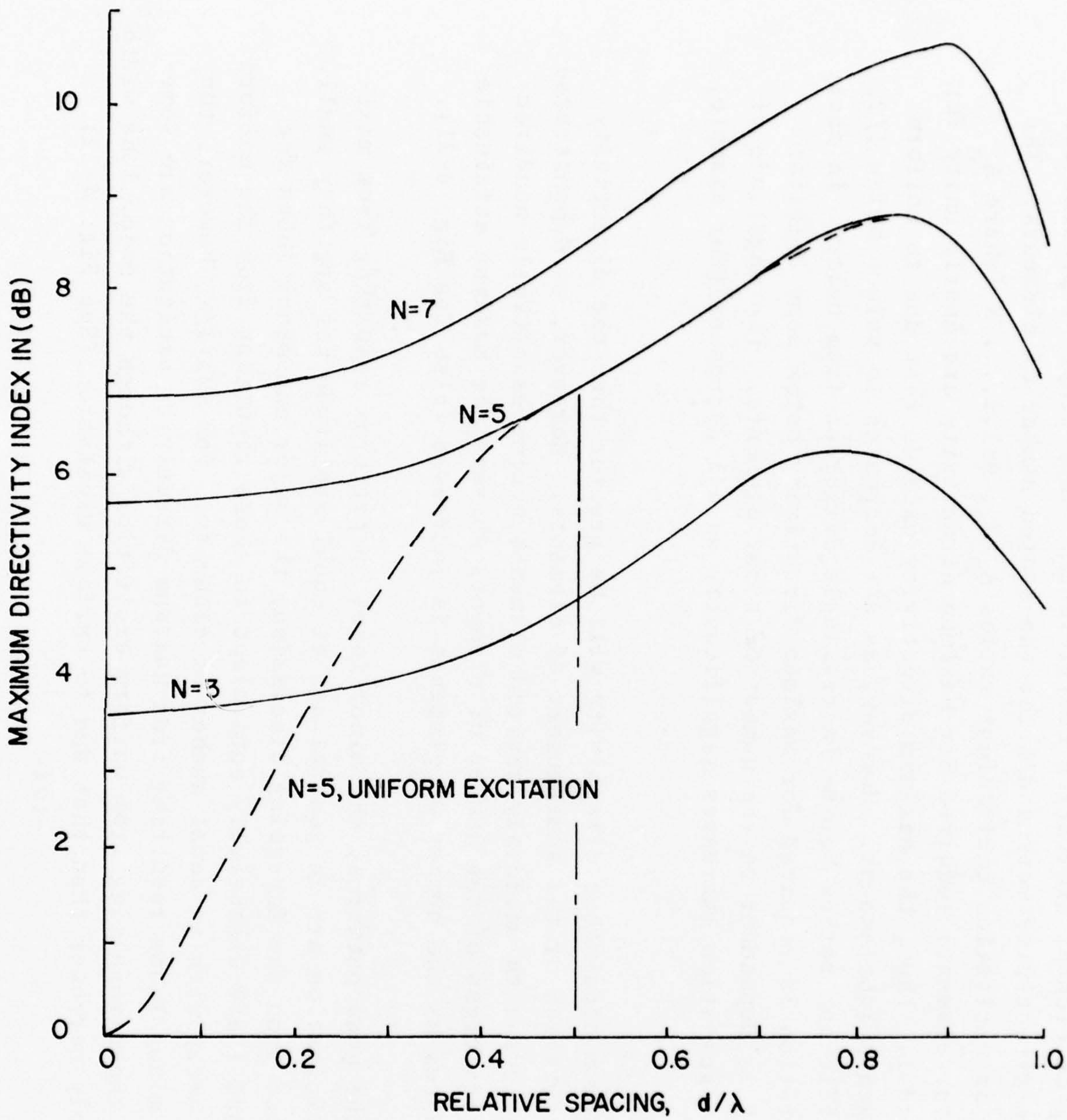

MAXIMUM D.I. AS A FUNCTION OF ELEMENT SPACING (d/λ) FOR BROADSIDE LINE ARRAYS WITH 3, 5 AND 7 POINT ELEMENTS.

FIGURE 4-20

uniform weighting or element excitation coefficients. They simply represent the maximum attainable directivity versus d/λ for the stated number of elements. The element weighting or excitation coefficient ratios A_m/A_o, $m=1,2,\ldots N$ (where A_o refers to the center element) required for maximum directivity are nearly unity for d/λ between 1/2 and 1. Thus, the maximum directivity exceeds that due to uniform excitation by only a slight amount. However, as d/λ decreases to values below 1/2, the weighting coefficient ratios become increasingly different from unity. In fact, out-of-phase excitation is required for maximum directivity below some critical value of d/λ which is dependent on the number of array elements. The magnitude of this out-of-phase excitation increases significantly as d/λ decreases (for example, See Fig. 4-23).

- As $d/\lambda \to 0$, the maximum attainable directivity will be greater than the directivity due to uniform excitation of the same number of elements. Moreover, as demonstrated in Figure 4-20, arrays with uniformly excited elements become essentially nondirectional as $d/\lambda \to o$ regardless of the number of elements whereas the maximum attainable directivity increases as the number of elements is increased (also See Fig. 4-21).

- With respect to the beam patterns, the minor lobes in patterns resulting from maximum directivity excitation are in general not of equal amplitude nor are they small. As one might expect from the foregoing discussion, the major and minor lobes for d/λ between 1/2 and 1 are essentially equivalent to those resulting from the uniform excitation of an array with an equal number of elements. For $d/\lambda<1/2$, however, the amplitude of the minor lobes resulting from maximum directivity excitation are somewhat larger than those resulting from uniform excitation although the major lobe width can be considerably narrower than that due to uniform excitation (See Fig. 4-22).

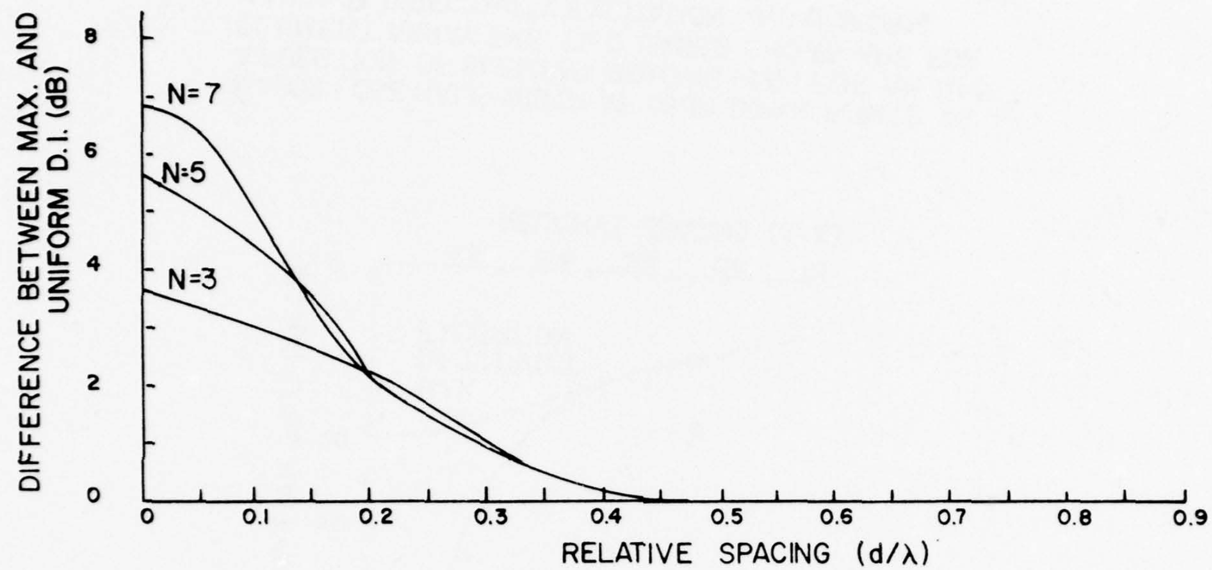

DIFFERENCE BETWEEN MAXIMUM AND UNIFORM D.I. AS A FUNCTION OF ELEMENT SPACING (d/λ) FOR N=3,5 AND 7 ELEMENTS.

FIGURE 4-21

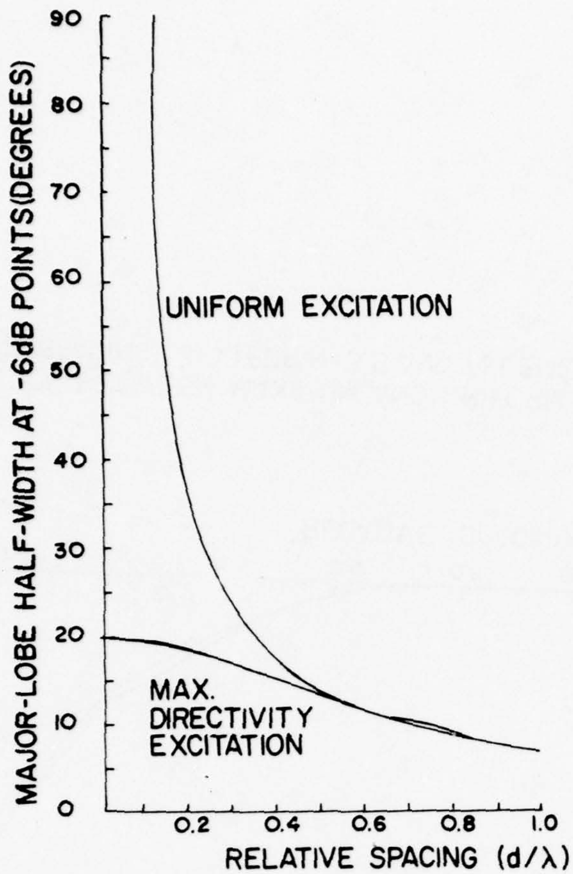

MAJOR LOBE HALF-WIDTH AT -6dB DOWN POINTS AS A FUNCTION OF ELEMENT SPACING (d/λ) FOR AN N=5 ELEMENT ARRAY. THE TWO CASES SHOWN ARE FOR MAXIMUM DIRECTIVITY EXCITATION AND UNIFORM EXCITATION.

FIGURE 4-22

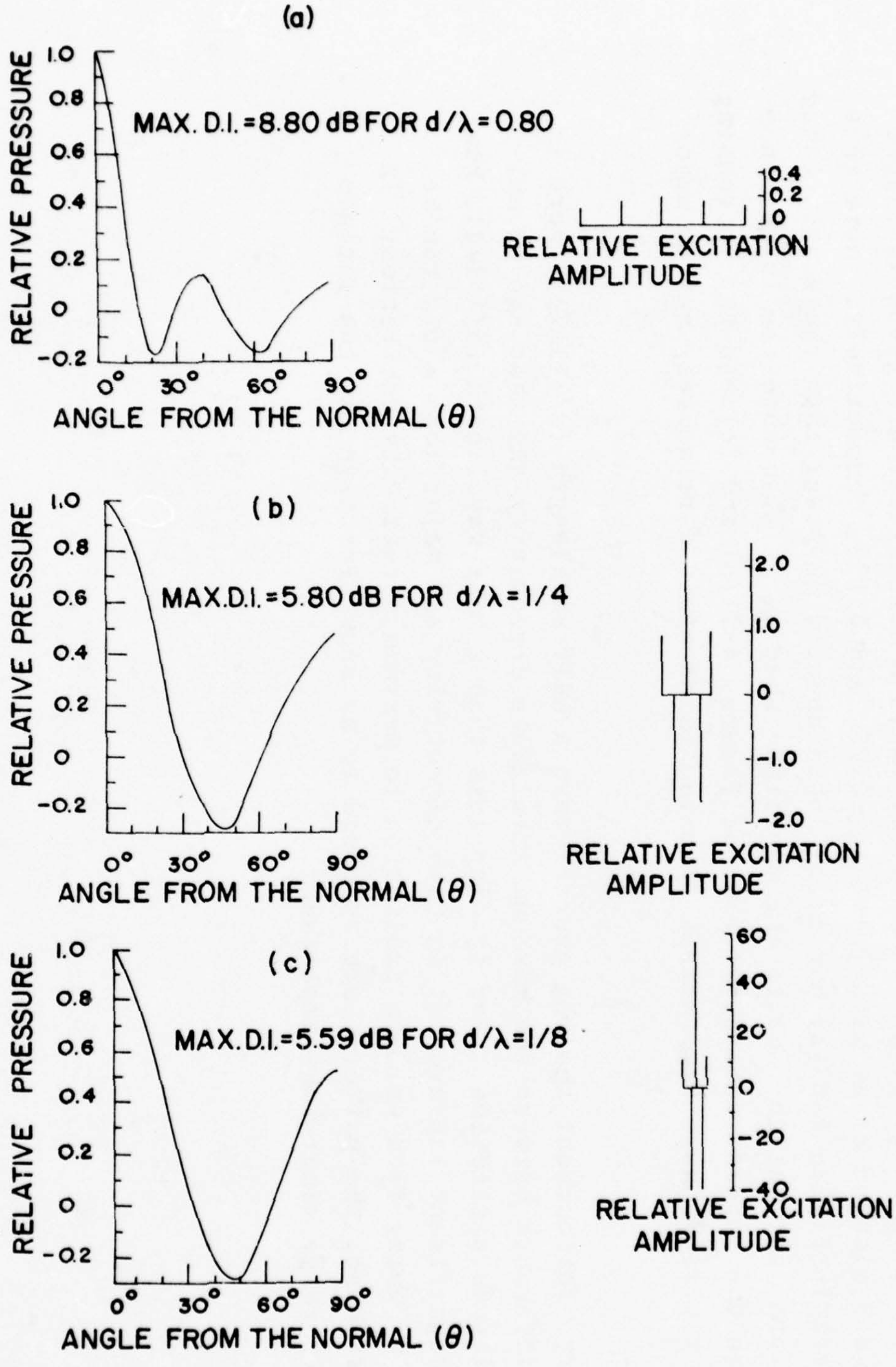

FAR-FIELD AMPLITUDE PATTERN AND RELATIVE EXCITATION AMPLITUDES FOR AN N=5 ELEMENT ARRAY WITH MAXIMUM DIRECTIVITY EXCITATION.

FIGURE 4-23

As we saw above, this narrower major lobe is obtained as $d/\lambda \to o$ only by requiring large out-of-phase excitations. Patterns of this type are called "Superdirective" and will be discussed in the following section. A typical example of the patterns and corresponding excitations required for maximum directivity are given in Figure 4-23 for a 5-element array with $d/\lambda=0.80$, 0.25, and 0.125, respectively. Note that the pattern in Figure 4-23(a) has minor lobes about 2 dB lower than those associated with uniform excitation due to the amplitude shading. Also note the large minor lobe(s) in the superdirective patterns of Figures 4-21(b) and (c) and the increasingly large reversed phase excitations required to maintain a relatively narrow major lobe.

- In summary, for element spacing greater than a half-wavelength ($d/\lambda \geq 1/2$), there is little difference between the maximum attainable directivity and that due to uniform amplitude excitation. For spacing less than a half-wavelength ($d/\lambda < 1/2$), however, a *significant improvement in both* directivity and major lobe width can be obtained by going from uniform excitation to maximum directivity excitation. In the latter case, the patterns are referred to as superdirective and can include relatively large minor-lobe amplitudes.

4.9 Supergain

- Until now, with the exception of the previous section, our discussions have concentrated on aperture distributions with uniform phase designs where the phase is such that the radiation from each element propagates in phase in the steered direction. Uniform phase distributions, however, cannot be used to obtain the maximum possible directivity for a given array. Directivity higher than that allowed by uniform phase is called superdirectivity or supergain and occurs as the result of interference phenomena produced by the aperture phase oscillating over a broad range of values.

- We have seen that the optimum spacing d of elements in an array is such that d/λ is slightly less than 1/2. The effect on a specified pattern of increasing this element spacing, or the overall array length L/λ, is not only that the main beam will narrow (See Fig. 4-22) but that the pattern will repeat itself. In a line array as d/λ approaches unity, a large lobe will begin to occur in the pattern $\pi/2$ radians from the main lobe. On the other hand, for a compressed array or one with element spacing less than a half wavelength ($d/\lambda<1/2$) there are no problems with a repeated pattern. However, assuming uniform phase excitation, the effect of compressing the array will be that the main beam broadens and the directivity decreases (See Fig. 4-20).

- If the uniform phase criteron is relaxed, then the decrease in directivity need no longer occur as the array is compressed. In fact, in certain cases where the array element excitation coefficients are allowed to become negative and large in magnitude, the width of the major lobe of the resulting pattern may be appreciably less than

that of a pattern from a similar array of uniformly excited elements (See Fig. 4-23, for example). It is this very feature of superdirectivity that is of greatest interest to the array designer. That is, by adjusting the phase and amplitude of individual element excitations, the beamwidth can be maintained at a nearly constant value as the overall array length L/λ (or d/λ) is compressed. Thus, the array does not become nondirectional as $d/\lambda \to o$, as it would for excitation with uniform phase, but rather is made superdirective with the beamwidth tending to a finite limit.

- The finite limit as $d/\lambda \to o$ of the beamwidth of an N-element line array corresponds to a maximum directivity which is given by

$$D_{max} = \sum_{n=o}^{N-1} (2n+1)[P_n(\sin\theta_o)]^2 ,$$

where θ_o is the scan direction (measured from broadside) and the P_n are the Legendre Polynomials.

- For the <u>endfire</u> condition, the above expression for D_{max} reduces to

$$D_{max} = \sum_{n=o}^{N-1} (2n+1) = N^2, \text{ (endfire)}.$$

For <u>broadside</u> it becomes

$$D_{max} = \left[\frac{1\cdot 3\cdot 5\cdot 7 \cdots N}{2\cdot 4\cdot 6 \cdots (N-1)}\right]^2, \text{ (broadside)}$$

which can be approximated very well by

$$D_{max} = (2N+1)/\pi \ . \quad \text{(broadside)}$$

- Unfortunately, superdirectivity is somewhat difficult to achieve in practice because, as the element spacing d/λ is decreased and the beamwidth tends to a finite limit, the excitations required tend to become infinite in magnitude. A reversed-phase excitation presents no problems in theory but is normally avoided in practice because of the large excitation magnitudes required for a given response which lead to a decrease in the over-all efficiency of the array. Moreover, a superdirective pattern requires that close tolerances be imposed on the sensitivities of the array elements and upon the operating wavelength. Thus, such a pattern will be very sensitive to frequency changes and therefore unsuitable for broadband operations.

4.10 Gain Beamwidth Product

- **Uniform Distribution**

  For a line array, both the beamwidth and the directivity depend linearly on the array length. As a result, when the (3dB down) broadside beamwidth BW_3 is expressed in degrees and when the array distribution is uniform, the directivity D of the array can be expressed simply as

$$D = 101.5/BW_3 .$$

- **Cosine-On-Pedestal Distribution**

  The expression given above for the directivity of a uniform array changes only marginally when a cosine-on-pedestal distribution is used. Even for the extreme taper $a_1=0.5a_o$ (See Section 4.6.1.6), the magnitude of D changes by less than 10%.

- **Dolph-Chebyshev Distribution**

  For a Dolph-Chebyshev distribution, the expression given above for the directivity D of a uniform distribution is quite accurate until an array length is reached at which the directivity begins to limit.

- **General Distributions**

  The expression given above relating the beamwidth and directivity of a uniformly illuminated array provides a good working relation for most useful distributions. In fact, the expression can be rounded off and it can be said that the product of the broadside beamwidth (in degrees) and directivity for a line array is about one hundred.

THIS PAGE INTENTIONALLY LEFT BLANK.

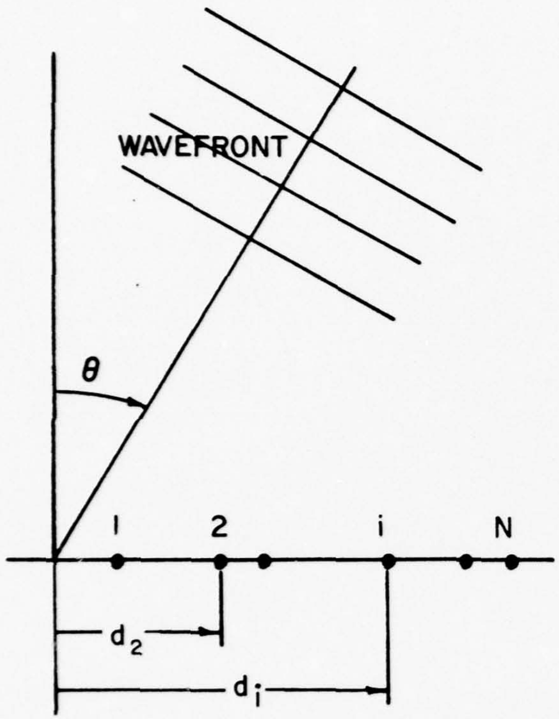

d_i = location of the i^{th} element

s_{max} = maximum interelement spacing

s_{min} = minimum interelement spacing

λ = signal wavelength

λ_o = wavelength parameter which constrains the range of u such that $|u| \leq 2$ for all $\lambda > \lambda_o$ and all steering angles between broadside and endfire

α = beamsteer direction

$u = \frac{\lambda_o}{\lambda} (\sin\theta - \sin\alpha)$

$V(\theta)$ = beam voltage output

ARRAY AND SIGNAL PARAMETERS

FIGURE 4-24

4.11 Nonuniformly Spaced Arrays*

4.11.1 Introduction

- The control of the beamwidth and the sidelobe level of transmitting and receiving arrays can be achieved by the proper design of the aperture distribution function. The aperture distribution, which produces the desired radiation pattern, can be synthesized by shading the element output and/or tapering the element spatial density.
- Adjusting the element output voltage or amplitude shading an N-element array gives the array designer N degrees of freedom by enabling him to match the N amplitudes to the N coefficients of the Fourier series representing the pattern function. Allowing the element positions to be arbitrary adds another degree of freedom to each element. Normally, however, only one of these approaches is used, amplitude shading being the traditional one.
- *Unequal spacing of elements is analogous to nonuniform temporal sampling of a signal.* Moreover, as we shall see shortly, there exists an equivalence between the amplitude shading of a uniformly spaced array and the interelement-distance variation in a nonuniformly spaced array.
- Although the history of hydrophone arrays dates back to World War I, the design possibilities of nonuniform spacing have been considered only during the past 25 years. Figure 4-24 provides some of the array and signal parameters that are typically used when dealing with nonuniformly spaced arrays.

---

*This subject is also treated in the literature under the heading of " Aperiodic Arrays".

4.11.2 Examples

- Figure 4-25(a) shows the arrangement of elements in a geometrically tapered array; in addition to the asymmetric configuration presented, the geometric space taper can also be implemented symmetrically with respect to the center point of the array.

- The degree of taper is specified by the number R, defined as the ratio of the maximum interelement spacing to the minimum interelement spacing.

- The common ratio,or the factor by which the successive spacings in Figure 4-25(a) increase,is given by

$$r = R^{1/(N-2)} .$$

- Figure 4-25(b) shows an 11-element array designed for maximum resolution. The numbers indicate relative interelement spacing. The array spacing rule in this example was determined by minimizing the number of redundant spacings in the array since repetition of an interelement spacing gives redundant information.

- Determination of the element positions in a minimally redundant array with even a moderately large number of elements is generally associated with extreme computational difficulties.

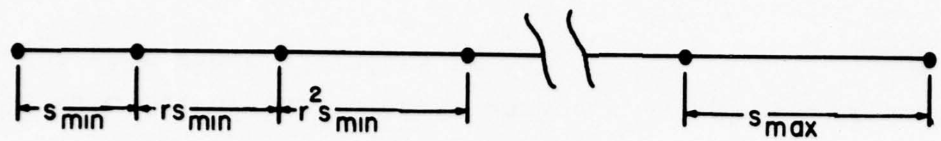

GEOMETRICALLY SPACE TAPERED ARRAY

FIGURE 4-25 (a)

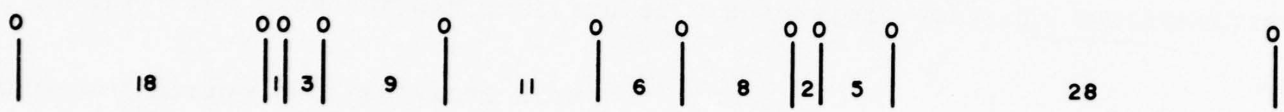

MINIMUM-REDUNDANCY ARRAY

FIGURE 4-25 (b)

- In addition to deterministic methods for finding the spacing rules, a statistical approach has been tried with arrays having a large number of elements. According to this method, the elements are placed at random over an aperture according to a given distribution function.

4.11.3 Important Properties

- The array properties to be described fall into two general categories: the beam pattern function and the array gain.

- In general, the beam pattern function of a nonuniform array is characterized by a sharp main beam followed by a region of very low sidelobes called the clean-sweep region which is followed by a region of moderately high sidelobes called the plateau region. (See Fig. 4-26).

- Array gain at low frequencies is controlled by properties of the main beam; at high frequencies it is controlled by the properties of the sidelobe plateaus. It is generally a much smoother function of frequency.

- The half-power beamwidth is given by

$$BW_3 \simeq F\lambda/L,$$

where F is a factor that depends on N and R. When R is in the neighborhood of 3, $F \simeq 1$ for a wide range of values of N.

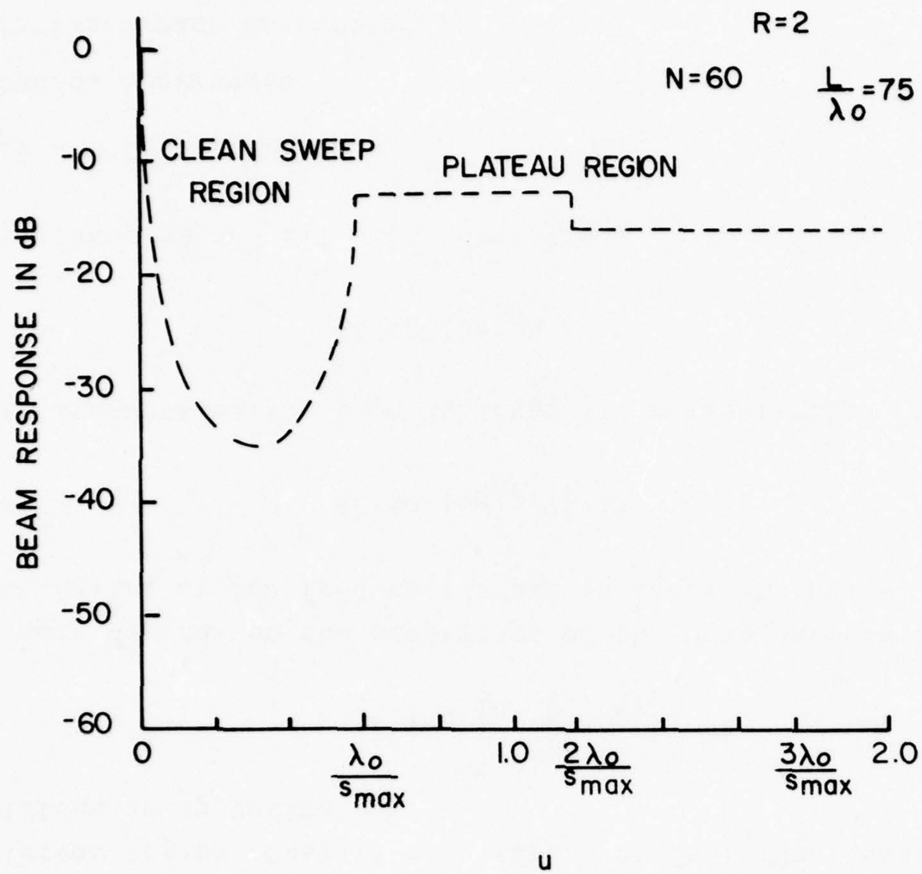

ENVELOPE OF THE BEAM PATTERN OF A GEOMETRICALLY TAPERED ARRAY

FIGURE 4-26

- The clean-sweep region extends from the main beam to the point where

$$u = \lambda_o / s_{max} .$$

- The plateau region consists of a series of individual plateaus. The level of the m^{th} plateau is approximately

$$-10 \log_{10}\left(\frac{mN}{2} \log_r R\right) \text{ dB}.$$

- Array gain depends on the properties of the beam pattern and of the noise field. In particular, at low frequencies and in isotropic noise,

$$AG \simeq 10 \log_{10}(2L/\lambda) .$$

At high frequencies the gain achieves its nominal value, namely,

$$AG \simeq 10 \log_{10} N$$

for all steering and all noise densities.

4.11.4 Analysis and Design Methods

- Two General Approaches

Convolution (space as variable)
Spectrum (spatial frequency as variable)

- Analytical and Design Procedures

  Exact solutions are available only for simple cases

  Optimum spacing rules are difficult to derive

  Conventional optimization is generally required in the sense of finding the minimum beamwidth for a given sidelobe level

  Constrained optimization is also frequently required where the array is designed subject to specified conditions such as maximum resolution, maximum signal-to-noise ratio or special radiation pattern requirements.

- Short-cut Approaches

  Usually begin by imposing additional restrictions such as selecting the taper function to be geometric, logarithmic, etc.

  They generally involve iterative procedures, usually with the aid of a computer

  The array design frequency is often based on the mean interelement spacing

  An example is a 760-element nonuniform circular configuration yielding the same beamwidth as a uniformly packed array of 6350 elements.

4.11.5 Advantages of Spatial Taper

- Much higher resolution or a significant reduction in the number of elements can be obtained with a spatial taper. For example, consider an array of fixed length L. Suppose a 35-meter resolution ρ at a range R=10 km is specified. The required beamwidth is $\theta \simeq \lambda/L = \rho/R$ = 3.5 milliradians. Hence, the aperture length (L) must be at least 280λ. Even at 1000 Hz this corresponds to $L \simeq 500$m, which requires more than 500 equally spaced hydrophones if the appearance of grating lobes is to be prevented. The prospect of reducing the number of hydrophones to, say, 150 by a properly designed nonuniform spacing is certainly an attractive one.
- Bandwidths of up to several octaves can be achieved without grating-lobe interference.
- The first-sidelobe level can be reduced to more than 13.6 dB below the main lobe level while retaining uniform amplitude shading.
- Reduction in cost and weight of arrays.
- Greater latitude in array design.
- Many of these advantages and others can be obtained at the expense of a slight increase in the level of the sidelobes and a decrease in the maximum value of array gain.

4.12 Planar Arrays

4.12.1 Far-field Amplitude Pattern

- Consider the planar array of elements shown in Figure 4-27 where each row is parallel to the y-axis and the common spacing between rows is d_x. In addition, let the common spacing between the elements in each row be d_y. If each row has the same current (i.e., amplitude and phase) distribution, then the far-field amplitude* pattern of the planar array can be written as

$$F(\theta,\phi) = F_x(\theta,\phi)\ F_y(\theta,\phi).$$

That is, under the stated conditions, the far-field amplitude pattern of the planar array is the product of the patterns of the two line arrays, one along the x-axis the other along the y-axis. This is an example of the principle of pattern multiplication and effectively means that the results developed for line arrays in the preceding sections can be used in understanding planar arrays.

- The far-field amplitude pattern $F=F_xF_y$ of the planar array is the product of the two line array patterns. Thus, it essentially arises from the intersection of two conical main beams plus those sidelobes of each conical pattern that coincide with the main beam of the other conical pattern. This product of two conical patterns gives a pencil beam pointing into the half space $z>o$ (See Fig. 4-27) whose main axis is in the direction$(\theta_o,\ \phi_o)$, where

---

* Recall that the beampattern $b(\theta,\phi)$ is the square of the far-field amplitude pattern normalized to unity in the broadside direction.

$$\tan\phi_o = \alpha_y d_x / \alpha_x d_y.$$

$$\sin^2\theta_o = (\alpha_x^2/k^2 d_x^2) + (\alpha_y^2/k^2 d_y^2) .$$

Here, α_x is the uniform phase progression or interelement phase shift in the x-direction, α_y is the uniform phase progression in the y-direction and $k=2\pi/\lambda$ is the wave number. These equations yield a unique direction in the half space $z>o$. for the given spacings d_x and d_y and interelement phase shifts α_x and α_y.

4.12.2 Beamwidth and Beam Scanning

- The -3dB down contour of the planar array's pencil beam is approximately elliptical. The beam cross-section is shown in Figure 4-28. At large distances from the array, the size and shape of this elliptical contour are dependent on the beam direction (θ_o, ϕ_o) as is the rotational tilt of the axes of the ellipse. If the pencil beam lies in the xz plane in the direction $(\theta_o, 0)$, then the u',v' axes of the ellipse will be aligned with the u, v axes, respectively (See Fig. 4-28). The u axis is always in the direction of increasing θ while the v axis is always in the direction of increasing ϕ . The -3dB beamwidths in the noted directions are

$$BW_u = BW_{xo} \sec\theta_o, \ BW_v = BW_{yo} , \qquad (\phi_o = 0)$$

where the quantities BW_{xo} and BW_{yo} will be defined shortly.

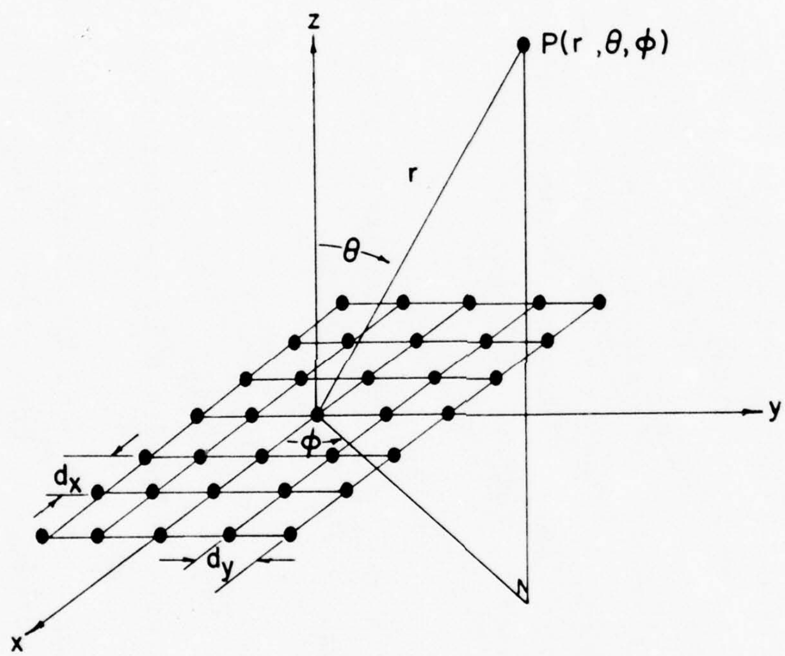

THE PLANAR ARRAY

FIGURE 4-27

If the pencil beam lies in the yz plane in the direction $(\theta_o, \pi/2)$, then the u' axis of the ellipse will point in the -v direction and the v' axis of the ellipse will be aligned with u. Thus, as indicated in Figure 4-28, the ellipse rotates in such a way that the angle γ rotates smoothly through 90^o as ϕ_o changes from 0^o to 90^o. In the latter case, the half-power or 3dB down beamwidth will be

$$BW_u = BW_{yo} \sec\theta_o, \; BW_v = BW_{xo} \qquad (\phi_o = \pi/2) .$$

- In order to calculate the -3dB beamwidths given above at the two positions $(\phi_o = 0^o, 90^o)$, it is necessary to know the quantities BW_{yo} and BW_{xo} in addition to θ_o. For uniform amplitude distributions, BW_{yo} or BW_{xo} can be determined by using L_y/λ or L_x/λ in place of L/λ in Figure 4-9 and reading the appropriate values (i.e., conical beamwidths) from the <u>broadside</u> curve. The quantities L_y and L_x are the dimensions of the planar array (Fig. 4-27). For cosine-on-pedestal or Chebyshev distributions, the beam broadening factors of Figure 4-17 must also be included in determining BW_u and BW_v.

- An area beamwidth B which is a measure of the area inside the elliptical -3dB contour of the pencil beam cross section is defined by

$$B = BW_{xo} \, BW_{yo} \, \sec\theta_o .$$

It should be noted that this area beamwidth B is independent of ϕ_o.

- The general effect of scanning a pencil beam is demonstrated in Figure 4-29. At position P, or broadside-broadside, the beam cross-section is approximately

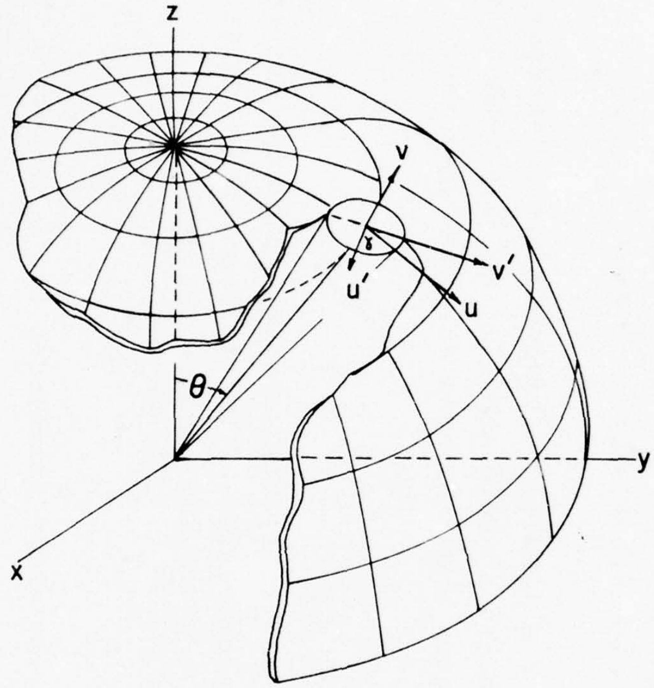

ORTHOGONAL BEAMWIDTHS OF A PLANAR ARRAY
PENCIL BEAM

FIGURE 4-28

elliptical with dimensions proportional to the inverse of the array dimensions (i.e., L_x^{-1} or L_y^{-1}). As the beam is scanned in the xz plane, its cross-section elongates in that direction (i.e., See Position P_1) As it is scanned in the yz plane, the cross-section elongates along the other beam dimension (i.e., See Position P_2). Comparing P_1 and P_2 we see that, for a constant θ_o measured from the z-axis, the elliptical cross section smoothly rotates and the two beamwidths smoothly change as the beam is scanned from $\phi_o=0$ to $\phi_o=\pi/2$. These effects combine in such a manner that the area beamwidth B stays constant.

- The relationships given above are all quite accurate to within several beamwidths of the limiting near-endfire condition where there is no main beam at all. It can be shown that this condition occurs when the beam is scanned so that

$$\sin^2\theta_o=1 \ .$$

Referring to Section 4.12.1, we see that this limiting condition determines the relationship between the phase progression or interelement phase shift (α_x, α_y), and the interelement spacing (d_x, d_y) for a given wavelength.

4.12.3 Directivity of Planar Arrays

- Suppose we are given a planar array whose dimensions are $L_x=(N_x-1)\ d_x$ and $L_y=(N_y-1)d_y$ where N_x and N_y represent the numbers of elements in each direction and d_x and d_y are the respective interelement spacings. Then, if the array is large and not scanned closer than several beamwidths from endfire, its directivity can be written as

$$D = \pi D_x\ D_y \cos\theta_o \ .$$

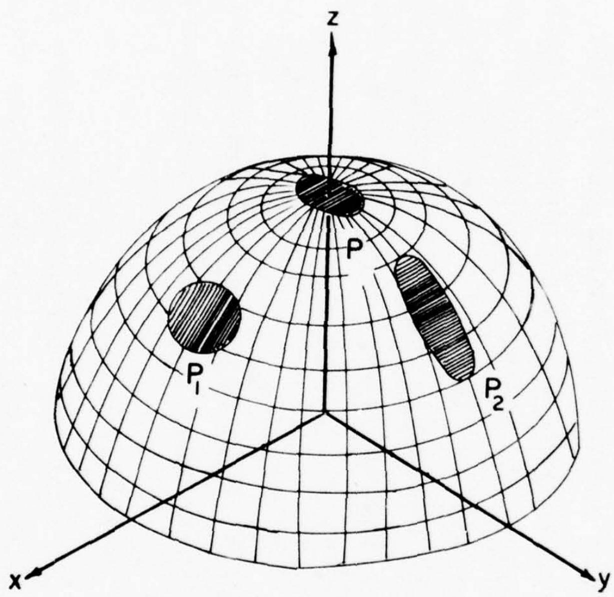

BEAM SHAPE VERSUS SCAN ANGLE FOR A PENCIL BEAM.

FIGURE 4-29

In this expression, $D_x(D_y)$ is the directivity of the constituent N_x (N_y) element line array with interelement spacing d_x (d_y). The $\cos\theta_o$ factor accounts for the decrease in projected aperture with scan. Thus, contrary to the directivity of a line array which is independent of scan angle (except at endfire), the directivity of a planar array depends on θ_o. It is, however, independent of the azimuthal coordinate of the beam, ϕ_o.

- Because of the form of the expression for D many of the results determined for the directivity of line arrays are applicable to planar arrays. For example, maximum directivity will again result from uniform amplitude excitation. Moreover, cosine-on-pedestal distributions will again give lowered sidelobes at the expense (although not very much) of some directivity. Dolph-Chebyshev distributions will again suffer a gain or directivity limit as shown in Figure 4-18 (Section 4.6.3.2) which is also applicable to planar arrays. The curves in Figure 4-18 can be used to determine D_x and D_y by using L_x/λ or L_y/λ for the abscissa in place of the denoted L/λ.

4.12.4 Gain-Beamwidth Product

- Similar to the case of line arrays, both the area beamwidth B and directivity D depend linearly on the area of the planar aperture. As a result, the relation

$$D = 32{,}400B$$

can be written for most practical aperture distributions where the area beamwidth B is now expressed in degrees squared rather than in radians squared. This expression is accurate for uniform amplitude distributions and Chebyshev distributions before gain limiting occurs (See Fig. 4-18). It is approximately correct for cosine-on-pedestal distributions.

5.0 ARRAY PERFORMANCE

- In the foregoing chapter we discussed the ideal performance that can be expected from an array of hydrophone elements. In the current chapter we shall present some major limitations to this performance incurred primarily through the medium in which the system operates.

- The ocean medium imposes severe constraints on the performance of any sonar system. Indeed, there is no known environmental parameter affecting the propagation of sound in the sea that is completely uniform, isotropic or homogeneous. External effects acting on and propagated through the medium such as wind, rain, shipping, etc. give rise to even more complications.

- In this chapter we shall develop the concept of array signal, noise and signal-to-noise gain. These parameters are very important since they provide a method for comparing the performance of arrays within their surroundings.

5.1 Array Self-Noise Limitations

5.1.1 Introduction

- In the following sections we shall discuss the limitations imposed on array performance by array self noise. In particular, we shall concentrate on the self-noise limitations of towed surveillance arrays.

- Self noise is a particular kind of background noise that occurs in sonars or in individual hydrophones, as well, whenever the mounting or suspension creates noise of its own. Although self noise is one of many different kinds of undesired sound in

a sonar system and originates in many ways, the following specific types of self noise are the most significant:

Electrical Noise

Flow Noise

Tow Ship Radiated Noise

and, Vibration Induced Noise.

5.1.2 Electrical Noise

5.1.2.1 Definition and Description

- Electrical noise refers to the noise generated by electrical equipment or external phenomena (i.e., magnetic fields) in the array output. This includes

  Thermal noise

  Cross talk noise between channels

  Noise induced by stray (or the earth's) magnetic fields

  60-cycle noise from the towship's power distribution system, etc.

- With the exception of the last of these, the electrical noises listed are easily controlled with the proper design and manufacturing techniques. In the case of the dominant 60-cycle hum, however, all sources must be carefully isolated through the use of high electrical impedances.

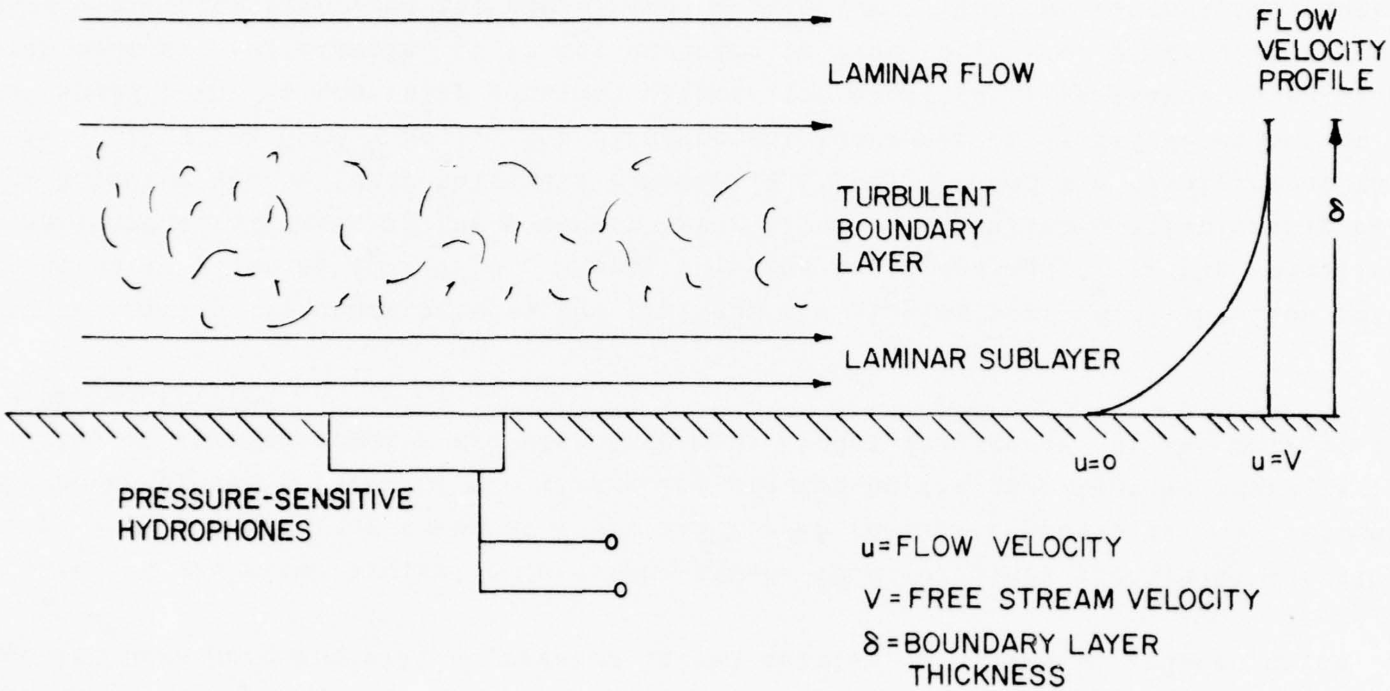
LAMINAR FLOW
FLOW VELOCITY PROFILE
TURBULENT BOUNDARY LAYER
δ
LAMINAR SUBLAYER
u=o
u=V
PRESSURE-SENSITIVE HYDROPHONES
u=FLOW VELOCITY
V=FREE STREAM VELOCITY
δ=BOUNDARY LAYER THICKNESS

FIGURE 5-1

5.1.3 Flow Noise

5.1.3.1 Definition and Description

- Flow noise refers to the pressure fluctuation at the array hydrophones caused by the turbulent boundary layer surrounding the array (See Fig. 5-1). It also extends to the noise arising from the surface roughness of the array. Cable strumming is not included here but will be treated in the section on vibration induced noise.

- Figure 5-2 gives two typical order-of-magnitude sound pressure spectra of the flow noise from a line array towed at $V = 2$ and $V = 15$ knots, respectively. As indicated, the sound pressure level of the flow noise created by the turbulent boundary layer is flat at low frequencies and slopes down at higher frequencies at the rate of about -9 dB per octave.

- The transition frequency between the flat and the sloping portion of the flow noise spectrum is given by $f_o = V/5\delta^*$. Here, V is the tow speed and δ^* is the so-called displacement thickness of the boundary layer (i.e. an approximate relationship between the actual boundary layer thickness δ shown in Figure 5-1 and the displacement thickness δ^* is given by $\delta = 5\delta^*$). The displacement thickness is itself dependent on the tow speed V and is generally obtained either from empirical data (water tunnels) or from models. For example, it is not uncommon to find the δ^* for a circular array to have been calculated from the expression derived for a flat two-dimensional plate.

- The displacement thickness δ^* of the boundary layer decreases with increased tow speed, V. However, if we neglect this effect, it can be shown that for frequencies less than $f_o = V/5\delta^*$, the power spectrum level of the flow noise will increase as

the cube of the tow speed (i.e., the sound pressure level will increase by about +9 dB for a doubling of the tow speed). For frequencies greater than f_o, the power spectrum level will increase as the sixth power of the tow speed. This latter case generally means that for the higher tow speeds ($V \geq 10$ knots) there will be an increase in the flow noise sound pressure level of about 1.8 dB/knot.

- Active research is currently being conducted in the area of flow noise. Some of this effort is directed toward finding materials that provide better flow noise attenuation. Still other research is oriented toward a better understanding of the relationship between flow noise and other noise sources. For example, a more detailed understanding of the coupling between the boundary layer and the induced "bulge wave" that propagates along the array wall would be of great value.

- Considering the typical sound pressure spectrum levels given in Figure 5-2, flow noise will generally be buried in cable strum, tow ship radiated noise, or even ambient noise at very low frequencies. This is true even at moderate tow speeds (i.e. say $V \approx 5$ knots). However, as tow speeds increase with future systems, flow noise will become more significant due to its dependence on the higher powers of V.

5.1.3.2 Reduction of Flow Noise

- Increasing the size of the array hydrophones causes them to become less sensitive to flow noise. A hydrophone will tend to average out the effect of a turbulent cell as it passes when the hydrophone size is comparable to that of the cell.

- Other methods for reducing flow noise which are applicable to towed arrays include moving the hydrophones further away from the turbulent boundary layer. This can be accomplished by physically recessing them further into the array wall.

- The ejection of polymers or long-chain unbranched molecules has also been found to be effective in reducing flow noise. The process appears to thicken the laminar sublayer (See Fig. 5-1) and thereby reduce flow noise by separating the hydrophones from the turbulent boundary layer.

5.1.3.3 Flow Noise Coherence

- Measurements with small hydrophones in the walls of tubes have shown that in a frequency band w Hz wide centered at frequency f, the crosscorrelation coefficient* $\rho(d,w)$ of the pressure at two points along the wall a distance d apart is

$$\rho(d,w) = \rho(s) \frac{\sin(\pi wd/u_c)}{\pi wd/u_c} \cos 2\pi s .$$

Here, s is the nondimensional Strouhal number defined by $s = fd/u_c$, where u_c is the "convection" velocity at which the turbulent patches are carried by the flow. Depending on the frequency f, u_c varies from 0.6V to 1.0V where V is the free-stream velocity. The coherence function $\rho(s)$ can be written as

$$\rho(s) = \exp\,[-0.7s]$$

for separations d parallel to the flow.

---

*Refer to sections 5.7.2 and 5.7.3 for definitions, examples and a discussion of coherence.

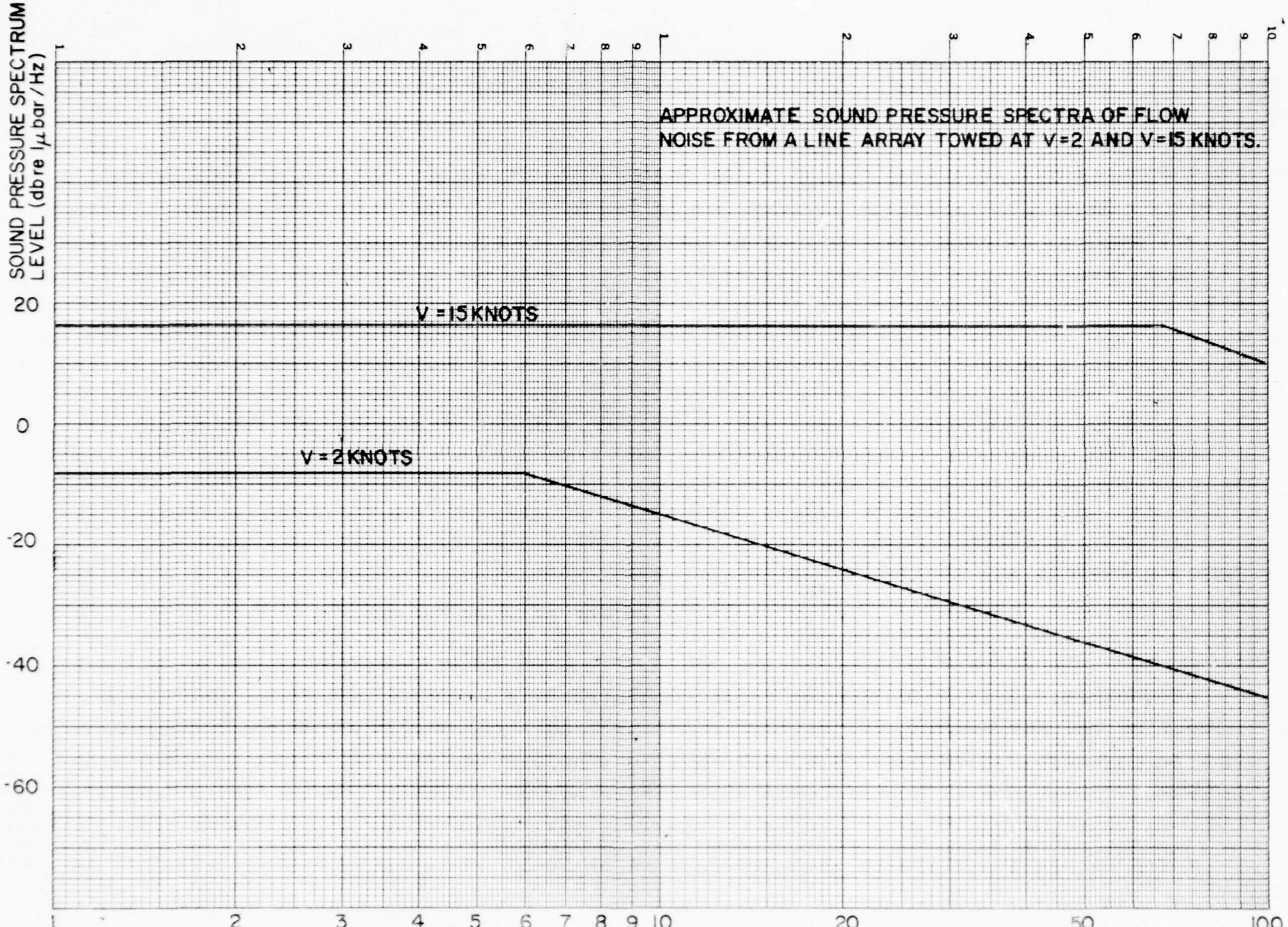
APPROXIMATE SOUND PRESSURE SPECTRA OF FLOW NOISE FROM A LINE ARRAY TOWED AT V=2 AND V=15 KNOTS.
SOUND PRESSURE SPECTRUM LEVEL (db re 1 μbar /Hz)
20
0
-20
-40
-60
V = 15 KNOTS
V = 2 KNOTS
1
2
3
4
5
6
7
8
9
10
20
50
100
FREQUENCY (Hz)
FIGURE 5-2

5.1.3.4 Discrimination Against Flow Noise

- The crosscorrelation coefficient given above suggests that an efficient way to discriminate against flow noise is to replace single hydrophones by groups of smaller independent hydrophones.* That is, we can obtain some gain against flow noise by replacing the N hydrophones in an array by N groups of M hydrophones, each phone separated by a distance d from its neighbor, so that the flow noise correlation between any two adjacent phones is minimized. This gain against flow noise, relative to that of a single hydrophone, is given at the beamformer output by

  $$G = 10 \log MN = 10 \log M + 10 \log N.$$

  The usual design frequency or half-wavelength spacing now refers to the spacing between the N groups and not the individual hydrophones. The value of M depends on the array design and is related to the crosscorrelation coefficient $\rho(d,w)$ given above. It generally ranges from $M=2$ to $M=20$.

5.1.3.5 Flow Noise Generated By *Surface Roughness*

- Noise due to surface roughness is generally insignificant if the roughness does not protrude above the laminar sublayer into the turbulent flow (See Fig. 5-1).

- In general, the surface of towed arrays is sufficiently smooth so that surface roughness is not considered a significant contributor to flow noise. However, if the tow speed increases sufficiently, the thickness of the laminar sublayer will decrease and roughness in the form of a joint or protrusion, etc., may penetrate it and produce noise.

---

* This is also known as hydrophone clustering.

5.1.4 Towship Radiated Noise

5.1.4.1 Definition and Description

- The overall spectrum of the towship radiated noise depends on the size, speed and construction of the ship and consists of three primary components; machinery noise, hydrodynamic noise and propeller noise.

5.1.4.2 Machinery Noise

- Machinery noise is defined as the noise arising from mechanical vibrations and transmitted through the hull of the ship into the water. These vibrations can originate in the engines, air compressors and other devices or equipment on board the ship. They appear as narrow band peaks in the spectrum with amplitude and frequency depending on the rotational speed of the machinery and are a significant source of 60 Hz energy in the array's output.

- Machinery noise can be significantly reduced by the proper and effective use of vibration isolation equipment.

5.1.4.3 Hydrodynamic Noise

- Hydrodynamic noise arises from the turbulent boundary layer of the ship and, as such, is not propagated to any great distances. It can, however, excite resonances in the ship's hull which are subsequently radiated toward the towed array. Like machinery noise, the hull resonances generally show up as peaked narrow band noise in the array output.

5.1.4.4 Propeller Noise

- The level of propeller noise is generally high when compared to machinery and hydrodynamic noise. Spectral peaks in the array output can be associated with blade rate frequencies given by

$$f = nR/60,$$

where n is the number of blades and R is the propeller speed in rpm. A three bladed ($n=3$) propeller, for example, turning at $R=800$ rpm will produce a blade rate peak at $f=40$ Hz.

- In addition to blade rate noise, the propeller blades will resonate at or near their natural frequencies due to flow induced vibrations. These resonances will appear as noise peaks in the array output and can extend to very low frequencies.

5.1.4.5 Reduction of Towship Radiated Noise

- Towship radiated noise is still not completely understood. At present, its effect on the towed array is reduced by simply increasing the distance between the array and the towship.

5.1.5 Vibration Induced Noise

5.1.5.1 Definition and Description

- Vibration induced noise is the array hydrophone response to static and dynamic pressure changes and accelerations caused by vibrating forces applied to the array. These forces include those from the towship which are propagated down the cable, cable strum due to vortex shedding and even vortex shedding by the array itself. Vibration induced noise is generally the predominant low frequency noise component for towed arrays (See Fig. 5-3).

5.1.5.2 Towship Vibrations Propagated Down the Cable

- Hull and equipment vibrations such as those from compressors, generators, screws, etc., can propagate down the cable to the array.

- Motion of the towship end of the cable as the ship reacts to the sea also causes noise to be introduced in the form of higher frequency harmonics of this motion.

- Towship noise generally occurs as peaks throughout the frequency band 5 Hz to 100 Hz.

5.1.5.3 Cable Strum

- Cable strum is a vibration induced noise in the array output caused by the periodic shedding of vortices from the cable. The vibrations caused by the vortex shedding extend over the entire length of the cable. Cable strum is currently the predominant source of noise in the 5 Hz to 20 Hz frequency range. Generally, it occurs

as a narrowband peak in this frequency range with a maximum sound pressure amplitude some 6 to 24 dB above a similar case where no strum occurs (See Fig. 5-3).

- The vortex shedding frequency for a flow normal to the cylindrical cable is given by

$$f = sV/d,$$

where s is the dimensionless Strouhal number, V is the flow velocity and d is the cable diameter. This expression is approximately correct even when there is a tangential flow component along the cable as long as V is taken as the normal component of the flow velocity. The Strouhal number has a constant value of about 0.18 over most of the tow speeds and cable sizes occuring in practice. Thus, for a 1-knot towing speed (51.5cm/sec) and a 1cm. diameter cable, the strum frequency will be about 9 Hz.

- Pitching motion of the towship at higher sea states can also produce vortex shedding and thereby cable strum of sizable amplitude by creating a flow across the cable. This particular type of strum is readily discernible since it appears in short bursts at a rate which is dependent upon the operating configuration and the sea-state.

5.1.5.4 Reduction of Vibration Induced Noise

- As in the case of towship radiated noise, vibration induced noise can also be attenuated somewhat by increasing the distance from the noise source.

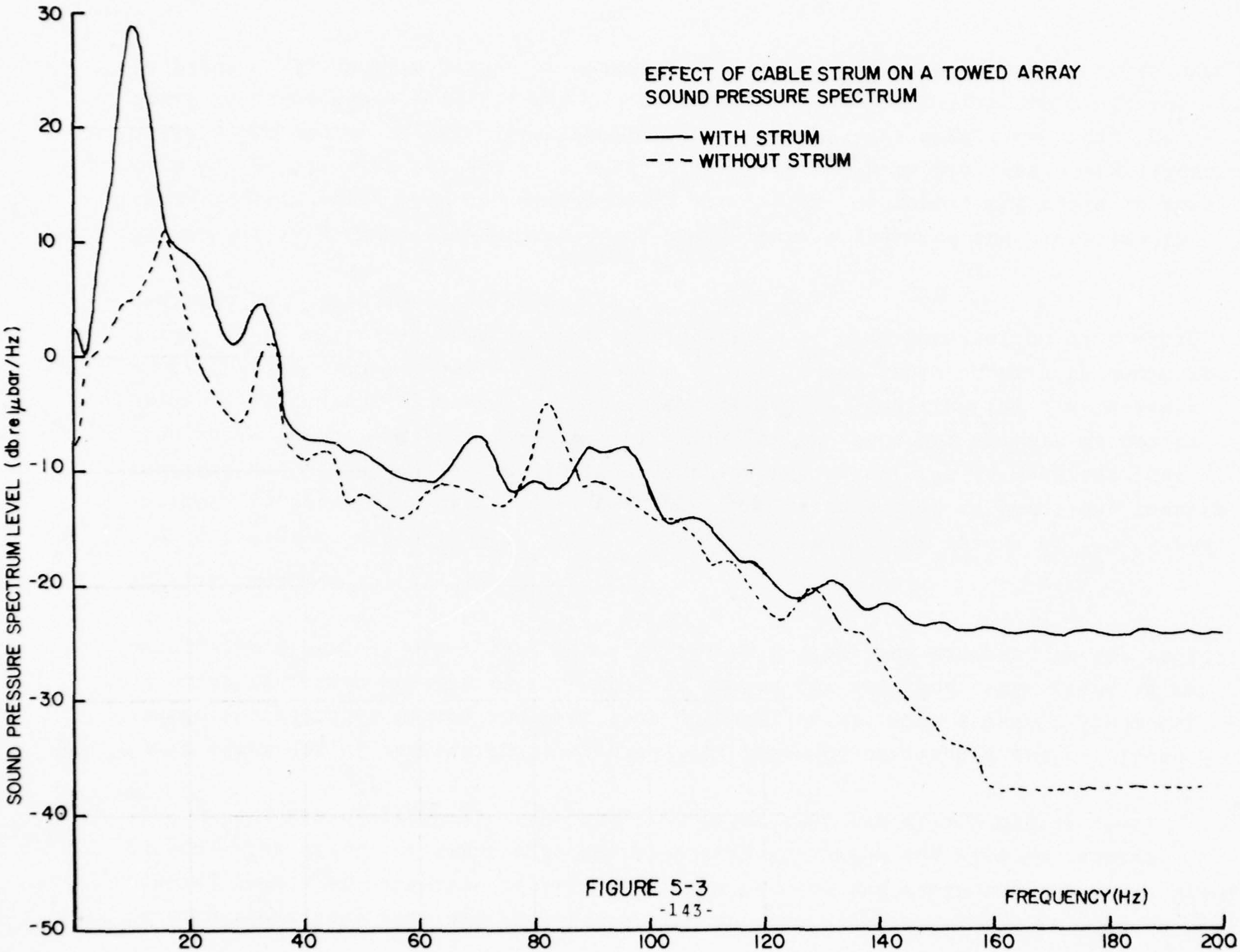

EFFECT OF CABLE STRUM ON A TOWED ARRAY
SOUND PRESSURE SPECTRUM
WITH STRUM
WITHOUT STRUM
SOUND PRESSURE SPECTRUM LEVEL (db re μbar/Hz)
30
20
10
0
-10
-20
-30
-40
-50
20
40
60
80
100
120
140
160
180
200
FREQUENCY(Hz)

FIGURE 5-3

- Towship vibrations that are propagated down the cable and array can be reduced by placing compliant vibration isolation modules between the cable and the array hydrophones. The effect of transverse vibrations in the array can also be reduced through the use of properly suspended or acceleration cancelling hydrophones.

- Cable strum can be reduced by using a faired, ribboned or stubbed cable. These reduce the periodic vortex shedding that normally occurs with a bare cylindrical or untapered cross-section cable. Another method for reducing cable strum is by using stress members other than steel (i.e., polyester, for example) in the cable.

5.1.5.5 Typical Examples for a Towed Array

- Figure 5-4 gives three typical sound pressure spectra at tow speeds of V=6, 8 and 10 knots in sea states of 0 to 1. Each spectrum is comprised of the flow, towship radiated and vibration induced noise as seen by the array. It is apparent that flow noise is not dominant for this particular array since the spectra do not increase with increasing speed as fast as theoretically predicted for flow noise alone (See Section 5.1.3.1). Cable strum of the faired cable appears to dominate around 10 Hz while the remainder of each spectrum is some combination of towship radiated and vibration induced noise.

- Figure 5-5 is a comparison of the total flow, towship radiated and vibration induced noise spectra with and without a faired cable. Moreover, the cable in this case has a polyester instead of a metal stress member which provides a significant noise reduction by itself. Generally, when a steel stress member is used, the total sound pressure level is about 3 to 9 dB lower with a fairing than without. In Figure 5-5, where a polyester member is used, the total noise reduction is even

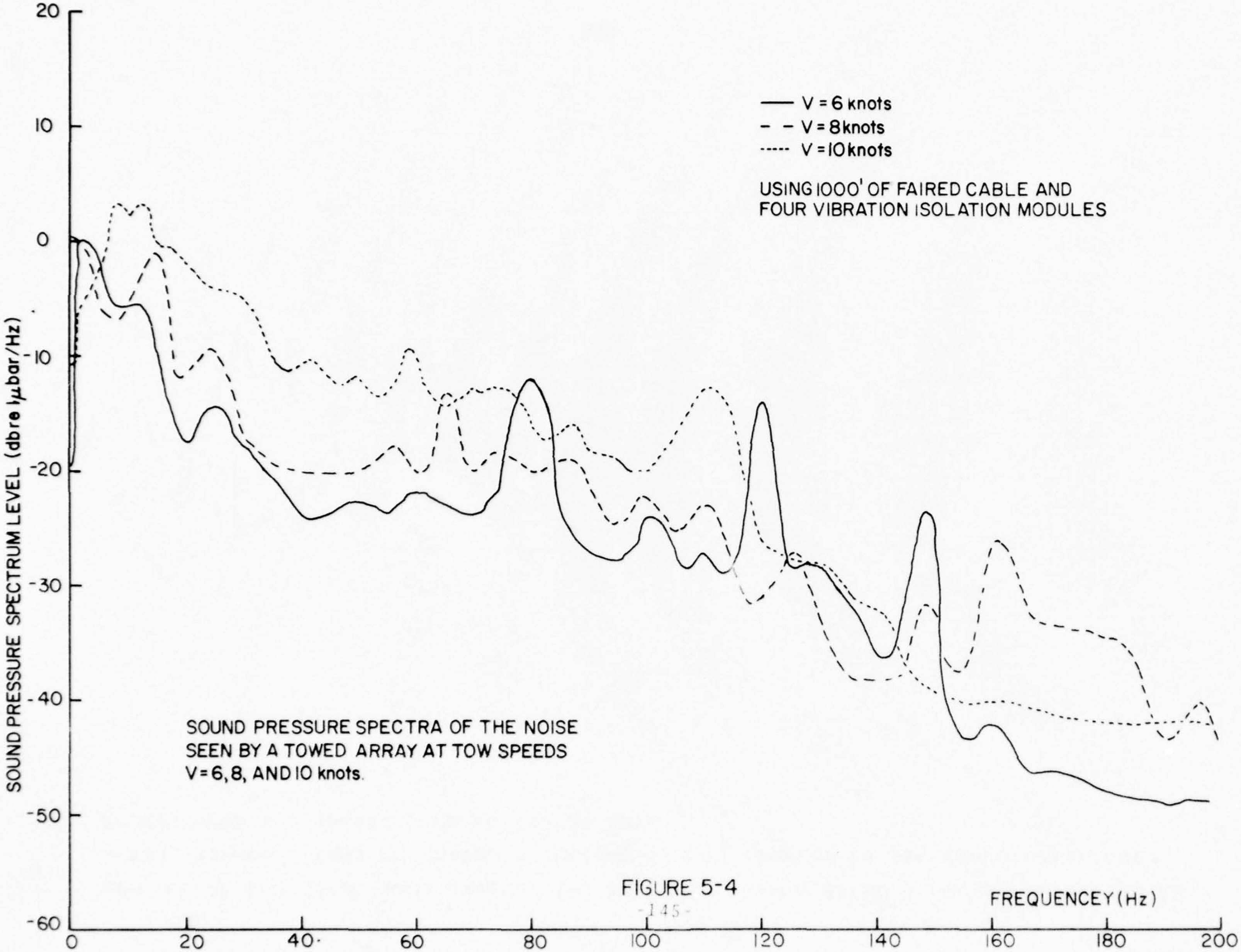

SOUND PRESSURE SPECTRA OF THE NOISE SEEN BY A TOWED ARRAY AT TOW SPEEDS V=6, 8, AND 10 knots.

FIGURE 5-4

greater than 9 dB at some frequencies but less than 3 dB at others. It should be noted, however, that the noise reduction is not limited to low frequencies but occurs over the entire 5 Hz to 140 Hz band.

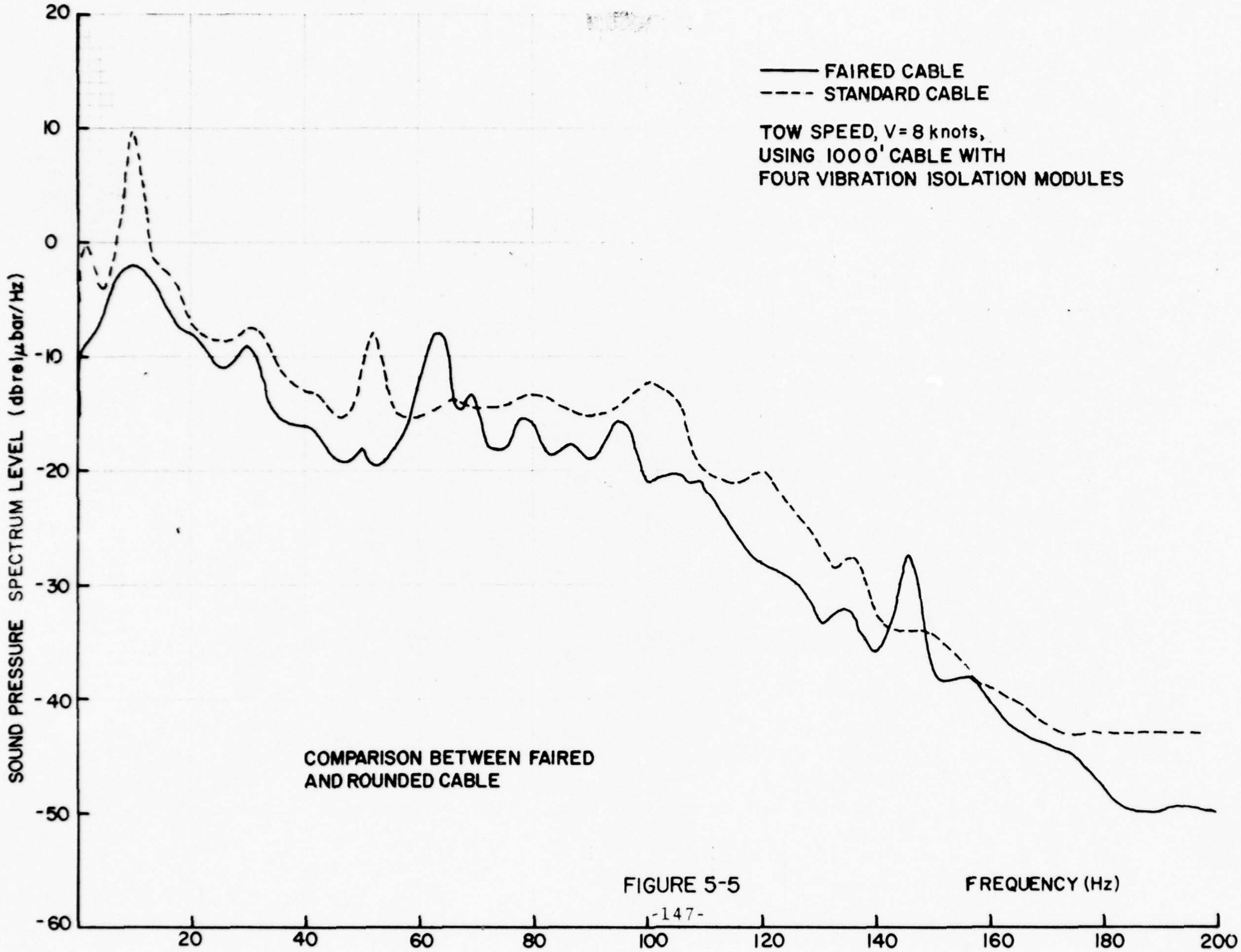
FAIRED CABLE
STANDARD CABLE
TOW SPEED, V = 8 knots,
USING 1000' CABLE WITH
FOUR VIBRATION ISOLATION MODULES
COMPARISON BETWEEN FAIRED
AND ROUNDED CABLE
SOUND PRESSURE SPECTRUM LEVEL (db re l μbar/Hz)
FREQUENCY (Hz)
20
10
0
-10
-20
-30
-40
-50
-60
20
40
60
80
100
120
140
160
180
200

FIGURE 5-5

THIS PAGE LEFT INTENTIONALLY BLANK.

5.2 Performance as a Function of Depth

5.2.1 Introduction

- In this section, we shall briefly consider the effect of depth on the performance of an array. More exactly, we shall consider the performance of a receiving array as a function of the relative depth of that array to the depth of some radiating source. Special attention shall be given to the cases when either the source or receiver (or both) are in the surface duct.

- In order to assess the performance of a receiving array as a function of depth we shall examine a series of graphs where transmission loss is plotted against range. These graphs do not represent experimental data, but are results generated by the FACT-X propagation model.

5.2.2 Performance

- In the following Figures, the transmission loss TL (in dB) between the source and receiver is plotted as a function of the range or distance between them (in miles). All curves were generated by the FACT-X model for the same general ocean area at the same time of year with the same bearing angle between the source and receiver and at the same frequency. The only difference from one figure to the next is the relative depth between source and receiver. The ocean depth for the area under consideration was in excess of 17,000'.

- Performance of a receiving array as a function of depth is typified in Figures 5-6 through 5-9 where the source depth is maintained at a constant 600'. The receiving system can tolerate a maximum transmission loss (TL_{MAX}) of, say, 100 dB and still detect the source. Thus, its detection range at a depth of 300' will be about 300 miles (Fig. 5-6). At a receiver depth of 500', or near the source depth, the detection range will be more than 400 miles which is also the case at a depth of 1000'. However, as shown in Figure 5-9, when the receiver is in the surface duct (i.e., at 60') its detection range will drop to a value below 70 miles.

- Similar results are obtained with the source maintained at a constant depth of 300'. That is, with the receiver at the same depth as the source (300') and assuming a required TL_{MAX} of 100 dB for detection as before, the FACT-X model indicates a detection range of over 450 miles. This range diminishes to about 375 miles at a receiver depth of 1000' and to about 80 miles at a depth of 3000' or greater. Again, with the receiver in the surface duct (60'), the model predicted a detection range of less than 60 miles.

- Completely analagous results were obtained for the different receiver depths when the source was maintained at a constant depth of 800'.

- As one would expect, when the source was maintained in the surface duct (60') and the receiver depth again varied from 60' through 4000', very poor detection ranges were predicted. In fact, using the same criterion as above (TL_{MAX}=100 dB), no detection range exceeded 100 miles for these cases.

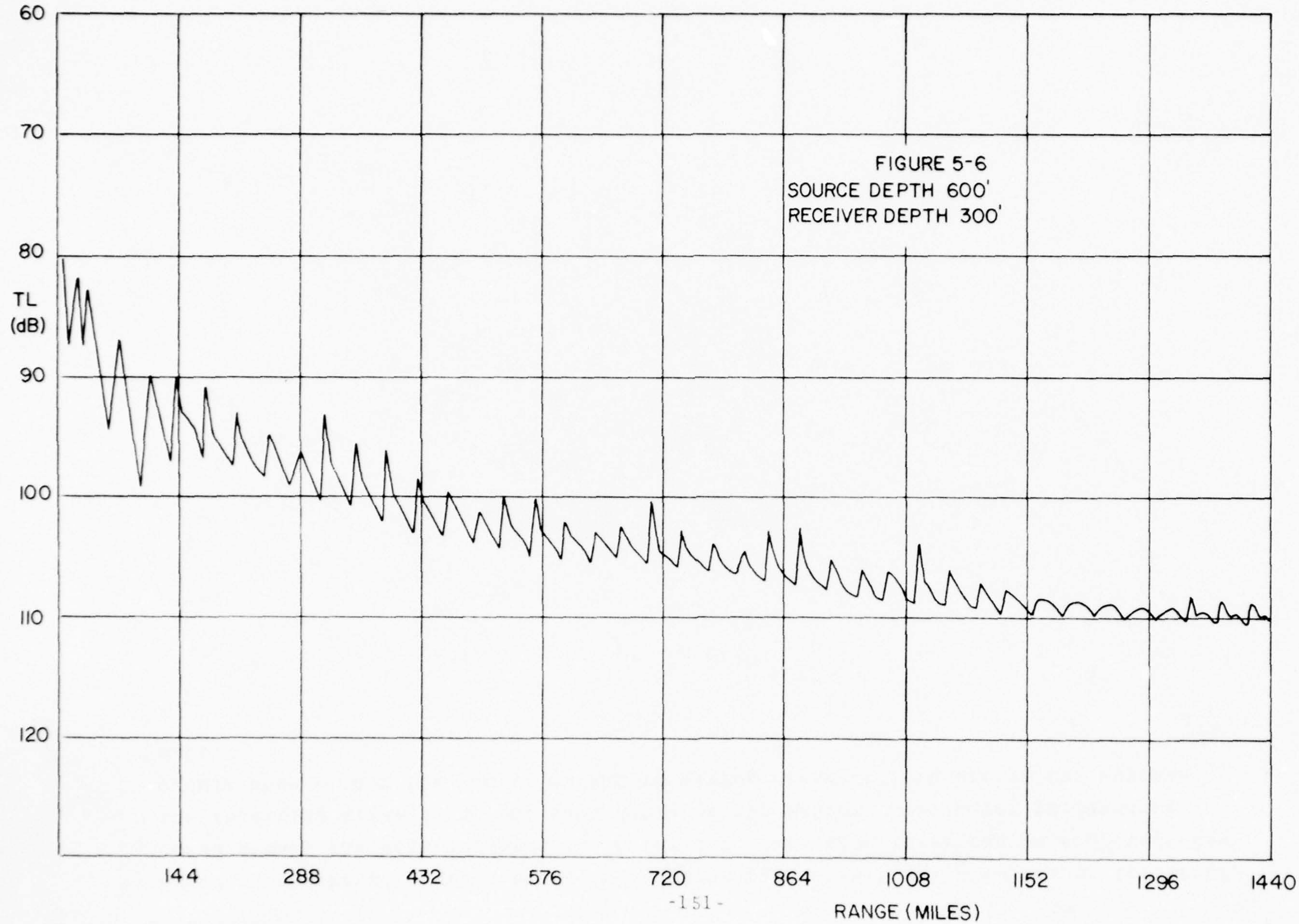
FIGURE 5-6
SOURCE DEPTH 600'
RECEIVER DEPTH 300'
TL
(dB)
60
70
80
90
100
110
120
144
288
432
576
720
864
1008
1152
1296
1440
RANGE (MILES)

5.2.3 Conclusions

- Based on the results given above in addition to FACT-X model predictions for other ocean areas, the best performance in terms of detection range can be expected when the receiving array is at the same depth as the source. The worst performance occurs when either the source or the receiving array or both are in the surface duct.

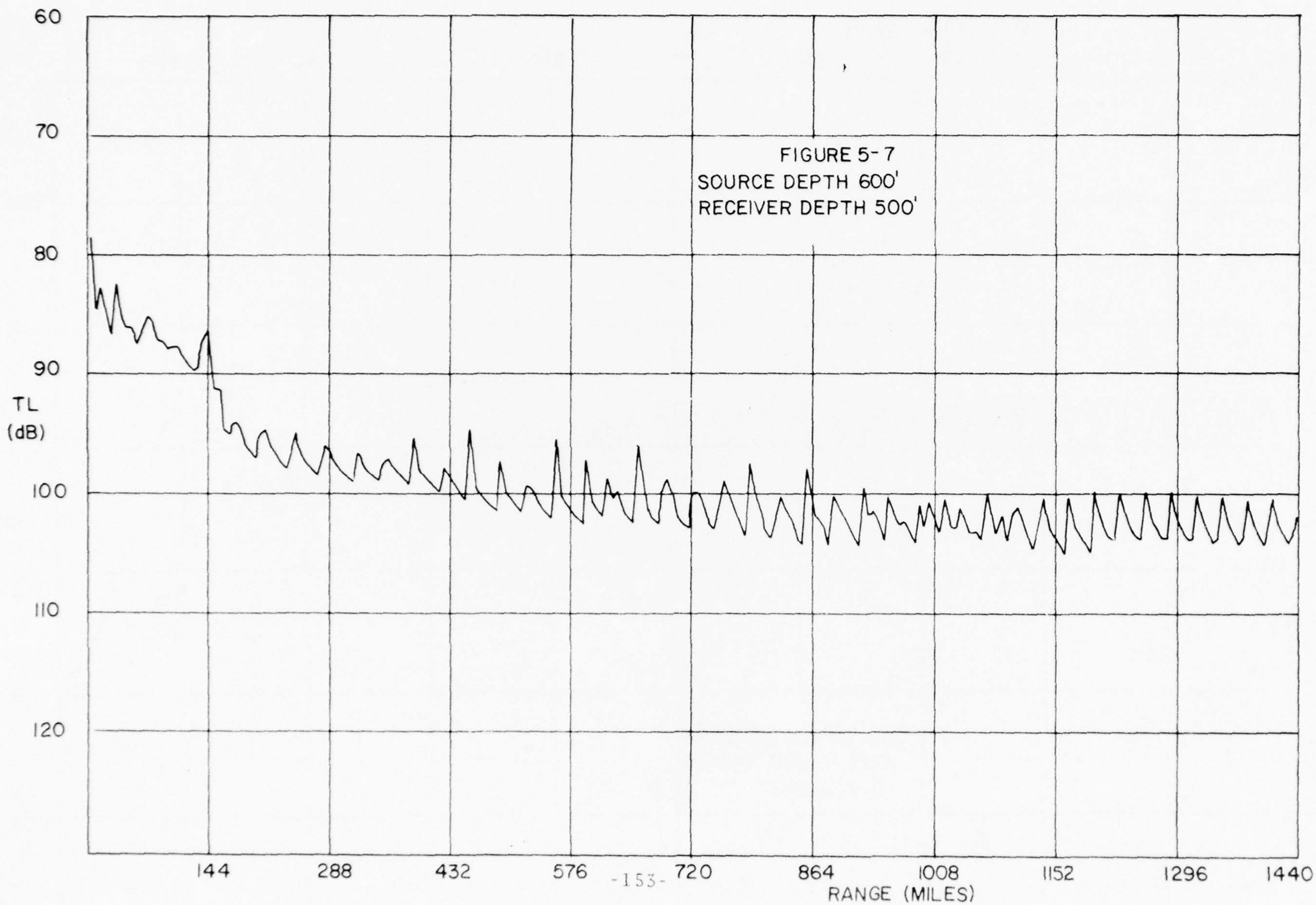

FIGURE 5-7
SOURCE DEPTH 600'
RECEIVER DEPTH 500'

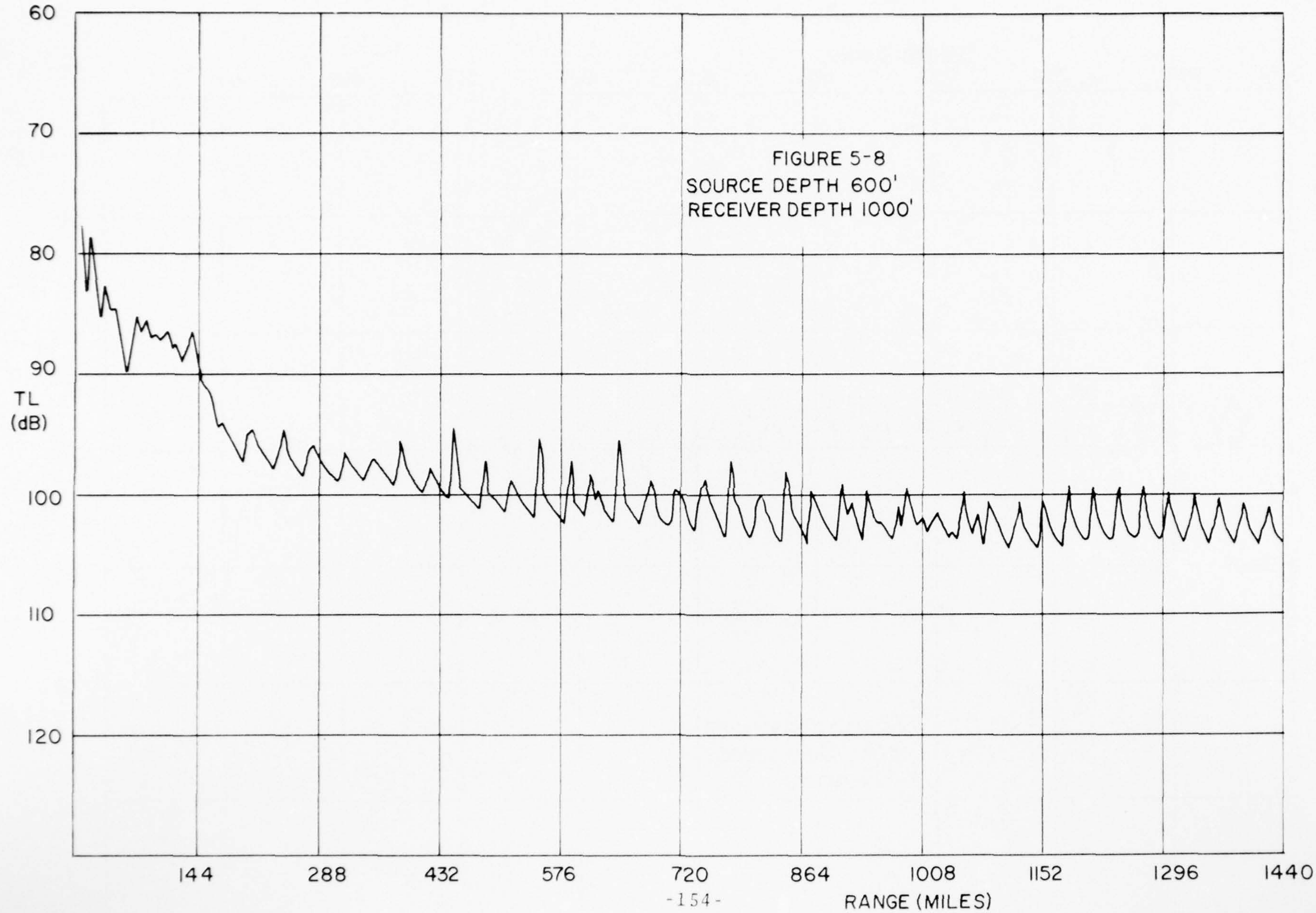
FIGURE 5-8
SOURCE DEPTH 600'
RECEIVER DEPTH 1000'
60
70
80
90
TL
(dB)
100
110
120
144
288
432
576
720
864
1008
1152
1296
1440
RANGE (MILES)

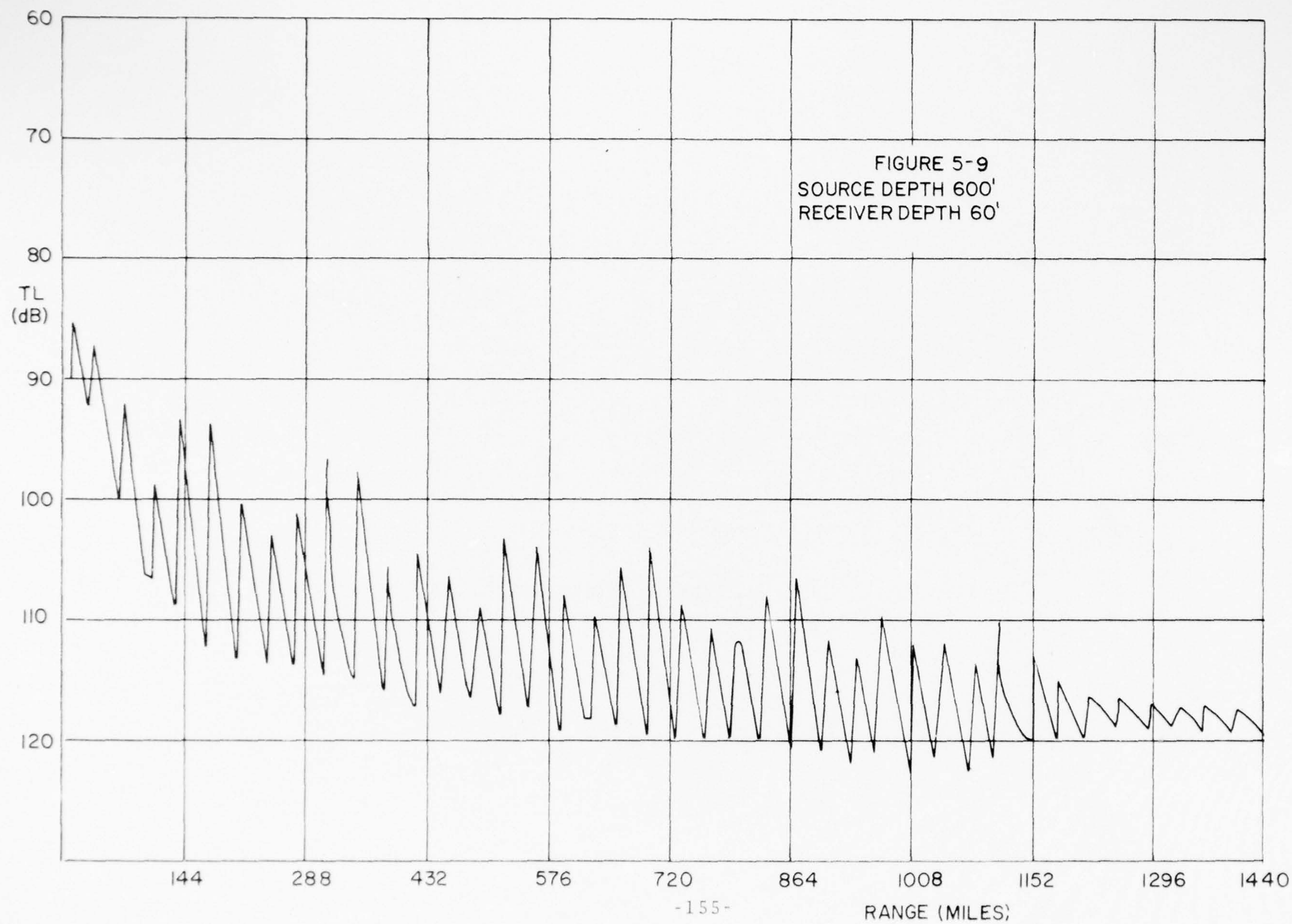
FIGURE 5-9
SOURCE DEPTH 600'
RECEIVER DEPTH 60'
TL
(dB)
60
70
80
90
100
110
120
144
288
432
576
720
864
1008
1152
1296
1440
RANGE (MILES)

THIS PAGE LEFT INTENTIONALLY BLANK.

5.3 Performance in a Multipath Environment*

5.3.1 Introduction

- Rays of acoustic energy arriving at a receiving array from more than one elevation angle ϕ(See Fig. 5-10) can affect the performance of the array and its associated beamformer. This condition, of course, is very common in the ocean environment where its seriousness depends on the source and receiver depths, the water depth, and on the sound velocity profile. An exact array performance analysis would be quite difficult if not impossible to conduct since it would depend on the detailed elevation arrival structure and its variability. Multiple elevation arrivals, however, should at least be considered in array design if only to estimate their effect on some of the more salient design features such as size and number of hydrophones.

5.3.2 General Problem

- The general problem of multipath arrival structure is demonstrated in Figure 5-10 where the plane of the paper represents a specific azimuth angle θ. Two rays are depicted which, because of the particular geometry involved (i.e., source depth, water depth and receiver depth), are entering two different preformed beams. This, of course, can lead to bearing ambiguity problems for the sonar operator, a subject with which we shall not be concerned.

- It is possible to calculate a loss due to multiple elevation arrivals across the (-3dB) beamwidth of a single beam. This will be presented in the following section.

---

*This section deals only with the effect of multiple arrivals at an array, an aspect of the "multipath problem" which is not very well documented in current texts.

5.3.3 Performance of a Line Array

- The performance of a line array is quite sensitive to the arrival elevation structure ϕ of acoustic rays. To demonstrate this fact, consider the beampattern of a line array of length L lying along the y-axis in Figure 5-11, which can be written as

$$b(\theta,\phi) = \frac{\sin^2[\pi L_y(\sin\theta\cos\phi-\sin\theta_b\cos\phi_b)]}{[\pi L_y(\sin\theta\cos\phi-\sin\theta_b\cos\phi_b)]^2} .$$

Here $L_y=L/\lambda$ is the array length in wavelengths, (θ,ϕ) the ray arrival azimuth and elevation, respectively, and (θ_b, ϕ_b) the beam steering azimuth and elevation, respectively.

- If only those ray arrivals at angles (θ,ϕ) near the main beam axis (θ_b,ϕ_b) are considered and if it is assumed that the total energy of the multiple arrivals is uniformly distributed over the elevation range $\phi_1\le\phi\le\phi_2 (\phi_1\ge 0)$, where

$$\phi_b = \frac{\phi_1+\phi_2}{2} ,$$

and if it is further assumed that adjacent beams are similar and that they overlap at their respective 3dB down points $(\theta_b+\theta_3,\theta_b-\theta_3)$, then one can calculate the following loss expression:

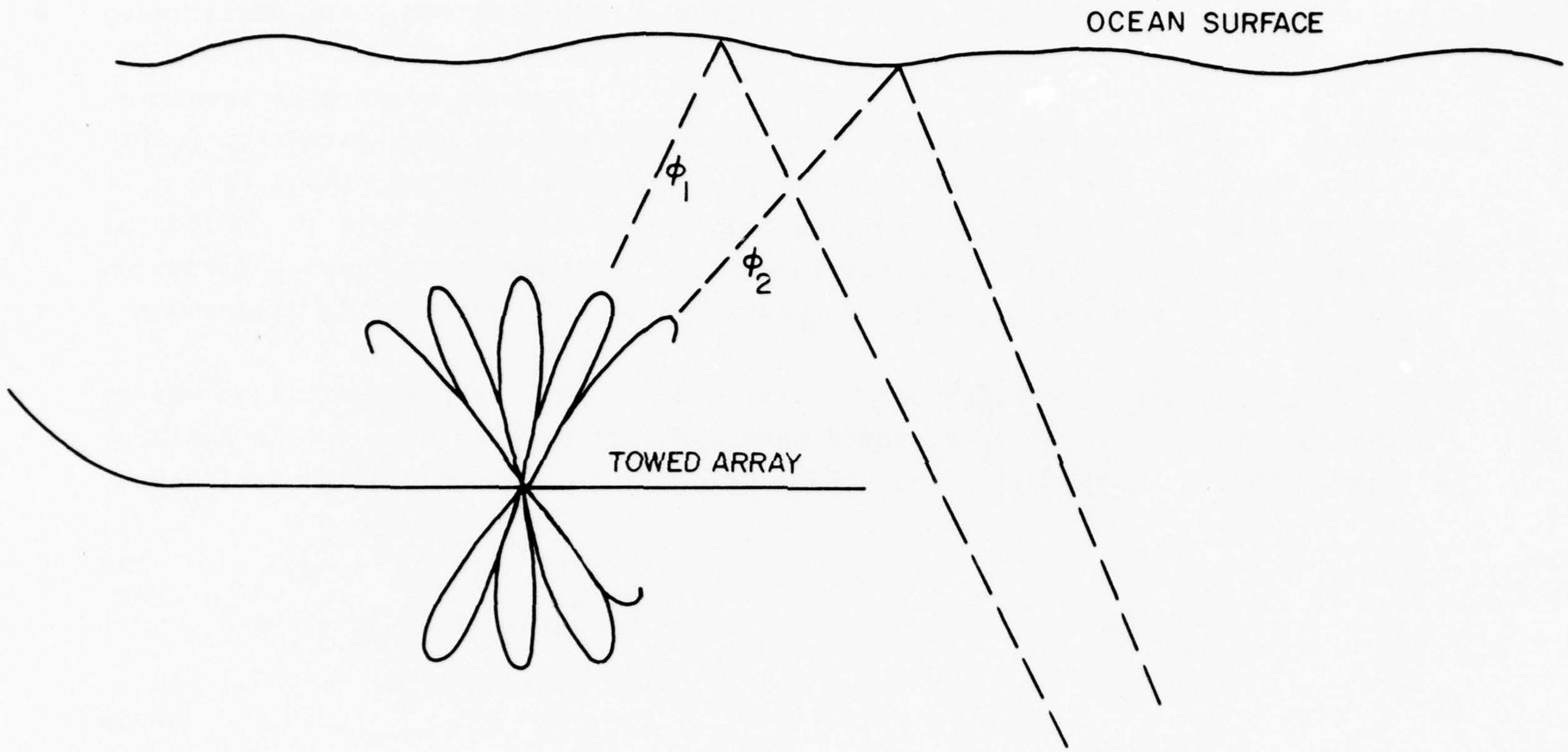

MULTIPATH RECEPTION

FIGURE 5-10

$$L(\gamma) = \frac{\displaystyle\int_{\eta(\theta_b-\theta_3)}^{\eta(\theta_b+\theta_3)} \int_{\eta+\frac{\pi\gamma}{2}}^{\eta-\frac{\pi\gamma}{2}} \frac{\sin^2 u}{u^2}\, du\, d\eta}{\displaystyle\int_{\eta(\theta_b-\theta_3)}^{\eta(\theta_b+\theta_3)} \frac{\sin^2\eta}{\eta^2}\, d\eta} .$$

Here, $u = \xi+\eta$,

$$\xi(\phi) = -\pi L_y(\phi-\phi_b)\sin\theta_b\sin\phi_b,$$

$$\eta(\theta) = \pi L_y(\theta-\theta_b)\cos\theta_b\cos\phi_b,$$

and $\gamma = [\phi_2-\phi_1]\, L_y\sin\theta_b\sin\phi_b$.

As written, the expression for $L(\gamma)$ represents the ratio of the average power received by the beam between its 3dB down points and elevation angles ϕ_2 and ϕ_1 to the power received for the "zero-multipath" condition or when $\phi_2=\phi_1=\phi_b$.

- The quantity $L(\gamma)$, which lies in the range $0\leq L(\gamma)\leq 1$, represents a "Loss" due to multipath reception as compared to zero-multipath or single elevation ($\phi_2=\phi_1=\phi_b$) reception. A plot of $L(\gamma)$ versus γ, the multipath parameter, is given in Figure 5-12. It should be noted that for a given range of elevation arrivals, the loss ($L(\gamma)$) increases with steering angle θ_b from a zero dB value at broadside and also increases with array length.

- Considering this loss $L(\gamma)$ due to multiple elevation arrivals, it is important from a practical viewpoint to determine whether a specific "gain" can be obtained and the

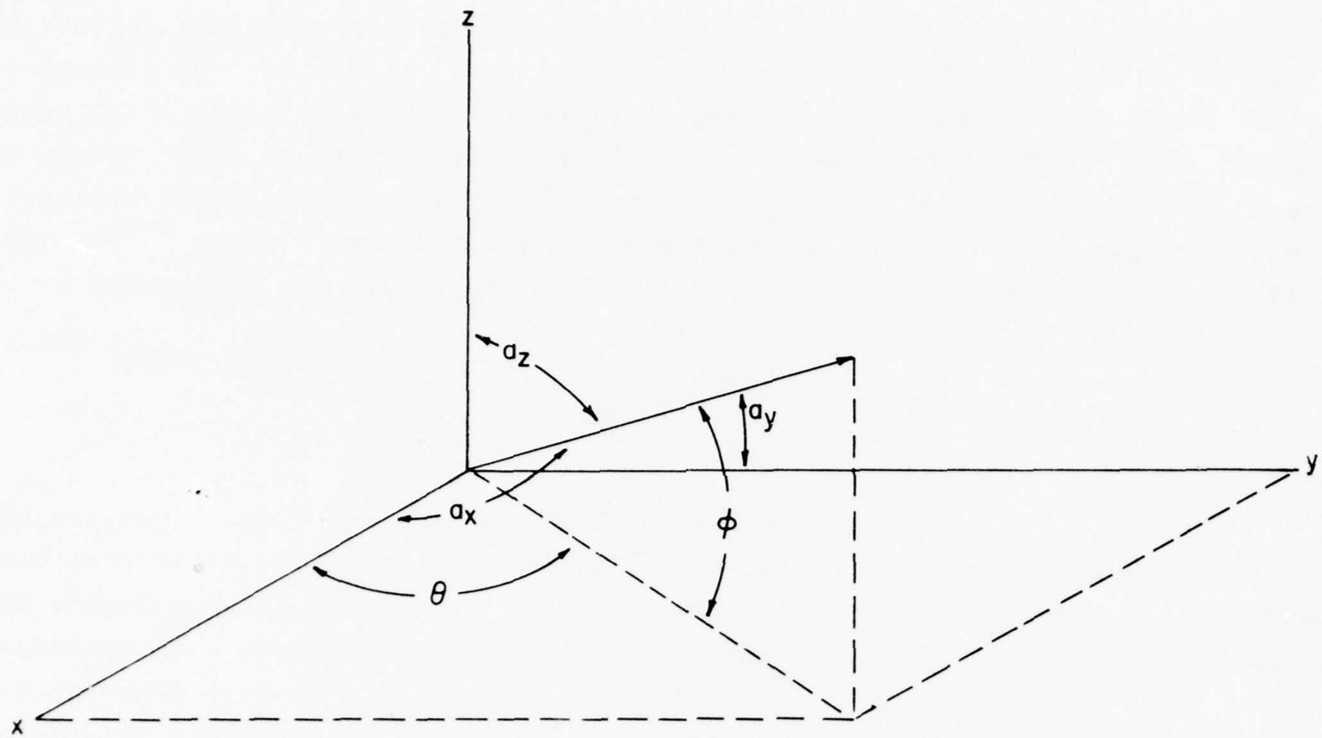

COORDINATE SYSTEM FOR ARRAY CALCULATIONS

FIGURE 5-11

array length necessary to obtain it. In the present case gain will be defined as the product of the array's directivity ($\approx 2L_y$ at half-wavelength spacing) and the loss factor $L(\gamma)$ given above*. Figure 5-13 is a plot of this gain versus array length with the quantity

$$\gamma_1 = (\phi_2 - \phi_1)\sin\theta_{bmax}\sin\phi_b$$

serving as a parameter. Here, θ_{bmax} is the maximum allowable steering angle whose significance will be demonstrated shortly. Thus, for a specified gain, one can determine the required array length from Figure 5-13 and therefore the corresponding number of hydrophones (at half-wavelength spacing) necessary to achieve this gain in a given multipath environment. A detailed example is given in the following section. The number of hydrophones is given by

$$N = 2L_y + 1 \ .$$

5.3.4 Example

- As an example of the use of Figure 5-13, determine the maximum allowable steering angle θ_{bmax} for a given gain requirement (say 18 dB) in an environment where the elevation angles range from up $\phi_1 = 5^o$ to $\phi_2 = 25^o$. Figure 5-13 shows that in order to obtain an 18 dB gain a value of $\gamma_1 \leq .02$ is required. Thus, from the definitions of γ_1 and ϕ_b (i.e., $\phi_b = (\phi_1 + \phi_2)/2$) it can be shown that the steering angle should be be limited to $-13^o < \theta_b < 13^o$ from broadside. Steering angles in excess of this limitation for the same elevation structure will result in some gain degradation. This

* Note that for the "no-multipath" condition, the loss becomes 0 dB and the defined gain simply reduces to the array directivity.

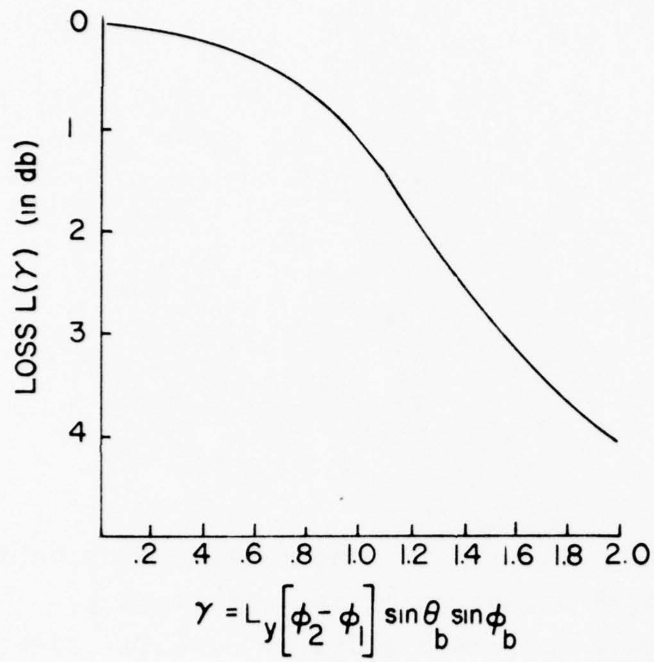

LOSS AS A FUNCTION OF THE MULTIPATH PARAMETER γ

FIGURE 5-12

is shown for another case in Figure 5-14 where the desired gain of 17 dB is not quite achieved in a multipath environment due to steering beyond the allowable θ_{bmax}.

5.3.5 Planar Array Performance

- To obtain improved performance in a multipath environment over that provided by linear arrays, it is necessary to use planar or multidimensional arrays. These are practically insensitive to multiple elevation arrivals, a fact which is demonstrated in Figure 5-15 where the variation in the gain of a planar array due to multiple elevation arrivals is negligible.

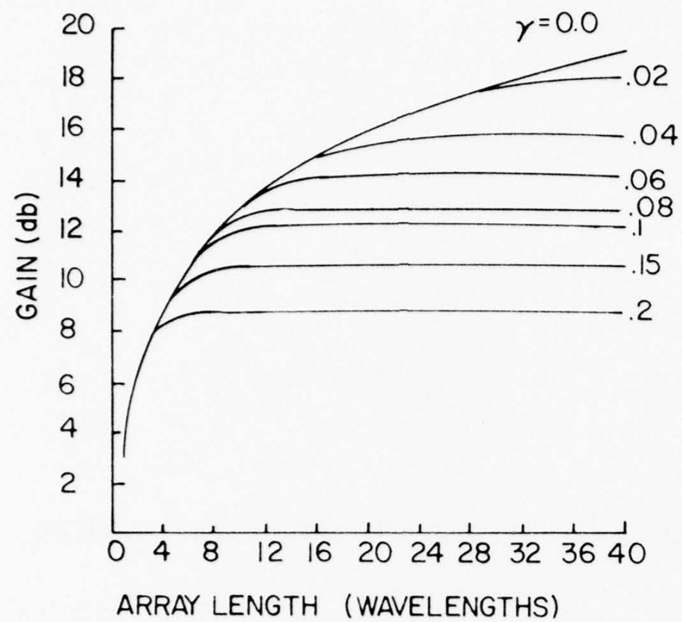

GAIN OF AN ARRAY AS A FUNCTION
OF LENGTH

FIGURE 5-13

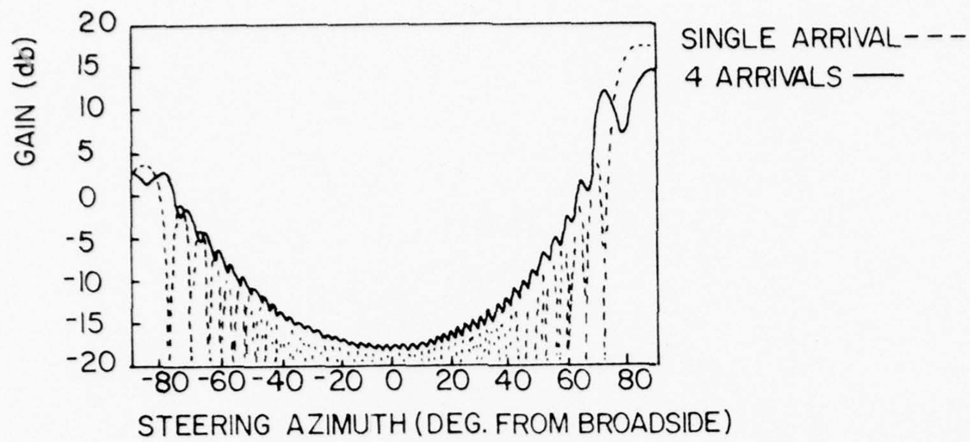

RESPONSE AS A FUNCTION OF STEERING ANGLE

FIGURE 5-14

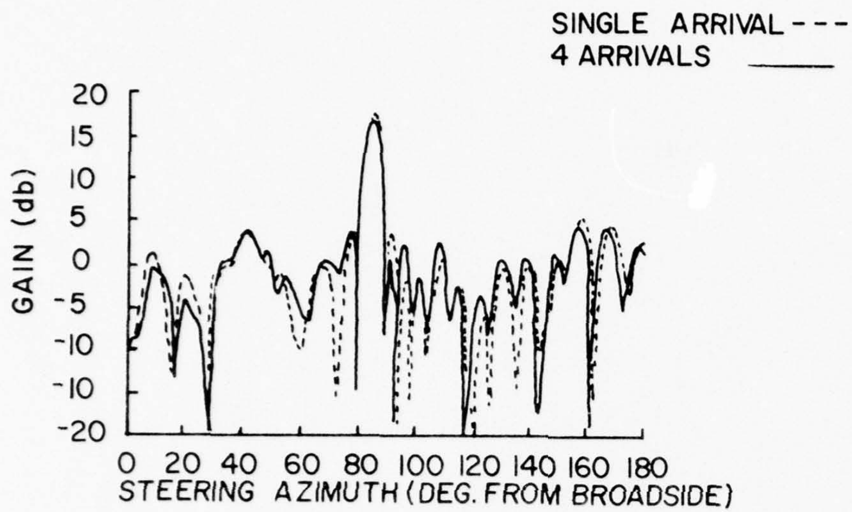

RESPONSE OF A PLANAR ARRAY AS A FUNCTION OF STEERING FOR A SOURCE 85° OFF BROADSIDE

FIGURE 5-15

THIS PAGE INTENTIONALLY LEFT BLANK.

5.4 Performance With Random Errors

5.4.1 Introduction

- Once an array has been designed to produce a desired pattern, it is usually found that the measured result falls short of the expected result, particularly where the sidelobes are concerned. One reason for this is that errors have been incorporated into the structure of the aperture. Certain types of errors are deterministic in that they are the effect of a known cause and can be predicted. For example, the structure that supports the array in many cases interferes with and thereby causes errors to occur in the radiation pattern. Still other types of errors are random and their effects must be determined through statistical analysis. An example of this type can be found in modularly constructed arrays where the individual module lengths vary randomly and cause similar variations in the inter-element hydrophone spacings.

- The following presentation will deal with the effects of random errors on the

  Beampattern,

  Directivity,

  Sidelobe Level, and

  Direction of the Main Beam (Beam Pointing).

  Moreover, it will dwell on planar arrays with the corresponding results for linear arrays obtained as a special case by letting one dimension shrink to a limit.

5.4.2 Effect of Output Amplitude and Phase Errors on the Beampattern of an Array

- Consider a two-dimensional MxN element array with elements spaced a distance d apart with the following conditions: the amplitude* and phase-errors at the output terminals of each element are independent of each other and also from element to element and, the amplitude error is distributed uniformly across the aperture while the phase error distribution is Gaussian. The beampattern $\bar{b}\,(\theta,\phi)$ then becomes

$$\bar{b}\,(\theta,\phi) = b_o(\theta,\phi)+S(\theta,\phi)\,\overline{\varepsilon^2}\,\frac{\sum_{m=1}^{M}\sum_{n=1}^{N} I_{mn}^{2}}{\left[\sum_{m=1}^{M}\sum_{n=1}^{N} I_{mn}\right]^2} .$$

In this expression,

$b_o(\theta,\phi)$ = desired errorless beam pattern

$S(\theta,\phi) = \cos\theta(\cos^2\theta\cos^2\phi+\sin^2\phi)$ = obliquity factor

$\overline{\varepsilon^2}$ = total mean-square error = $\overline{\Delta^2}+\overline{\delta^2}$

$\overline{\Delta^2}$ = normalized mean-square amplitude error

$\overline{\delta^2}$ = mean-square phase error in radians, and

I_{mn} = output amplitude (i.e. current) of the mnth array element.

---

* The amplitude errors mentioned here are equivalent to errors in tne element amplitude weighting coefficients.

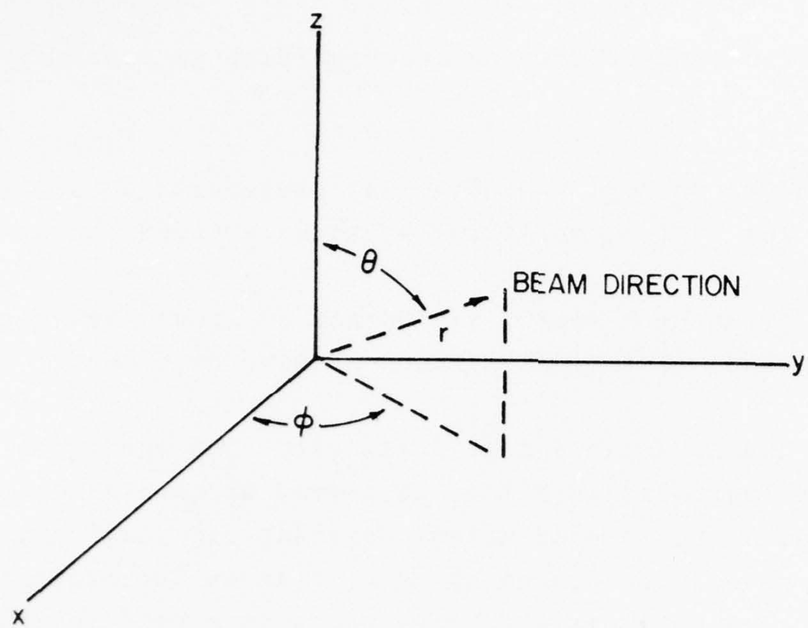

FIGURE 5-16

The angles ϕ and θ are shown in Figure 5-16 where the MN elements lie in the xy plane. In the case of a line array, simply ignore the summation over the index m.

5.4.3 Effect of Output Amplitude and Phase Errors on the Sidelobe Level

- The (statistical) sidelobe level distribution of a beampattern under the error conditions given in the previous section is described by a modified Rayleigh distribution. That is, the distribution of the sidelobe level about its mean value obeys modified Rayleigh statistics.

- An example of such a sidelobe level distribution for a 25-element Dolph-Chebyshev array designed for an errorless -29 dB sidelobe level is given in Figure 5-17. This Figure gives the fraction (percentage of the total distribution) of sidelobe levels below a certain number of decibels (ordinate) as a function of the total rms $(\varepsilon^2)^{1/2}$ amplitude and phase error in the array output (abscissa).

- Figure 5-17 can also be made *roughly applicable to a 50-element array with the same* Dolph-Chebyshev taper by moving all curves down by -3 dB.

- A limit to the total acceptable rms error $(\overline{\varepsilon^2})^{1/2}$ for the given Chebyshev shaded array(s) can be determined from Figure 5-17 once one has decided upon a "worst-case" sidelobe level.

5.4.4 Effects of Errors in Array Element Postion and Orientation on the *Sidelobes*

- In a two-dimensional array of (MxN)dipole* elements, consider the three-dimensional translational position errors of each element *along* with the two-*dimensional angular*

* Any conclusions drawn here will also be approximately correct for omnidirectional elements.

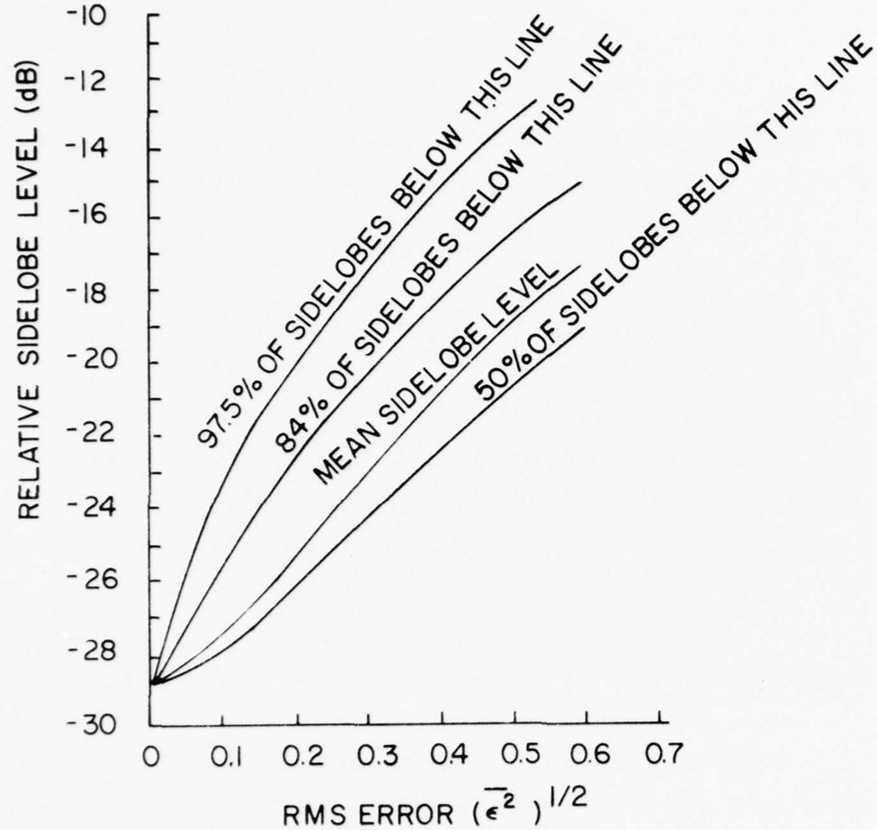

SIDELOBE DISTRIBUTION DUE TO RANDOM OUTPUT ERRORS FOR A 25 ELEMENT DOLPH-CHEBYSHEV ARRAY DESIGNED FOR -29 dB SIDELOBE SUPPRESSION.

FIGURE 5-17

(θ,ϕ) errors in each element's orientation. The random errors in the outputs of each element, as discussed in Section 5.4.2, are also included in this consideration and assumed to be independent of the translation and orientation errors. Moreover, the translation errors and the orientation errors are assumed to be independent of each other and described by Gaussian statistics. An analysis of these errors has led to the following conclusions:

Translational errors in element position have the most significant effect on sidelobe level and on the beampattern in general;

As one might expect, the effects of dipole orientation errors are essentially negligible;

Additional results are provided in Figure 5-18 where the ordinate is the upper limit of the average sidelobe level in a variety of *Dolph-Chebyshev arrays*. *The* abscissa is the rms error σ in element translation which is assumed to be equal along any of the three rectangular coordinate axes. The parameter F is defined by the ratio σ_{mn}/I_{mn}, where σ_{mn} is the rms error in the output amplitude I_{mn} of the mn^{th} dipole element (i.e. See Section 5.4.2).

5.4.5 Effect of Output Errors on the Array Directivity

- The effect of the random errors described in Section 5.4.2 on array directivity has also been determined. If the errorless directivity of the array is denoted

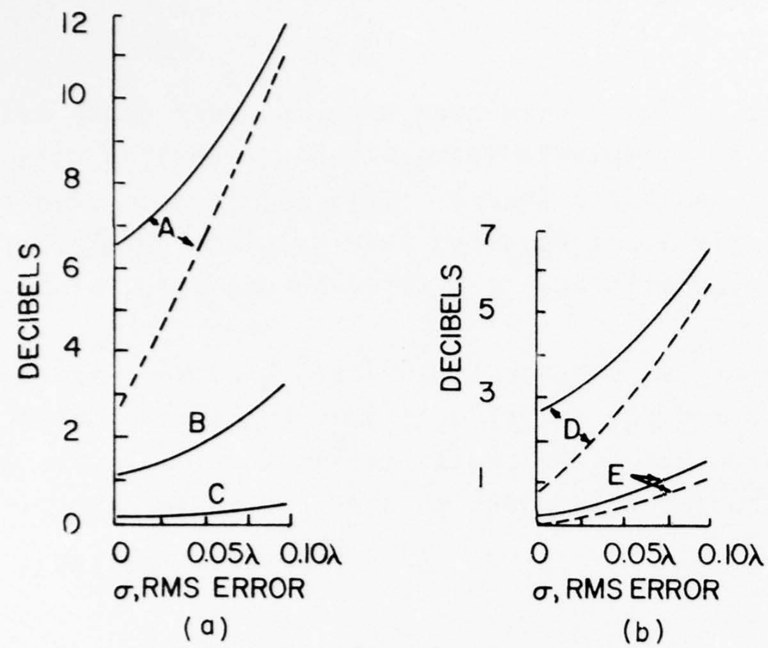

FIGURE 5-18 Upper bound on the mean rise in sidelobe level due to random errors for various Dolph-Chebyshev arrays as a function of the tolerance σ (in wavelength fractions) and the current parameter, F. F=0.25 for the solid curves and F=0.125 for the dashed curves. Curves A: 24 elements, 40 dB sidelobe design; Curve B: 24 elements, 30 dB design; Curve C: 24 elements, 20 dB design; Curves D: 48 elements, 40 dB design; Curves E: 144 elements, 40 dB design.

FIGURE 5-18

by D_o and the directivity with errors is denoted by D, then the reduction in the broadside directivity due to these errors is approximately

$$D = \frac{D_o}{1+\frac{3\pi}{4}\left(\frac{d}{\lambda}\right)^2 \overline{\varepsilon^2}}$$

Here, d is the interelement spacing, λ is the wavelength and $\overline{\varepsilon^2}$ is again the total mean-square output amplitude and phase error. This expression, which is independent of the actual element outputs and array size is valid if; there is negligible coupling between array elements, there are no grating lobes (i.e., $d/\lambda<1$) and the number of array elements is large.

5.4.6 *Beam Pointing Error*

- The results of an analysis of the beam pointing error associated with a line array with a uniform aperture distribution is given in Figure 5-19. In the analysis, it was assumed that the output amplitude and phase errors from each array element were independent of each other and described by Gaussian statistics.

- In Figure 5-19, the quantity E is the allowable rms interelement phase error (in radians) such that the beam pointing error will lie in the interval $(-\theta,\theta)$ with the indicated probability $p(\theta)$. Curves are given for three separate array lengths L, all with half-wavelength element spacing. The normalizing angle θ_N of the abscissa is the angle from the main beam axis ($\theta=0$) to the first null.

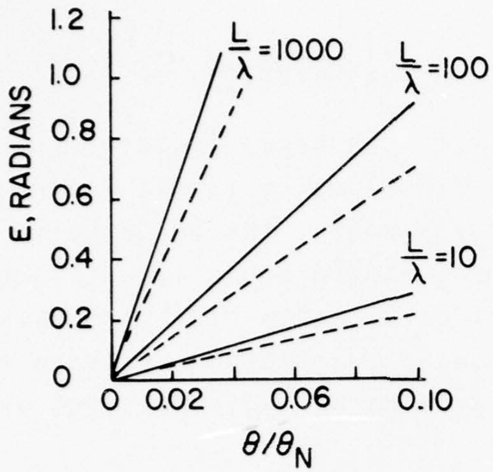

FIGURE 5-19 E versus θ/θ_N, where E is the rms interelement phase error such that the beam pointing error will lie in the interval $(-\theta,\theta)$ with a probability $\rho(\theta)$; $\rho(\theta) = 0.95$ for the solid curves, $\rho(\theta) = 0.99$ for the dashed curves. θ_N is the angle to the first null and L is the array length. Element spacing is half-wavelength.

FIGURE 5-19

- Aside from this general analysis, a specific source of beam pointing error arises from the variation in the local sound propagation speed near the array. Defining the percent sound speed error α as

$$\alpha = 100\left|\frac{s_o - s}{s}\right|$$

where s_o is the assumed sound speed and s is the actual sound speed, the beam pointing error $\delta\theta$ is given by

$$\delta\theta=\theta-\sin^{-1}\left[\frac{100\sin\theta}{100+\alpha}\right].$$

Here, θ is the assumed beam pointing direction referenced to broadside. A plot of $\delta\theta$ versus θ is given in Figure 5-20 for various values of α.

- Applying the proper phase shift or steering to only one frequency in a band results in a beam pointing error at the other frequencies (and also a loss in response to a wideband signal). This degradation in performance can be reduced by filtering to sufficiently small bands before beam forming. To describe this effect, consider that a given phase shift steers the band center frequency f to the angle θ and the frequency $(f+\Delta f)$ to the angle θ'. Defining $\rho=100\Delta f/f$ as the percent bandwidth, the beam pointing error $\delta\theta$ will be

$$\delta\theta=\theta-\sin^{-1}\left[\frac{100\sin\theta}{100+\rho}\right],$$

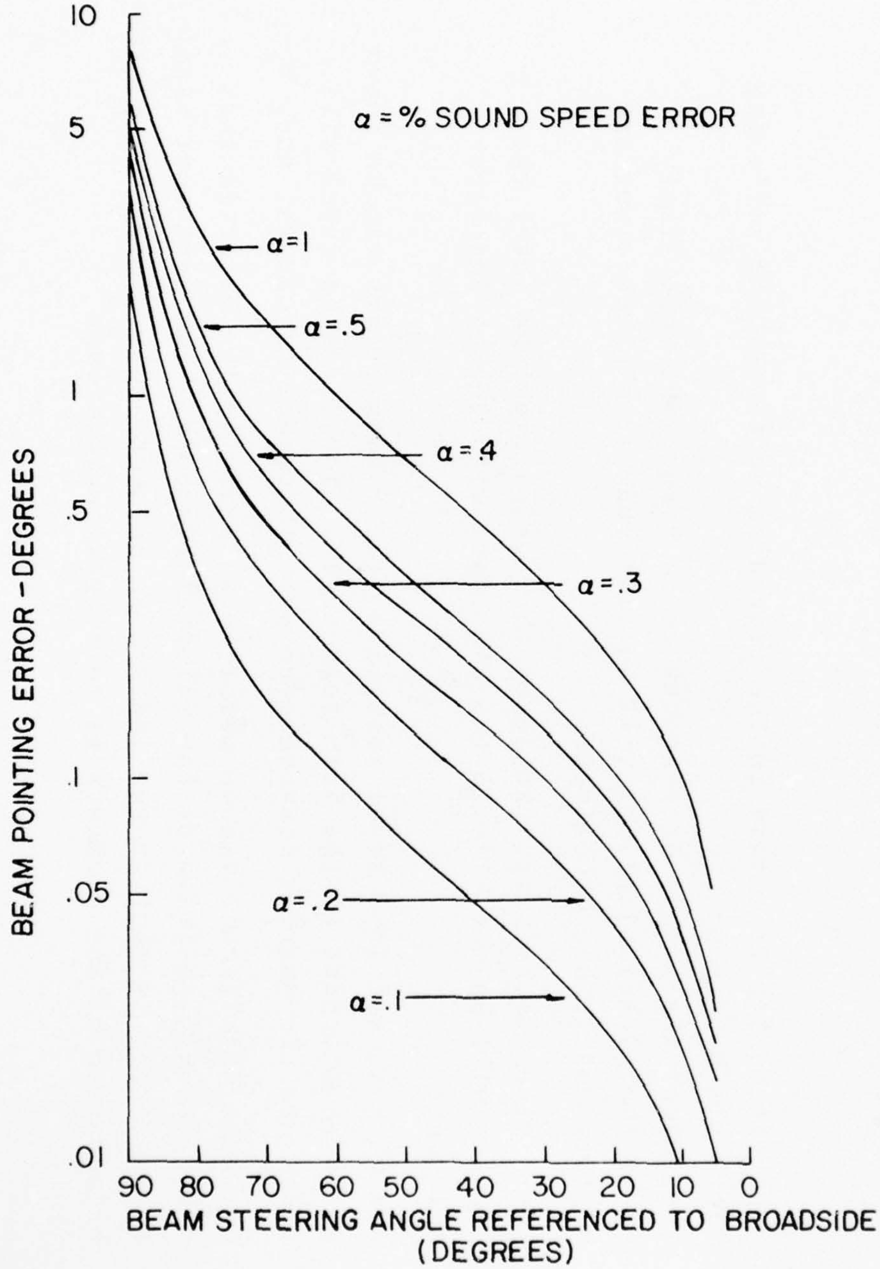

BEAM POINTING ERROR DUE TO SOUND SPEED ERROR

FIGURE 5-20

where θ is the assumed beam pointing direction referenced to broadside. This expression for $\delta\theta$ can also be represented by Figure 5-20 merely by interchanging the α values therefor ρ values. Thus, in Figure 5-20, the beam pointing error $\delta\theta$ for an $\alpha = 0.1\%$ sound speed error is the same as the beam pointing error for a $\rho=0.1\%$ bandwidth error at any beam steering angle. Note that there is no error at broadside ($\theta=0$) and that the maximum error occurs at endfire.

5.4.7 Summary

In summarizing the discussion of errors in the preceding sections, the following general conclusions can be drawn:

The larger the number of elements in an array, the more likely it is that lower sidelobes will be achieved for a given error and a given design sidelobe level;

For a given array size, the lower the design sidelobe level the greater will be the rise in the sidelobes with increasing error tolerance;

The rise in sidelobe level resulting from random errors can be shown to be independent of the beam scan angle. The sidelobe level will rise when the beam is scanned even when there are no errors; and,

The most significant random error in an array is the error in the translational position of the (dipole) elements. The next most significant error is that in the individual element amplitudes. The angular orientation of the elements is relatively unimportant.

5.5 Array Signal Gain with Phase and Amplitude Fluctuations

5.5.1 Introduction

- In this section we shall present the results of an analysis of the effects of normally (Gaussian) distributed signal amplitude and phase fluctuations on the signal gain of an array. This will be followed by a similar treatment of noise gain and finally a determination of array signal-to-noise gain. It might be noted that the results given herein are valid for all (normally distributed) phase and amplitude errors between the source and the array output, wherever they occur, and are not limited to those errors caused by the medium only.

- Random amplitude and phase fluctuations in the signals and noise arriving at each element of an array can lead to the degradation of the array signal-to-noise gain from its errorless or ideal value. The effect of these fluctuations on the array signal gain can be determined from their effect on the value of the squared time-averaged output signal voltage. An analogous procedure will determine their effect on array noise gain and a consistent definition of both of these gains will then allow the determination of the resulting degradation in the array signal-to-noise gain.

5.5.2 Squared Time-Averaged Output Signal Voltage (Average Signal Power)

- The signal voltage at the output of the k^{th} omnidirectional hydrophone in an array of N such elements can be written in the form

$$V_k = a_k \cos(\omega t + \delta_k + b_k) ,$$

where ω = angular frequency of the signal

a_k = random amplitude of the output from element k

δ_k = non-random component of phase in the output from element k such as that associated with steering angle

b_k = fluctuating or random component of phase from the output of element k.

The output voltage from the entire N element array is then the summation given by

$$V = \sum_{k=1}^{N} a_k \cos(\omega t + \delta_k + b_k) = C \cos(\omega t + m) ,$$

where the quantity C is dependent on the randomly distributed amplitudes a_k and phases b_k, as is m. Since the squared time-averaged output signal voltage of the array $\overline{V^2}$ is given by

$$\overline{V^2} = (1/2)\, C^2 ,$$

then the expectation value (i.e. mean value) of C^2 can be used as a measure of $\overline{V^2}$.

AD-A038 073 APPLIED HYDRO-ACOUSTICS RESEARCH INC ROCKVILLE MD F/G 17/1
HANDBOOK OF ARRAY DESIGN TECHNOLOGY. VOLUME I.(U)
JUN 76 N00039-76-C-0015

UNCLASSIFIED NL

3 OF 3
ADA038073

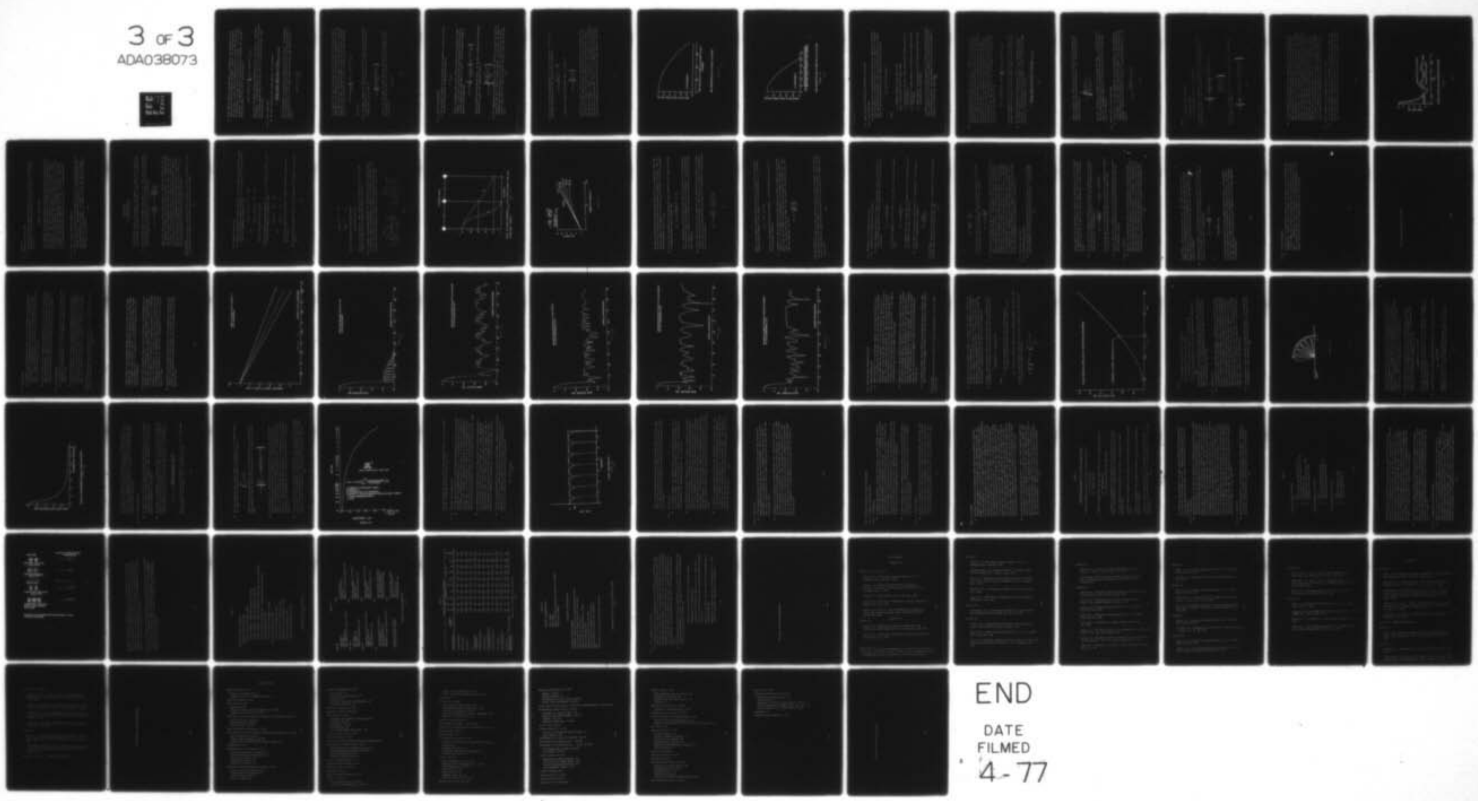

END
DATE
FILMED
4-77

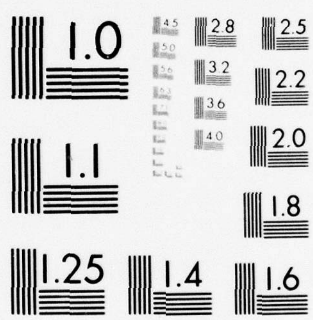

MICROCOPY RESOLUTION TEST CHART
NATIONAL BUREAU OF STANDARDS-1963-A

- Assume that the phase b_k and amplitude a_k distributions are independent of each other and that both are normally distributed. Moreover, let the amplitudes have the mean value, a, and an rms (or standard) deviation, A, about this mean and let the phases have a zero mean and an rms deviation, B (in radians). If it is further assumed that the amplitudes are not correlated whereas the phases are, then the expectation value of C^2 or $E[C^2]$ can be written as

$$E[C^2] = N(A^2+a^2)+a^2 \sum_{k\neq j}^{N}\sum \cos(\delta_k-\delta_j)\exp[-B^2(1-\rho_{kj})] ,$$

where ρ_{kj} is the phase correlation coefficient and B^2 is the variance f the phase distribution. As indicated above, $E[C^2]$ is twice the expectation value of the squared time-averaged output voltage of the array, $\overline{V^2}$, or twice the average output signal power of the array.

5.5.3 Array Signal Gain

- The array signal gain at a given frequency can be defined as

$$G = \frac{\text{average output signal power of array}}{\text{average output signal power of reference receiver}} ,$$

where the numerator is one-half of the expression for $E[C^2]$ above. The denominator in this definition is one-half of the expression for $E[C^2]$ for the special case of a single element or N=1. For a single element the average output signal power is given by

$$\frac{1}{2} E[C^2] = \frac{1}{2} (A^2+a^2) .$$

It is apparent that phase fluctuations contribute nothing to the average output signal power of the reference receiver and that amplitude fluctuations result only in an additional term of one-half the square of the rms deviation, A. Using this expression in the array signal gain definition along with the general expression for $\frac{1}{2} E[C^2]$, the following result in (dB) is obtained for the array signal gain

$$G=10 \log\{N+\frac{1}{1+d^2} \sum_{k\neq j}^{N}\sum \cos(\delta_k-\delta_j)\exp[-B^2(1-\rho_{kj})]\} ,$$

where $d \equiv A/a$.

- As an example, consider the expression for the array signal gain in the direction of peak response (i.e., $\delta_k-\delta_j=0$) for the case of completely uncorrelated phase fluctuations ($\rho_{kj}=0$), which is

$$G = 10 \log\left\{\frac{Nd^2+N(1-e^{-B^2})+N^2e^{-B^2}}{d^2+1}\right\} .$$

Moreover, for the ideal case where there are no amplitude fluctuations ($A=d=0$) and no phase fluctuations ($B=0$), this expression reduces still further to the familiar form

$$G=10 \log N^2 .$$

5.5.4 Signal Gain Degradation

- One can define a quantity D that describes the degradation in signal gain resulting from the fluctuations in amplitude and phase as

$$D = G_F - G_I \ .$$

Here, D is defined so that it will always be negative in the direction of peak response ($\delta_j - \delta_k = 0$) with G_F being the signal gain including fluctuations and G_I the ideal signal gain, given above as $10 \log N^2$. For the direction of peak response it can be shown that

$$D = 10 \log \left\{ \frac{1}{N} + \frac{1}{N^2(1+d^2)} \sum_{k \neq j}^{N}\sum \exp\left[-B^2(1-\rho_{kj})\right] \right\} ,$$

where all terms have been defined above. If the phase fluctuations are completely uncorrelated ($\rho_{kj}=0$), this expression reduces to

$$D = 10 \log \left\{ \frac{\frac{d^2}{N} + \frac{1-e^{-B^2}}{N} + e^{-B^2}}{d^2+1} \right\} .$$

- It is apparent that the numerator of this last expression is always less than the denominator (for N>1) so that D is always negative. In other words, the effect of amplitude and/or phase variations is to reduce the signal gain in the direction of peak response below the value that would be obtained if there were no fluctuations.

- Two cases of signal gain degradation are of special interest. If there are no amplitude fluctuations (d=0) the expression for D reduces to

$$D = 10 \log \left[\frac{1-e^{-B^2}}{N} + e^{-B^2} \right] .$$

If there are no phase fluctuations (B=0) it reduces to

$$D = 10 \log \left[\frac{\frac{d^2}{N} + 1}{d^2 + 1} \right] .$$

Figure 5-21 is a plot of the first of these expressions for a 40 element (N=40) array and shows the reduction in array signal gain due to phase fluctuations only. The abscissa in Figure 5-21 is the rms deviation B of the fluctuation in phase angle plotted in degrees. Figure 5-22 is a plot of the second of these expressions, also for the case N=40. It shows the reduction in array signal gain that results from amplitude fluctuations only, versus d. It is apparent that large phase fluctuations will degrade the array signal gain more than large amplitude fluctuations.

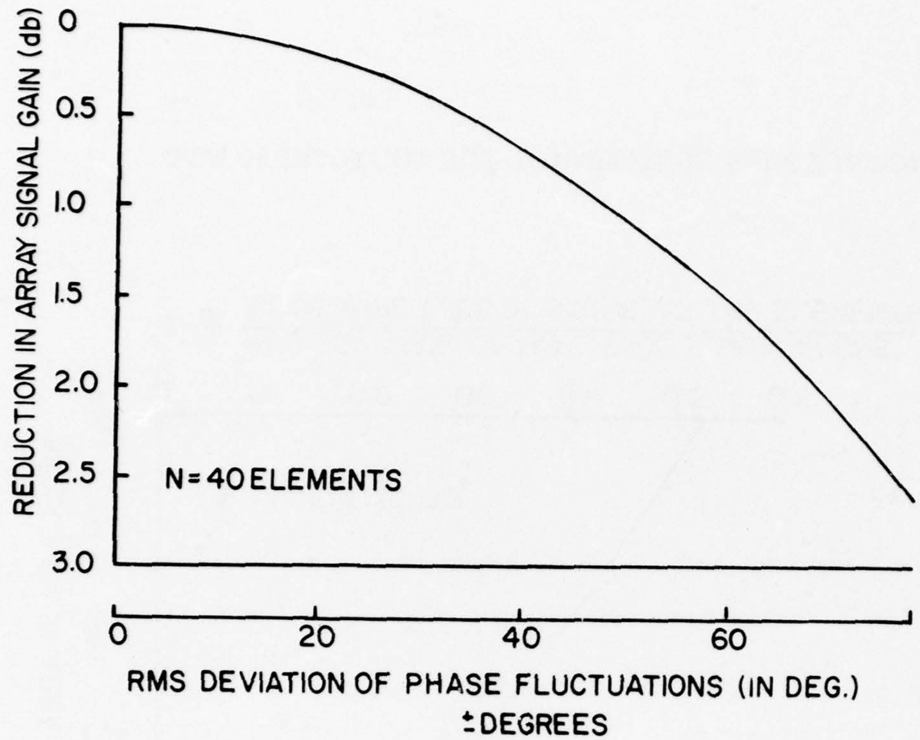

GAIN DEGRADATION DUE TO PHASE FLUCTUATIONS

FIGURE 5-21

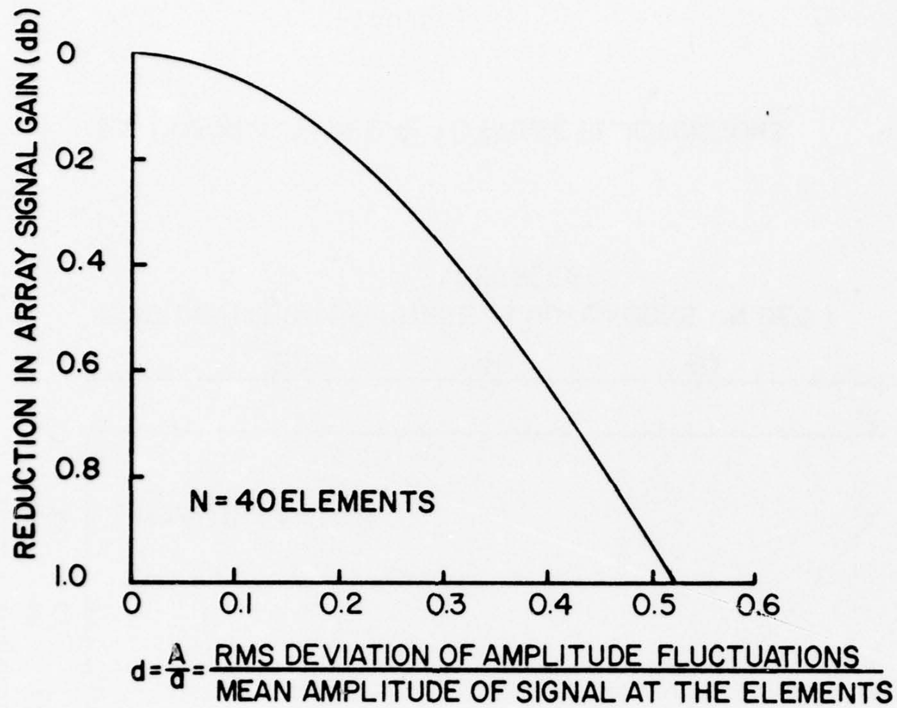

GAIN DEGRADATION DUE TO AMPLITUDE FLUCTUATIONS

FIGURE 5-22

5.6 Array Noise Gain with Phase and Amplitude Fluctuations

5.6.1 Array Noise Gain

- Array noise gain can be treated in much the same way as signal gain except that now it is necessary to consider the effects of the array response in directions other than the steered direction. Thus, for a typical element in an N element array, it will be assumed that the noise produces an output voltage of

$$N_k = h_k(\theta)\ \cos(\omega t+\delta_k+\phi_k)\ ,$$

where

ω = (angular) frequency of the noise source

$h_k(\theta)$ = amplitude of the k^{th} element *output*

θ = the direction of the noise source from the k^{th} element (relative to array broadside)

ϕ_k = fluctuating or random component of the phase of the output from the k^{th} element

δ_k = known component of the phase of the k^{th} element output such as that associated with steering angle.

It should be noted that the signal amplitude in the previous section was not taken to be a function of θ since the array was assumed to be steered in the direction of peak (signal) response. Only the response of the array in this direction is necessary to calculate the signal gain.

- The squared time-averaged output noise voltage is completely analogous to its signal counterpart given in the previous section. To see this, assume that the amplitudes $h_k(\theta)$ are normally distributed with mean $h(\theta)$ and rms deviation $H(\theta)$ about this mean and that the phases ϕ_k are normally distributed with zero mean and rms deviation ϕ(in radians). Moreover, assume that the amplitude and phase fluctuations in the noise are independent of each other and that the amplitude fluctuations are not correlated whereas the phase fluctuations are, with correlation coefficient ρ_{kj}. These assumptions are equivalent to those made in the previous section for the signal voltage and lead to an analogous expression for the expectation or mean value of C^2, or

$$E[C^2] = N[H^2(\theta)+h^2(\theta)] + h^2(\theta) \sum_{k \neq j}^{N}\sum \cos(\delta_k - \delta_j) \exp[-\phi^2(1-\rho_{kj})] ,$$

where the quantity $E[C^2]$ is now twice the expectation value of the squared time-averaged output noise voltage or twice the average output noise power of the array.

- The difference between this expression for $E[C^2]$ and its counterpart as given in the previous section (i.e., 5.5.2) becomes apparent when considering the array noise gain. The definition of array noise gain is similar to that for the signal gain and, at a given frequency, is given by

$$G = \frac{\text{Average output noise power of the array}}{\text{Average output noise power of reference receiver}}$$

However, contrary to the signal gain case, the average output noise power will contain components from all possible directions. Thus, the noise gain must be expressed as follows

$$G = \frac{\iint \frac{1}{2} E[C^2]\, d\Omega}{\iint \frac{1}{2} E[C_{ref}^2]\, d\Omega},$$

where $d\Omega = \cos\theta d\theta d\phi$ is an element of solid angle and $E[C_{ref}^2]$ is the value of $E[C^2]$ for the single reference receiver (obtained from the expression for $E[C^2]$ above with N=1). The general expression for the noise gain will not be included here due to its complexity.

5.6.2 Special Cases of Array Noise Gain

- In many cases it is simply assumed that the noise background is three-dimensional and isotropic. If this is indeed true, then the squares of the mean value and the standard deviation can be written as $h^2(\theta) = h^2$ and $H^2(\theta) = H^2$, where h^2 and H^2 are constants. Moreover, in the case of a line array, the phase differences $(\delta_k - \delta_j)$ are given by

$$\delta_k - \delta_j = \frac{2\pi(x_k - x_j)}{\lambda}(\sin\theta - \sin\theta_o)$$

where

x_k = position of the k^{th} element

λ = noise wavelength

θ_o = steering angle relative to array broadside.

If the phase correlation coefficient is a constant (i.e., $\rho_{kj}=\rho$), then the noise gain for a line array in a three-dimensional isotropic noise field becomes

$$G = 10 \log \left\{ N + \frac{h^2 e^{-\Phi^2}(1-\rho)}{H^2+h^2} \sum\sum_{k\neq j}^{N} \cos\left[\frac{2\pi(x_k-x_j)}{\lambda} \sin\theta_o\right] \frac{\sin 2\pi(x_k-x_j)/\lambda}{2\pi(x_k-x_j)/\lambda} \right\} .$$

If there are no fluctuations ($H=0$, $\Phi=0$) this expression reduces to the expression for the "ideal" noise gain, or

$$G = 10 \log \left\{ N + \sum\sum_{k\neq j}^{N} \cos\left[\frac{2\pi(x_k-x_j)}{\lambda} \sin\theta_o\right] \frac{\sin 2\pi(x_k-x_j)/\lambda}{2\pi(x_k-x_j)/\lambda} \right\} .$$

- It can be shown for a line array with a constant phase correlation coefficient ($\rho_{kj}=\rho$) in a three-dimensional isotropic noise field, that the amplitude and phase fluctuations at a given frequency modify the "ideal" or errorless noise gain given above so that it becomes closer to the value 10 log N. This is demonstrated in Figure 5-23 for an 8-element (N=8) equally spaced array with element spacing d ($x_k-x_j=d$) where the "ideal" noise gain is plotted as the solid line and the noise gain with fluctuations is plotted as the dashed line, both versus the parameter d/λ. This graph has a similar form for other values of N. It is apparent from Figure 5-23 that, for the typical line array employed with half-wavelength ($d/\lambda=1/2$) element spacing, the noise gain will be 10 log N where N is the number of elements in the array. For spacing less than half-wavelength (i.e. as in supergain) the noise gain can increase substantially whereas for spacing greater than half-wavelength it will remain close to the value 10 log N.

5.6.3 General Remarks on Array Signal Gain and Array Noise Gain

- It was tacitly assumed in the above presentations of signal and noise gains that the phase and amplitude fluctuations were caused by the medium between the source and the array elements. All results, however, are valid for any errors or fluctuations arising between the source and the point where the array output is measured.

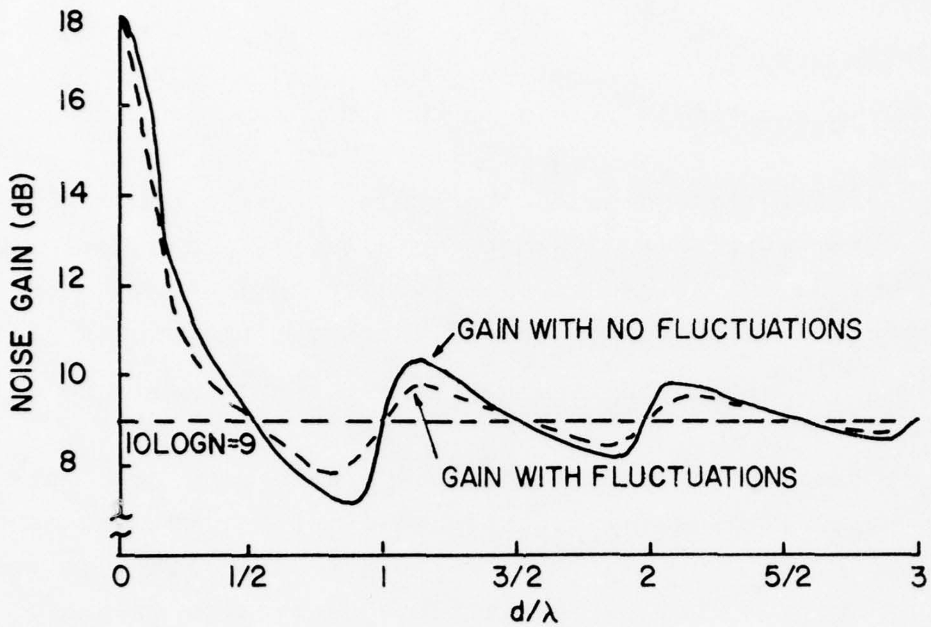

EFFECT OF AMPLITUDE AND PHASE FLUCTUATIONS

FIGURE 5-23

5.7 Array Gain

5.7.1 Definition of Array Gain

- Array gain AG or array signal-to-noise gain is the comparison of the signal gain G_S to the noise gain G_N which were given in the previous sections. It is defined, in dB, as

$$AG(dB) = G_S(dB) - G_N(dB).$$

It is important to note when calculating array gain that both the signal gain G_s and the noise gain G_N have been derived for wavelengths which do not necessarily have to be the same. Thus, one can calculate G_S for an array at the signal frequency corresponding to the typical half-wavelength element spacing $(d/\lambda=1/2)$. If one also desires G_N at this frequency then, according to Figure 5-23, it will be 10 log N. However, for lower noise frequencies the quantity d/λ, where λ is the noise wavelength, will become quite small $(d/\lambda<<1/2)$. Thus, according to Figure 5-23, G_N will become large thereby reducing the array gain by a corresponding amount.

5.7.2 Effect of Signal and Noise Coherence

- Array gain can be obtained from a knowledge of the noise and signal coherence between elements of the array. The coherence can be measured by crosscorrelating the outputs from different array elements. For example, if $V_1(t)$ and $V_2(t)$ are voltages generated by any two array elements as a function of time, then the crosscorrelation coefficient ρ_{12} is given by

$$\rho_{12} = \frac{\overline{V_1(t)\ V_2(t)}}{\left[\overline{V_1^{\,2}(t)}\ \overline{V_2^{\,2}(t)}\right]^{1/2}}$$

where the bars indicate time averages. Here again, as in the cases of signal gain and noise gain, the squared time-averaged output voltage $\overline{V^2}$ plays an important role.

- From the definition* of array gain as the ratio (in dB) of the average signal power-to-noise power ratio of the array, S^2/N^2, to the average signal power-to-noise power ratio of a single array element, s^2/n^2, it can be shown that

$$AG = 10 \log \frac{\overline{S^2}/\overline{N^2}}{\overline{s^2}/\overline{n^2}} = 10 \log \frac{\sum_i \sum_j (\rho_s)_{ij}}{\sum_i \sum_j (\rho_n)_{ij}} ,$$

where $(\rho_s)_{ij}$ and $(\rho_n)_{ij}$ are the crosscorrelation coefficients between the i^{th} and j^{th} elements of the signal and of the noise, respectively. It is apparent therefore, that the array gain is dependent on the signal and noise fields in which the array is located. For a unidirectional signal in isotropic noise, for example, the expression given above for array gain reduces to the directivity index. Moreover, both $(\rho_s)_{ij}$ and $(\rho_n)_{ij}$ are dependent on any time delays that may be used to steer the array. In fact, the purpose for steering the array at all is so that $(\rho_s)_{ij}$ will be maximized when it is steered in the signal's direction.

*This definition is entirely consistent with the definition of AG given in Section 5.7.1 and the definitions of signal and noise gains given in the previous sections.

5.7.3 Examples of Array Gain

- Using the expression for array gain above, it can be shown that when both the signal and noise are either completely coherent (i.e., $(\rho_s)_{ij} = (\rho_n)_{ij} = 1$ between <u>all</u> elements i and j) or completely incoherent so that

$$(\rho_s)_{ij} = (\rho_n)_{ij} = 0 \quad \text{for} \quad i \neq j$$

and

$$(\rho_s)_{ij} = (\rho_n)_{ij} = 1 \quad \text{for} \quad i = j \; ,$$

then the array gain will be zero dB.

- When the signal is perfectly coherent (i.e., $(\rho_s)_{ij} = 1$ between <u>all</u> elements i and j) and the noise completely incoherent so that

$$(\rho_n)_{ij} = 0 \quad \text{for} \quad i \neq j$$

and

$$(\rho_n)_{ij} = 1 \quad \text{for} \quad i = j \; ,$$

then it can be shown for an array with N elements that the array gain will be AG = 10 log N.

- When a perfectly coherent signal is in a background of only partly coherent noise, so that

$$(\rho_n)_{ij} = \sigma<1 \qquad i\neq j$$

$$(\rho_n)_{ij} = 1 \qquad i=j \; ,$$

then the expression for array gain becomes

$$AG = 10 \log N/1+(N-1)\sigma$$

which is less than 10 log N. Thus, array gain is reduced not only as the signal coherence decreases but also as the noise coherence increases.

- As an example of the general procedure for calculating array gain, consider Figure 5-24 where the signal ρ_s and the noise ρ_n coherence are plotted as continuous functions of element spacing d for an unshaded, equally spaced three-element array. For the given spacing, the (symmetric) signal and noise coherence matrices become:

$(\rho_s)_{ij}$

	j=1	j=2	j=3
i=1	1	0.6	0.2
i=2	0.6	1	0.6
i=3	0.2	0.6	1

$(\rho_n)_{ij}$

	j=1	j=2	j=3
i=1	1	0	0
i=2	0	1	0
i=3	0	0	1

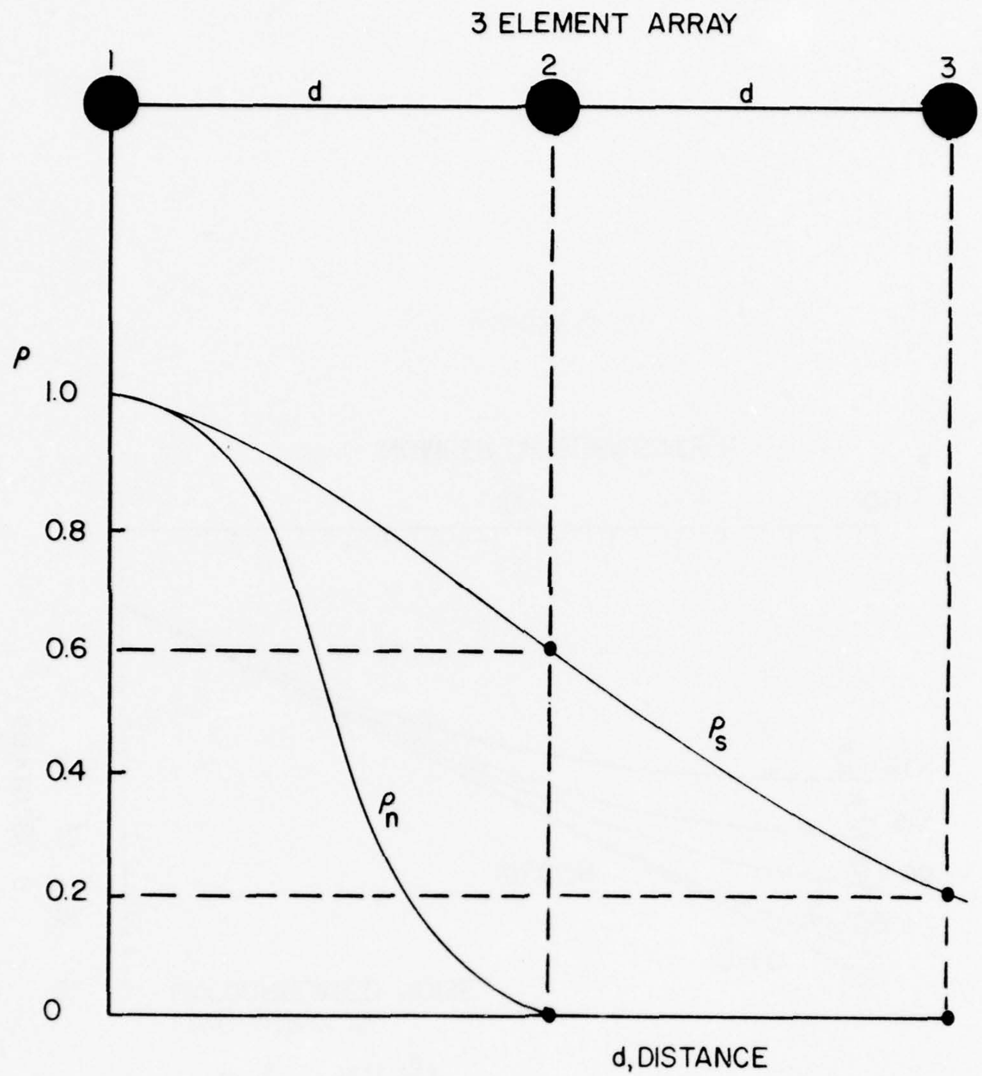

SIGNAL AND NOISE COHERENCE (ρ_s, ρ_n) FOR A THREE-ELEMENT ARRAY WITH INTERELEMENT SPACING, d.

FIGURE 5-24

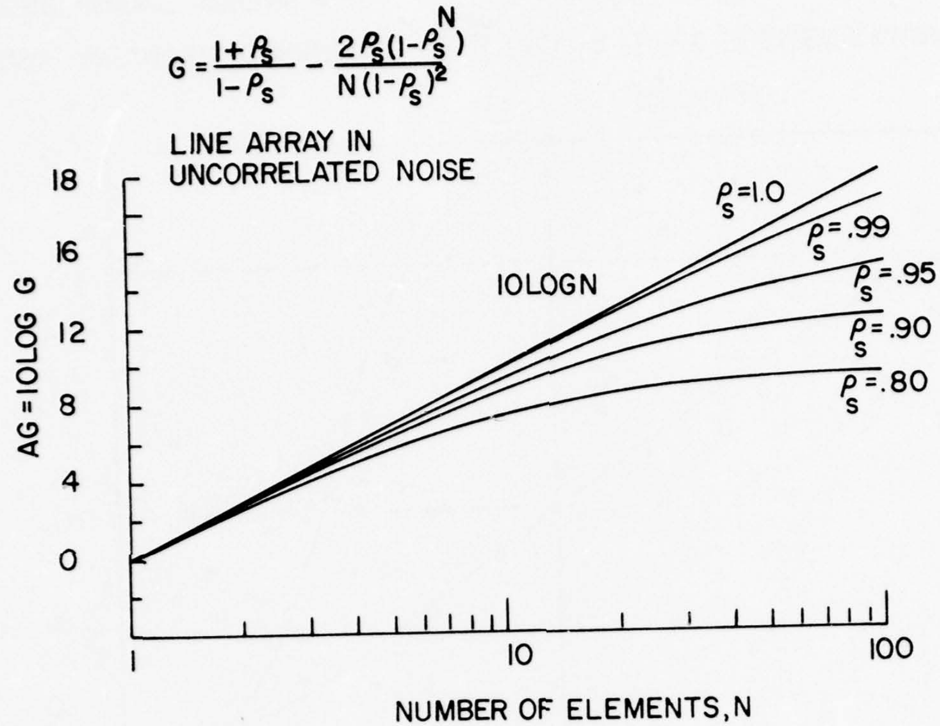

$G = \frac{1+\rho_s}{1-\rho_s} - \frac{2\rho_s(1-\rho_s^N)}{N(1-\rho_s)^2}$
LINE ARRAY IN UNCORRELATED NOISE
AG = 10LOG G
18
16
12
8
4
0
10LOGN
ρ_s=1.0
ρ_s=.99
ρ_s=.95
ρ_s=.90
ρ_s=.80
1
10
100
NUMBER OF ELEMENTS, N

FIGURE 5-25

In order to construct these matrices using Figure 5-24, it is necessary to note that the correlation coefficient between any two adjacent elements is the same. Thus, in the $(\rho_s)_{ij}$ matrix, for example, we can read $(\rho_s)_{12}$ from Figure 5-24, but $(\rho_s)_{23}$ comes from the equation $(\rho_s)_{23} = (\rho_s)_{12}$.

- If we use the expression for array gain given above (Section 5.7.2), then we can show by summing the sums of matrix columns that

$$AG = 10 \log \frac{1.8+2.2+1.8}{3} = 2.9 \text{ dB}.$$

This is approximately 2 dB less than the AG value (10 log N=10 Log 3) that would have been obtained had there been no degradation in signal coherence. It is apparent that as the number of elements N in the array increases, the coherence matrices will become quite cumbersome.

- In many signal fields the signal coherence $\rho_s(\omega)$ decreases with an increase in element separation relative to the wavelength. If this decrease is assumed to be exponential in form, then it can be shown that the array gain AG of a line array in an uncorrelated noise field is given by

$$AG = 10 \log\left[\frac{1+\rho_s}{1-\rho_s} - \frac{2\rho_s(1-\rho_s^N)}{N(1-\rho_s)^2}\right],$$

where N is the number of elements in the array and $\rho_s(\omega)$ $(0 \leq \rho_s(\omega) \leq 1)$ is the signal coherence between adjacent* array elements. The signal coherence $\rho_s(\omega)$ is given by

$$\rho_s(\omega) = \exp\{-\alpha(\omega)\, d/\lambda\}$$

where d is the spacing between array elements, λ is the wavelength and $\alpha(\omega)$ $(\alpha(\omega) \geq 0)$ is an adjustable parameter.

- A graph of the above expression for array gain AG is given in Figure 5-25 for various values of ρ_s. As an example, the array gain of a 100-element array when $\rho_s=0.95$ is about 15 dB, which is about 5 dB less than that for a perfectly coherent (i.e., $\rho_s=1$) signal. Also note that when the number of array elements N becomes very large, the array gain approaches the value

$$AG = 10 \log\left[\frac{1+\rho_s}{1-\rho_s}\right].$$

---

* For this particular model the signal coherence between all pairs of elements in the array is specified in terms of the signal coherence $\rho_s(\omega)$ between adjacent elements. Using this model, it can be shown that the signal coherence between the first and the $(k+1)^{th}$ elements will be $(\rho_s)_{1,k+1}=\rho_s^k$.

5.8 Performance in Directional Noise Fields

5.8.1 Performance in a Nondirectional Noise Field

- For an unshaded line array of N elements with uniform spacing d, the directivity index or ideal* array gain AG in a three-dimensional isotropic ambient noise field is given by

$$AG = 10 \log\left[\frac{2(N-1)d}{\lambda}\right] .$$

If the design frequency f_o is such that $d = \lambda_o/2$, then we can rewrite this expression as

$$AG = 10 \log\left[\frac{(N-1)\ f}{f_o}\right] .$$

It is apparent that, for a fixed number of elements N, the array gain will increase with frequency at a rate of 3 dB per octave.

- It was shown in the previous chapter that the -3 dB beamwidth of a line array at broadside is approximately (in degrees)

$$BW_3 = \frac{50.9^o \lambda}{(N-1)\lambda_o/2}$$

* For the ideal condition of a unidirectional signal in an isotropic noise field, array gain becomes simply the directivity index of the array.

or,

$$BW_3 = \frac{101.8^o}{(N-1)} \left[\frac{f_o}{f}\right] ,$$

where the array length is $(N-1)\lambda_o/2$. Thus, the broadside beamwidth varies inversely with frequency and the corresponding array gain can be written as

$$AG = 10 \log \frac{101.8^o}{BW_3} .$$

- It was shown in Chapter 4.0 that the beamwidth of a scanned line array varies as $|\cos\theta|$ where θ is measured from broadside. The beamwidth is minimal at broadside and increases toward endfire. Due to the slope of the cosine function, the rate of increase is slow near broadside and the beamwidth actually remains within 20% of its minimum value over a sector of almost 70^o centered at broadside. In a three-dimensional isotropic ambient noise field the array gain of a line array is independent of the steering angle θ since the $|\cos\theta|^{-1}$ beam broading factor is just cancelled by a geometrical $\cos\theta$ dependence of the solid or three-dimensional beam. As a result, array performance as measured, for example, by an estimated detection range is essentially independent of array heading and beam steer direction.

5.8.2 Directional Noise Field

5.8.2.1 Two-Dimensional Isotropy

- In most ocean areas the ambient noise field is not isotropic and can vary strongly with look direction in both the horizontal and vertical planes. In some of these

areas, however, and at frequencies of interest, the ambient noise field is dominated by components which arrive at shallow vertical angles. Thus, in the limiting case, the ambient noise field at these sites can be satisfactorily treated as two-dimensional.

- In the case of a horizontal two-dimensional isotropic noise field, the array gain of a line array can be approximated as the ratio of the full 360^o azimuth in the horizontal plane to the -3 dB beamwidth, or

$$AG = 10 \log\left(\frac{360^o}{2BW_3}\right). \qquad \text{Isotropic, 2-dimensional.}$$

In this expression, the -3 dB beamwidth BW_3 is assumed to be in degrees and is doubled to account for the bi-directional coverage of the axially symmetric beam.

- It can be shown that, at broadside, the limiting two-dimensional array gain, as given above, is about 2.5 dB less than the ideal array gain when the ambient noise has three-dimensional isotropy.

5.8.2.2 No Isotropy

- Generally, the ambient noise field is not even isotropic in the horizontal plane. When this is the case, the expression for array gain must be modified to reflect the particular quality of the noise field in question. For example, a directional noise field can be expressed as the total noise power (in dB) in, say, 10^o sectors of the horizontal plane. For a beamwidth BW_3 (assumed to be less than the sector width) steered into a given sector, the beam output will depend on the sector gain of 10

log $(10^{o}/BW_3)$ against the sector noise level. This output must then be power summed with the corresponding output from the other noise sector seen by the beam on the opposite side of the array axis to determine the total beam output. In a highly directional noise field, the outputs from the port and starboard sectors may differ considerably.

Generalizing the above, if the two dimensional ambient noise field is given in the form of noise power in each of n sectors in the horigontal plane, then the gain against the noise in a given sector is approximately

$$AG = 10 \log \frac{360^{o}}{BW_3} - 10 \log n$$

if,

$$BW_3 \leq (360/n) \text{ deg.}$$

Note that the first term in this gain expression omits the factor 2 which appeared in the gain expression for the two-dimensional isotropic noise field. The reason for this omission is that only the port or starboard side of the beam is considered. The total beam output still requires the power summation of the two beam components as described above.

5.8.2.3 Array Performance

- In the case of two-dimensional isotropy, the array gain is seen to depend on the beamwidth BW_3. There is, however, no geometrical factor of $\cos\theta$ as in the case of three-dimensional isotropy to offset the increase in beamwidth with steering angle θ . Consequently, the array performance as measured, for example, by the FOM or estimated detection range will depend on the directional properties of the ambient noise field, the array heading and the beam steer direction.

THIS PAGE INTENTIONALLY LEFT BLANK.

5.9 System Losses

- In Chapter 4.0 we discussed the effect of amplitude shading of array elements and how this widened the main beam (and reduced the sidelobes). Widening the main beam leads to a corresponding loss or reduction in the directivity index of the array. In the preceding sections we also discussed the loss due to multiple arrivals, the loss resulting from errors and more.

- In this section we shall summarize the remaining major losses that can detract from ideal array performance. With the exception of the loss introduced by the operator, these losses are incurred mainly in the beamformer where beams are formed from time sampled data originally collected by an imperfect array and telemetry system.

5.9.1 Lost Hydrophones

- The performance of an array will, of course, be sensitive to the loss of one or more hydrophones or hydrophone groups. By a lost hydrophone or group we mean one whose output is zero.

- In order to demonstrate this effect consider the computed normalized directivity index (D.I.) plotted as a function of the fractional number of lost hydrophones in Figure 5-26 for a very long line array.* The upper and lower solid lines represent the maximum and minimum values of the D.I. for a given percentage of lost hydrophones and the dashed line represents the average D.I. The D.I. of an array with

* Figure 5-26 was obtained for a long shaded array with a specified sidelobe level but the results are approximately valid for any long line array.

a given number of lost hydrophones depends on the exact location of these phones along the array. Thus, different configurations, each with the same total number of lost phones, cause a spread in the D.I. It is apparent from Figure 5-26 that, on the average, the D.I. of a long array will decrease by about 1 dB for a 20% loss in hydrophones.

- Not only is the directivity index of an array affected by lost hydrophones but the sidelobe level is affected as well. As an example, consider the broadside beam-pattern of the very long shaded array given in Figure 5-27. Figures 5-28 through 5-31 show the change in this pattern with increasing percentages of lost hydrophones. Generally, for long arrays, the indicated average increases in sidelobe level with an increasing percentage of lost hydrophones remains approximately the same for any lost hydrophone configuration as long as that configuration is relatively uniform across the array.

- In general, we can conclude that the effect of lost hydrophones on the directivity index of a very long array is rather minimal. The increase in the sidelobe level of that array, however, will be quite severe even if only four percent of the hydrophones are lost.

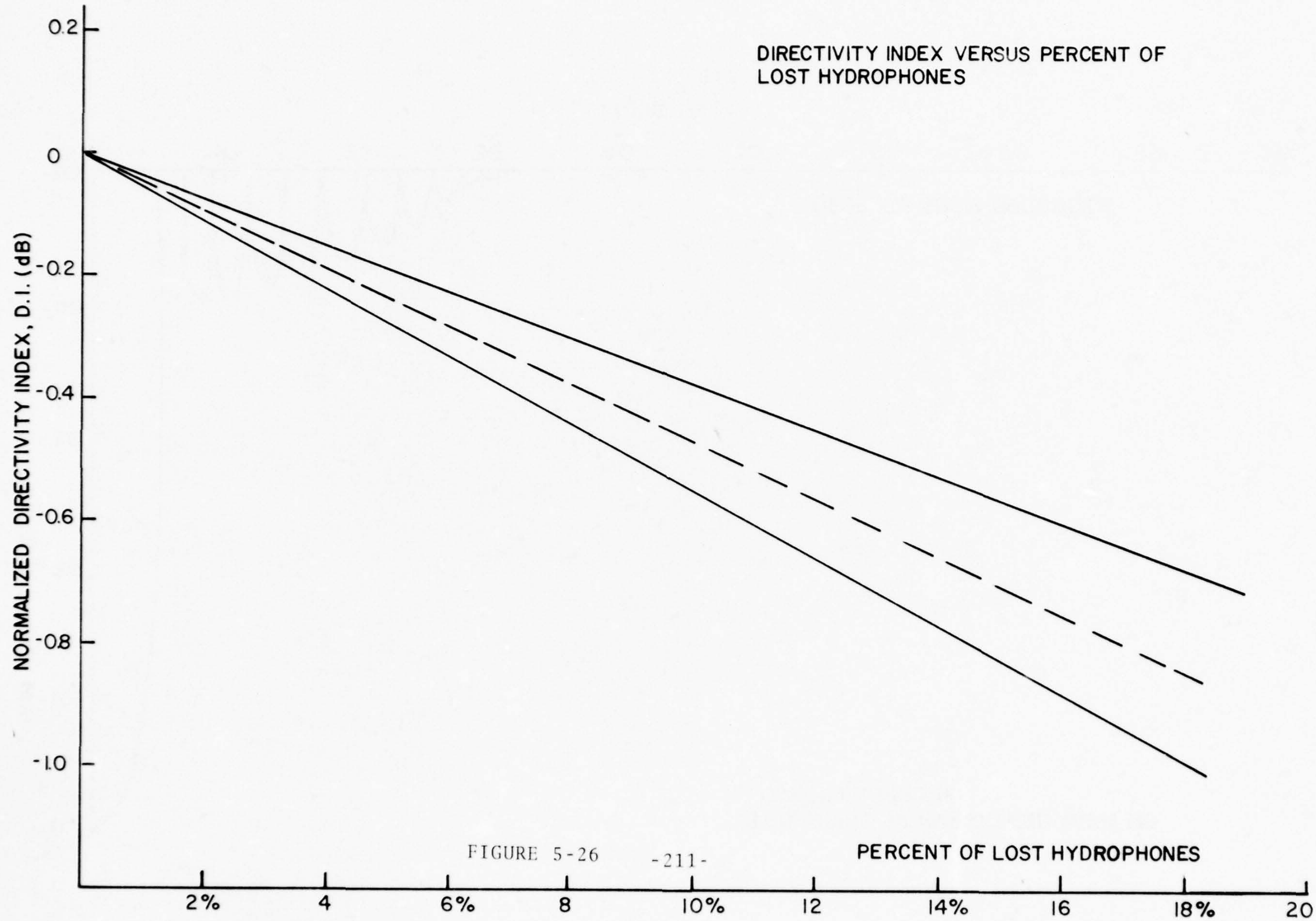
DIRECTIVITY INDEX VERSUS PERCENT OF
LOST HYDROPHONES
NORMALIZED DIRECTIVITY INDEX, D.I. (dB)
0.2
0
-0.2
-0.4
-0.6
-0.8
-1.0
PERCENT OF LOST HYDROPHONES
2%
4
6%
8
10%
12
14%
16
18%
20

FIGURE 5-26

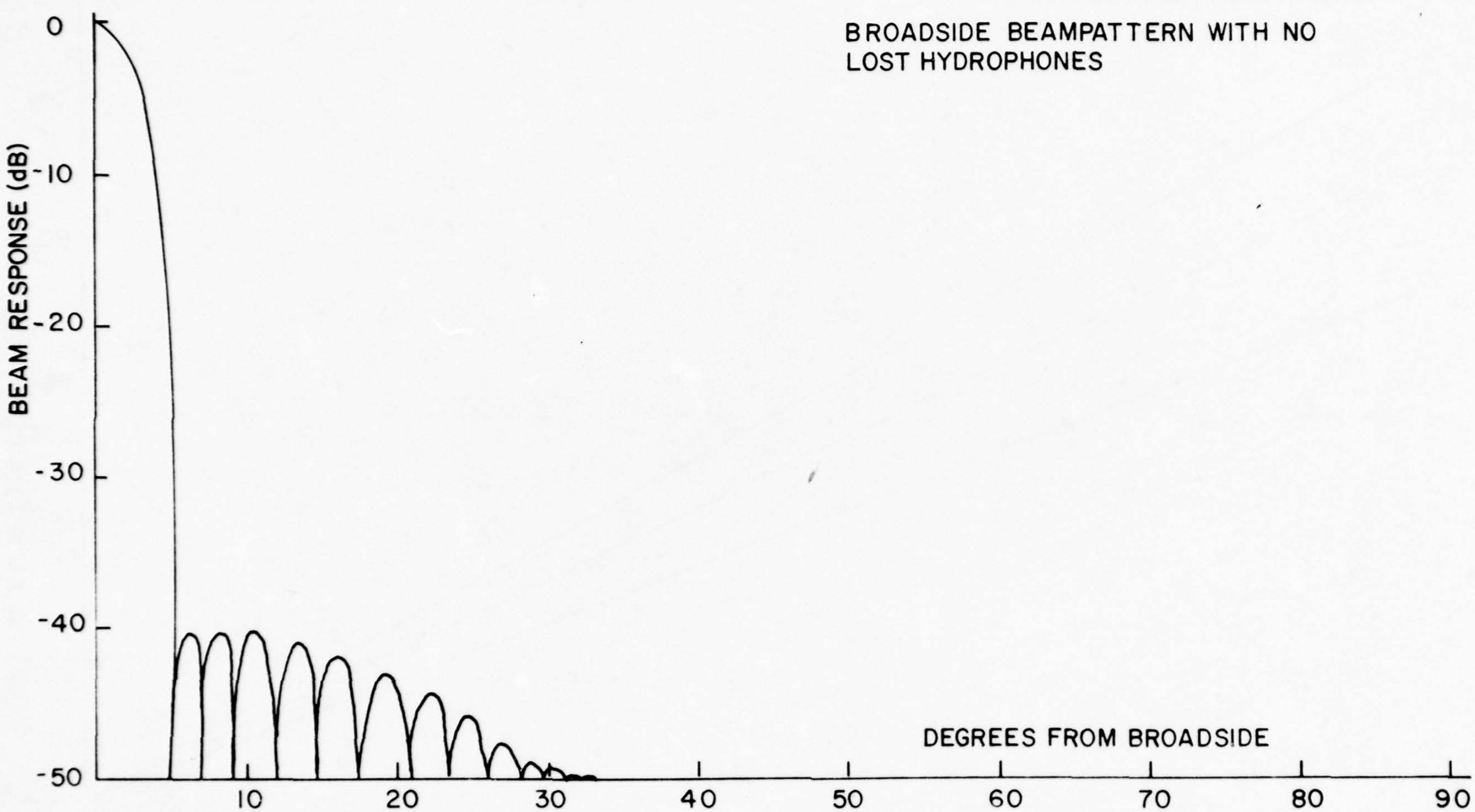
BROADSIDE BEAMPATTERN WITH NO
LOST HYDROPHONES
BEAM RESPONSE (dB)
0
-10
-20
-30
-40
-50
DEGREES FROM BROADSIDE
10
20
30
40
50
60
70
80
90

FIGURE 5-27

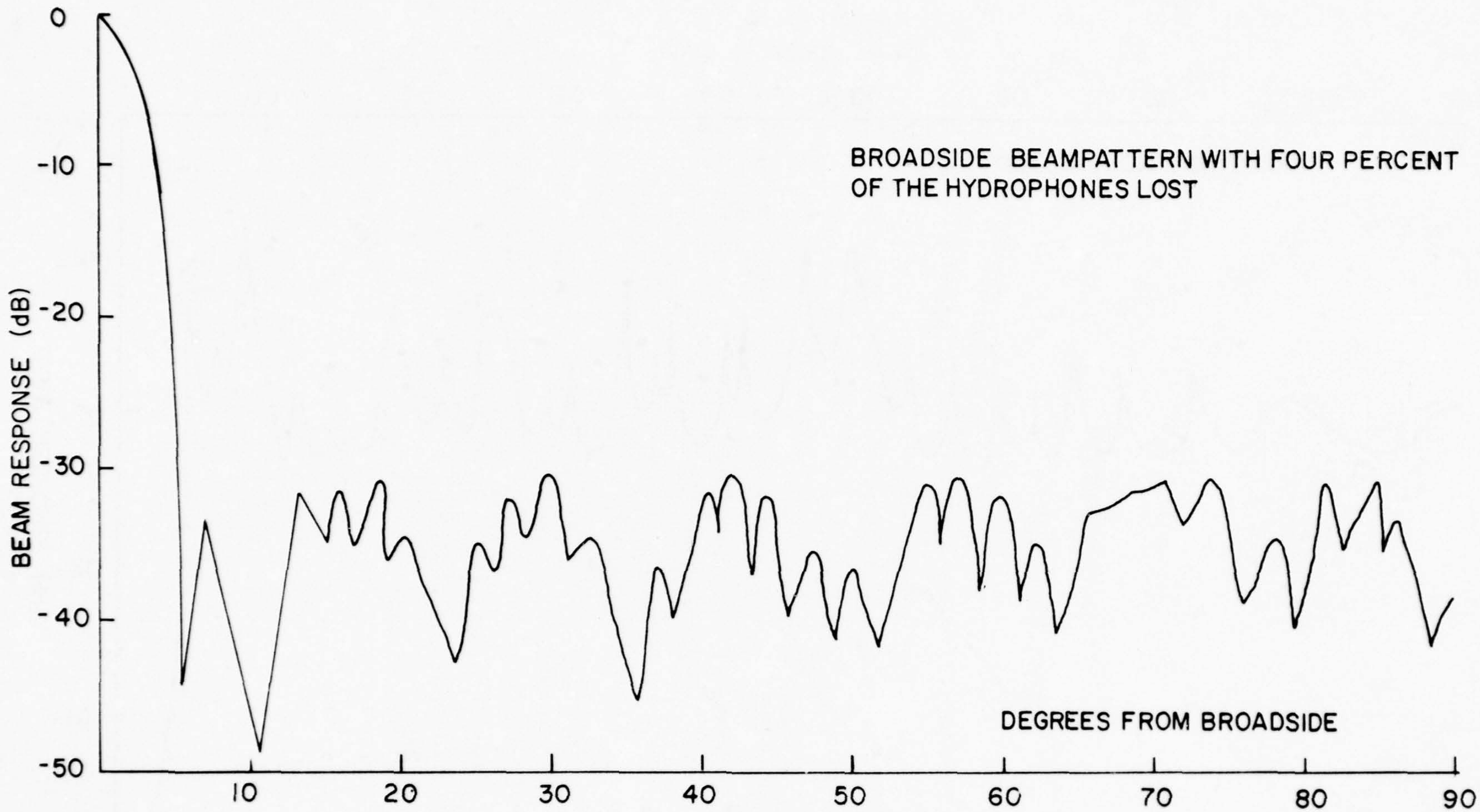
BROADSIDE BEAMPATTERN WITH FOUR PERCENT OF THE HYDROPHONES LOST
BEAM RESPONSE (dB)
0
-10
-20
-30
-40
-50
10
20
30
40
50
60
70
80
90
DEGREES FROM BROADSIDE

FIGURE 5-28

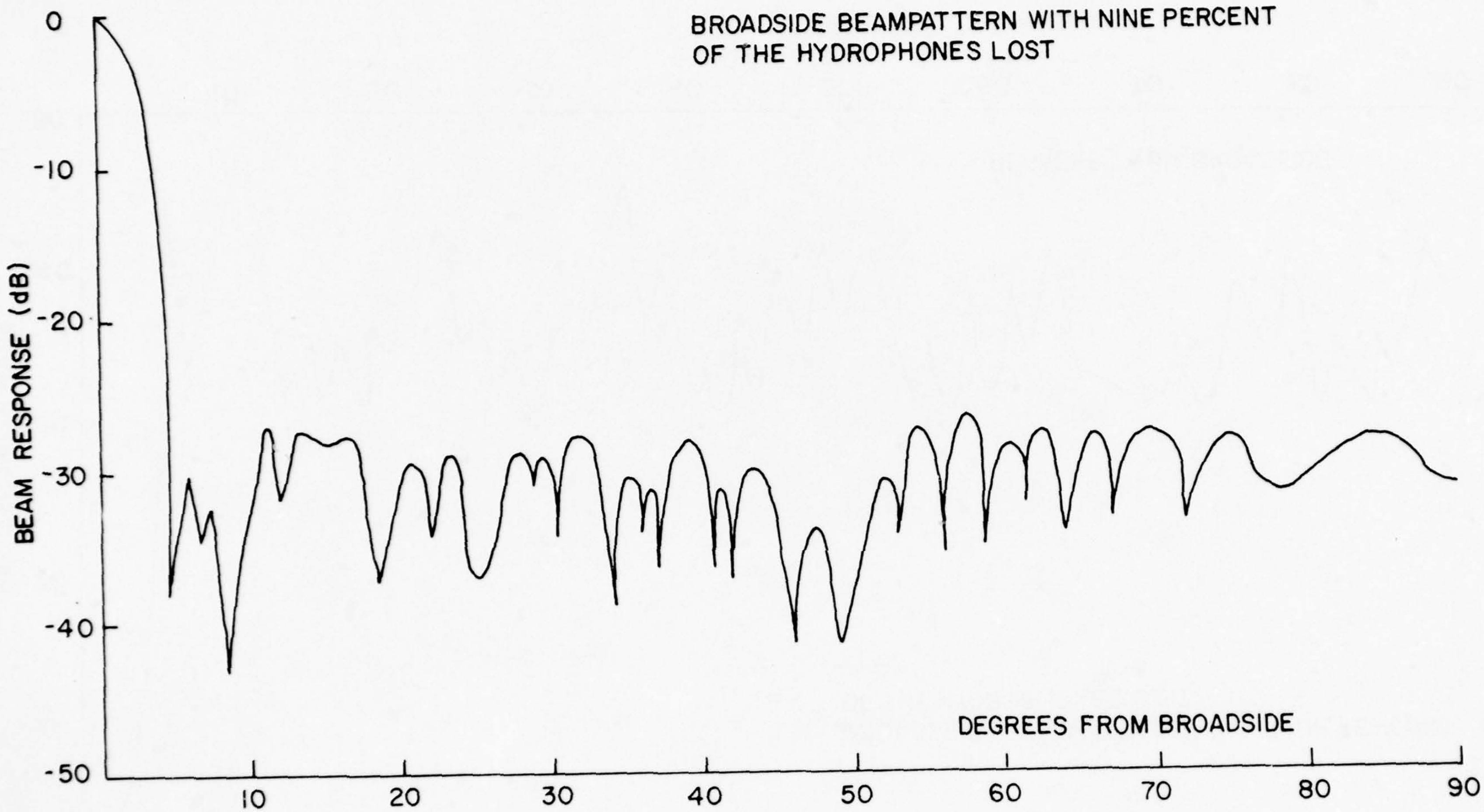
BROADSIDE BEAMPATTERN WITH NINE PERCENT
OF THE HYDROPHONES LOST
BEAM RESPONSE (dB)
0
-10
-20
-30
-40
-50
DEGREES FROM BROADSIDE
10
20
30
40
50
60
70
80
90

FIGURE 5-29

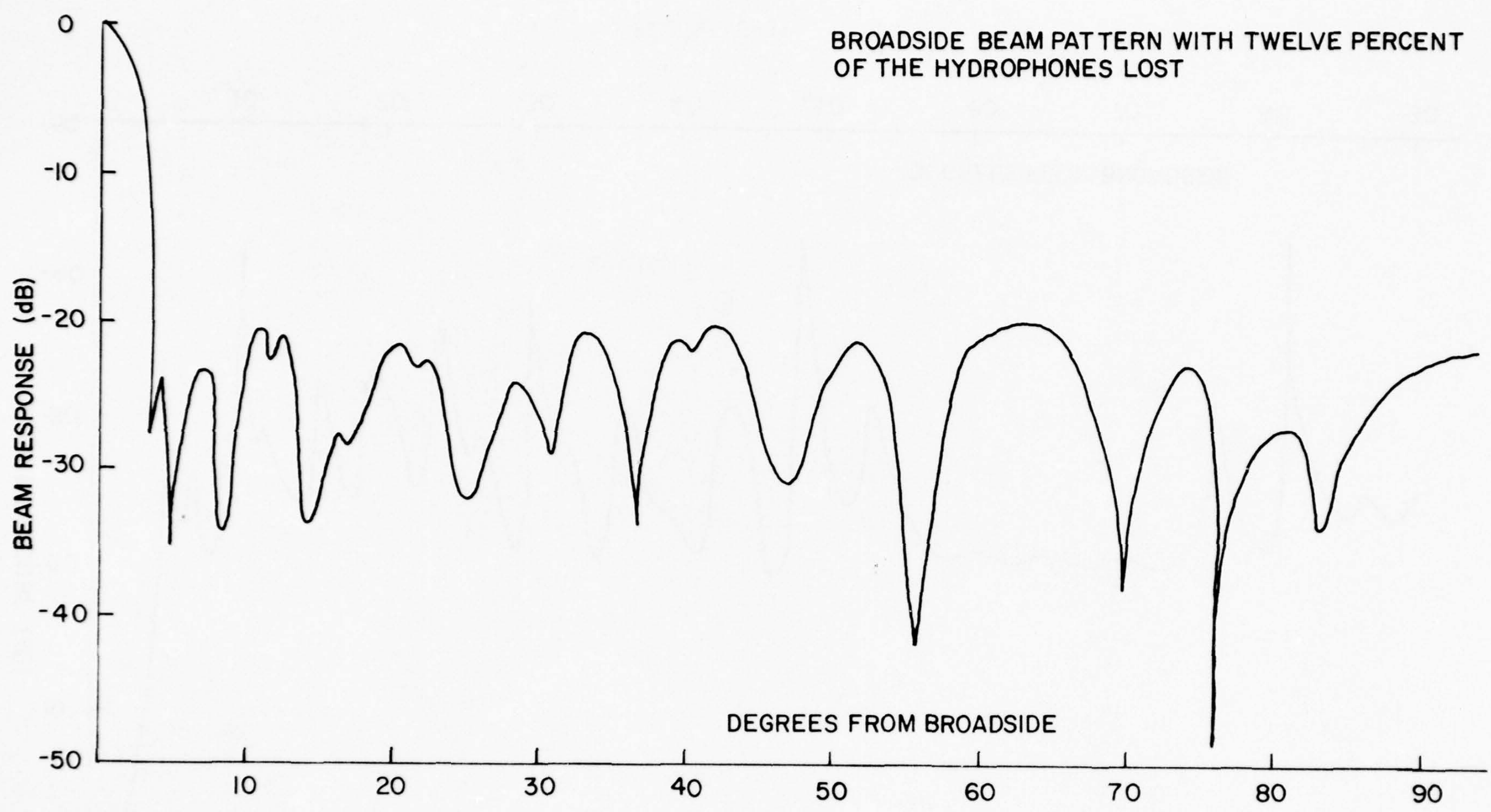
BROADSIDE BEAM PATTERN WITH TWELVE PERCENT
OF THE HYDROPHONES LOST
BEAM RESPONSE (dB)
0
-10
-20
-30
-40
-50
DEGREES FROM BROADSIDE
10
20
30
40
50
60
70
80
90

FIGURE 5-30

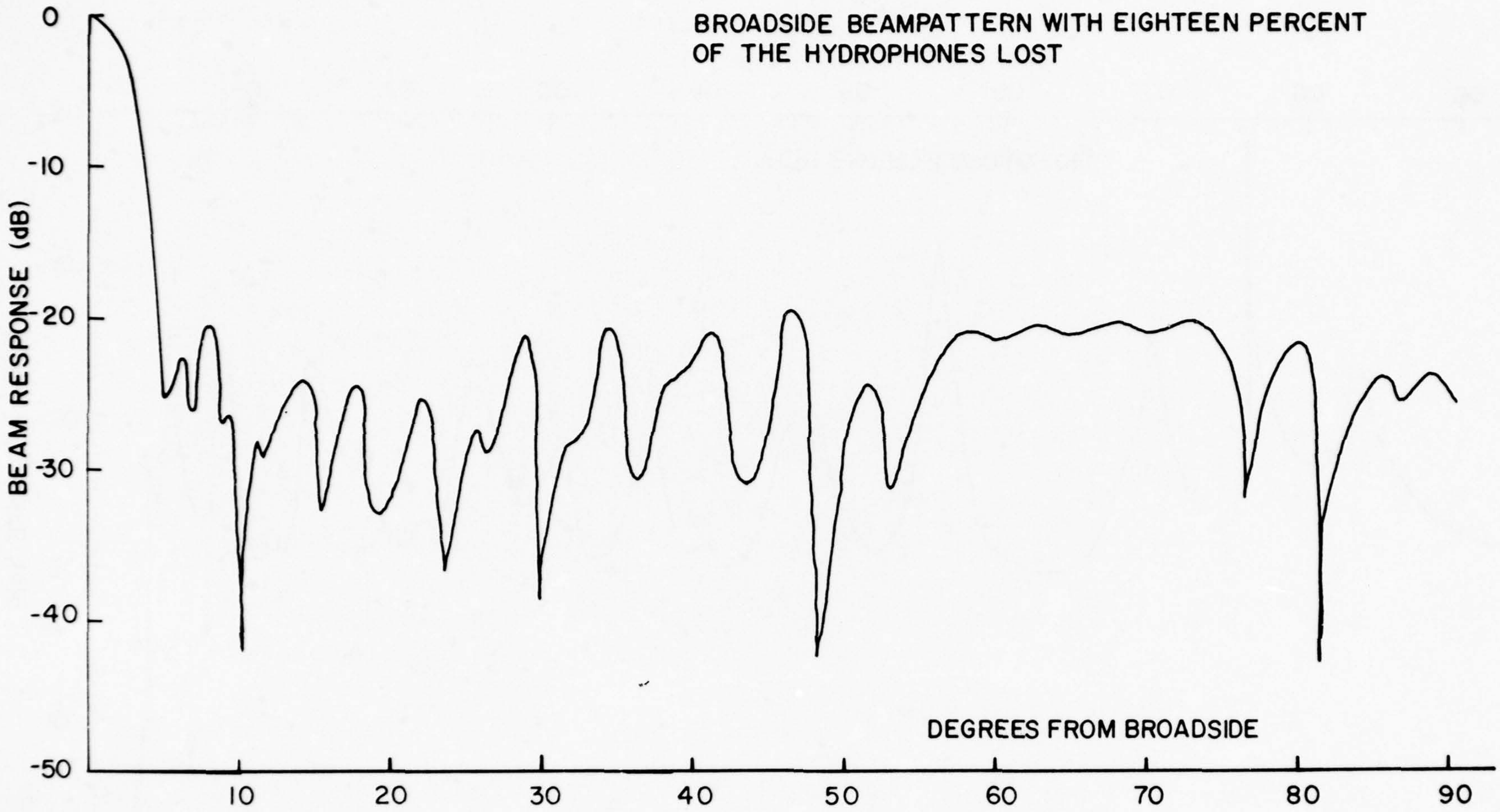
BROADSIDE BEAMPATTERN WITH EIGHTEEN PERCENT
OF THE HYDROPHONES LOST
BEAM RESPONSE (dB)
0
-10
-20
-30
-40
-50
DEGREES FROM BROADSIDE
10
20
30
40
50
60
70
80
90

FIGURE 5-31

5.9.2 Beam Processing and Operator Losses

5.9.2.1 Beam Scalloping Loss

- Beam Scalloping loss is an effective reduction in the design directivity index (D.I.) of an array that occurs when a (point) source or target is located between adjacent beams where the response is less than the maximum or design value of either beam. In other words, beam scalloping loss occurs when the (point) source or target is not located on the main response axis (MRA) of some beam in the pattern. The actual reduction in D.I. below the design or MRA value depends primarily on the response level at the beam crossover points (see Section 4.5). It also depends on the beamwidth and on the total number of beams formed.

- Figure 5-32 is a typical graph of scalloping loss versus d/λ where d is the hydrophone element (or group) spacing in the array. The curve in Figure 5-32 illustrates the case of conventional time-delay beamforming* in which the scalloping loss decreases with decreasing frequency (or increasing wavelength). That is, as frequency decreases from its design value (i.e., as $d/\lambda \to 0$), beamwidth increases and adjacent beams cross at response levels <u>above</u> the design level, thereby diminishing the scalloping loss.

- As frequency increases from its design value, beamwidth decreases, adjacent beams cross at response levels <u>below</u> the design level and scalloping loss becomes greater.

---

* Beam Scalloping loss may or may not vary with frequency depending upon the type of beam forming used.

- Actually, when full azimuthal coverage is desired, beam crossovers should be set well above -3 dB at design frequency. In this way, scalloping loss can generally be kept to a minimum ($\approx$1 dB) over most bands of interest. Even with such implementations as frequency independent beamformers, a sufficient number of beams should be formed at design frequency to assure a crossover level well above -3dB and therefore a scalloping loss of less than 1 dB at all frequencies.

- Assuming a threat probability that is constant with azimuth, scalloping loss can be defined for a line array as the area ratio given by the following expression

$$\text{Scalloping Loss} = 10 \text{ Log } (A_1/\pi/4)$$

where,

A_1 = the total area under the beams in one azimuthal quadrant ($0 \leq \theta \leq \pi/2$) as shown by the cross-hatched area in Figure 5-33, and

$\pi/4$ = the area of the unit circle in one azimuthal quadrant (see Figure 5-33).

The area A_1 under the beams in the unit circle can be computed from crossover point to crossover point from the expression

$$A_1 = \sum_{n=o}^{Q-1} \int_o^{\theta_n} v^2(\theta)\, d\theta + \int_{\theta(Q-1)}^{\pi/2} v^2(\theta)\, d\theta$$

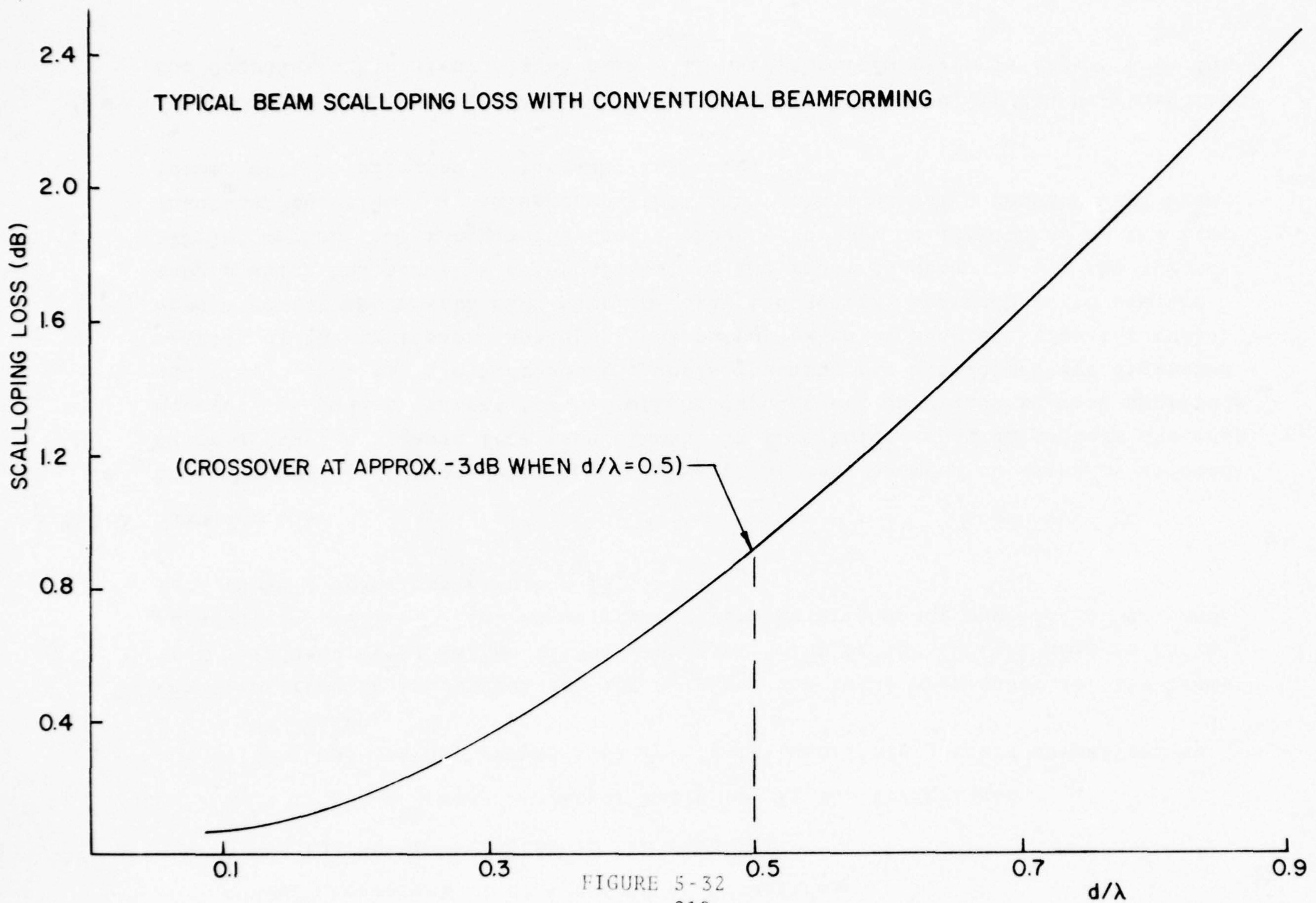

TYPICAL BEAM SCALLOPING LOSS WITH CONVENTIONAL BEAMFORMING
SCALLOPING LOSS (dB)
2.4
2.0
1.6
1.2
0.8
0.4
(CROSSOVER AT APPROX. -3dB WHEN d/λ=0.5)
0.1
0.3
0.5
0.7
0.9
d/λ

FIGURE 5-32

where,

$n = n^{th}$ beamsteer direction ($n=0$ is broadside)

Q = total number of beams in the quadrant

θ_n = is the n^{th} beam brossover angle (θ_o is the first), and

$v(\theta)$ = beam voltage response or far-field amplitude pattern normalized to unity.

The first term in the expression for A_1 gives the total area under all the beams from broadside ($\theta=0$) to the distal crossover point of the $(Q-1)^{st}$ beam which is adjacent to endfire. The second term gives the area under one half of the endfire ($\theta=90^o$) beam (See Figure 5-33).

5.9.2.2 Sampling Loss

- In conventional or time-delay beamforming , the main beam of an array is steered by delaying the signals from each element in time before summing to form the beam. However, in modern systems the hydrophone signals are quantized in both amplitude and time. That is, the hydrophone signals reaching the beamformer are digitized samples of the hydrophone analog signal output taken at discrete time intervals. When steering beams with time sampled data, the general approach is to use the sample which has the time delay closest to the required delay (i.e., the "closest sample" method) but recognizing that a phase error may be introduced by the time quantization. Thus, it is apparent that the performance of a conventional beamformer will be affected by the sampling rate.

- If the phase error due to sampling is uniformly distributed, it can be shown that the degradation in array signal gain will have the form given in Figure 5-34 for a

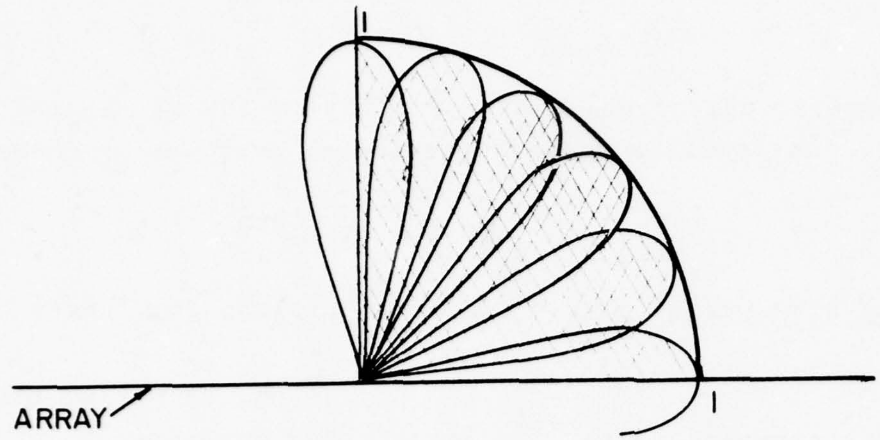

FIGURE 5-33

uniformly weighted array and a randomly steered beam. The absissa in Figure 5-34 is the "over sampling factor" or the ratio of the sampling rate f_s to twice the design frequency f_d. The graph shows that the degradation in array signal gain decreases as the sampling rate is increased and that the over sampling factor should at least be 3. Although the results given in Figure 5-34 are for a uniformly weighted array, they are also approximately valid for shaded arrays.

- The phase error caused by sampling or time-delay quantization can also lead to severe problems in controlling the sidelobe level of the beampattern. If the "closest sample" method is used for beam steering then it is apparent that the maximum phase error introduced by sampling is given by

$$\varepsilon_{max}(\text{degrees}) = \pm\ (f/f_s)180^{\circ},$$

where f_s is the sampling rate (or frequency) and f is the frequency of interest. For example, the maximum phase error ε_{max} for a periodic signal that is sampled twice during each period is $\pm 90^{\circ}$.

- It can be shown, for certain amplitude shaded arrays with design frequency f_d, that an

$$\varepsilon_{max} = \pm\ (f_d/f_s)180^{\circ}$$

greater than 9° may lead to severe sidelobe degradation. That is, if the sampling rate f_s is not at least 20 times the design frequency f_d, not only will

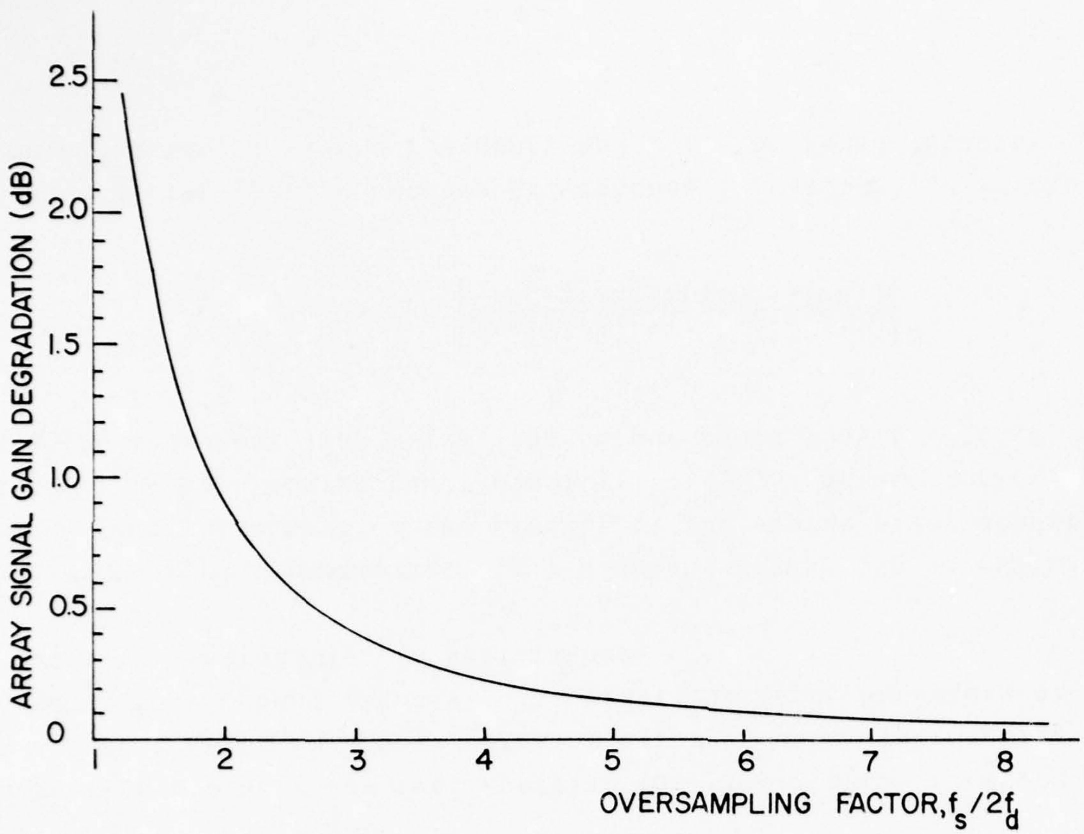

TIME DELAY BEAMFORMER LOSS DUE TO TIME QUANTIZATION

FIGURE 5-34

the sidelobe level increase above its shaded level but a significant number of grating lobes will also be introduced into the beampattern. Since sampling at this rate ($20 \times f_d$) is generally not feasible for a long array other approaches such as interpolating between fewer samples must be employed with time domain beamforming in order to reduce phase error.

5.9.2.3 Wideband Signal Loss

- In section 5.4.6 we saw that applying the proper phase steering to only one frequency in a band results in a beam pointing error at other frequencies and also a loss in response to wideband signals. The wider the input bandwidth of the beamformer the greater the degradation in performance.

- The response of a beamformer to a wideband signal can be evaluated by computing its output power density from the product of the source power density and the beampattern. That is, given a source power density $S(f,\beta)$ and an equally spaced uniformly weighted N-element line array, the output power density $P_o(f,\beta)$ of the beamformer is

$$P_o(f,\beta) = S(f,\beta)\left\{\frac{\sin[\pi N(d/c)f(\sin\beta-\sin\theta)]}{N\sin[\pi(d/c)f(\sin\beta-\sin\theta)]}\right\}^2 ,$$

where d is the spacing between hydrophones (or groups), β is the beam steering angle from broadside, f is the frequency and c is the sound velocity.

- The above expression can be used to define a beamformer loss for wideband sources. If a point source is assumed on boresight ($\theta=0$) with unit power, or

$$\int_{-B/2}^{B/2} S(f)\,df=1,$$

where B is the source bandwidth, and if, in the above expression, $\sin Nx/N\sin x$ is approximated by $\sin Nx/Nx$, then the beamformer loss L can be expressed in positive dB as

$$L = -10 \log \left\{ \int_{-B/2}^{B/2} S(f) \left[\frac{\sin[\pi N(d/c) f \sin\beta]}{\pi N(d/c)\ f \sin\beta} \right]^2 df \right\} .$$

- The beamformer loss L above has been evaluated for a zonal source power density spectrum and the results are given in Figure 5-35. The loss L is plotted as a function of $BN(d/c)\sin\beta$ and it is apparent that the maximum degradation occurs at endfire ($\beta=\pi/2$) while there is no loss at broadside ($\beta=0$). It might also be noted that the Nd/c term along the absissa in Figure 5-35 is roughly equal to the transit time τ of a sound wave along the entire line array. Thus, Figure 5-35 can be used to determine the beamformer loss L as a function of the transit time - bandwidth product, τB.

- For the very long arrays used today, transit times of the order of one or two seconds are not unusual. Thus, according to Figure 5-35 the input bandwidth B must be limited in order to minimize beamformer loss. The loss incurred by the zonal source (Figure 5-35) is very small. A greater loss is obtained with a Gaussian power density

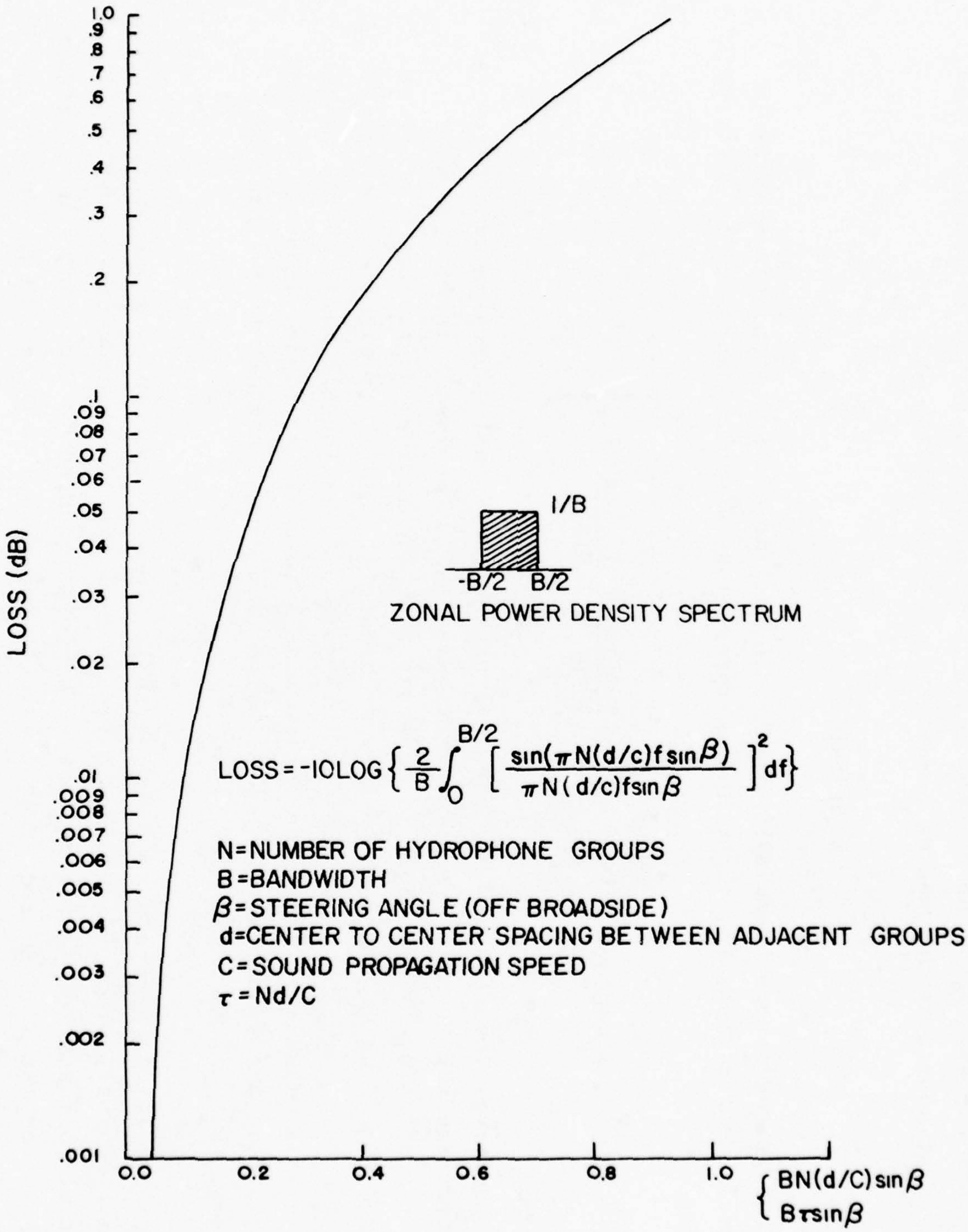

BEAMFORMER LOSS

FIGURE 5-35

spectrum although, for current transit time -bandwidth products, it is still within an order of magnitude of the loss in the zonal case.

5.9.2.4 Frequency Bin Scalloping Loss

- It is apparent from Figure 5-35 that narrowband prefiltering will result in a distinct advantage over the wideband beamformer loss, L. The narrowband filters are not perfect, however, and will give rise to "picket fence" or "frequency bin scalloping" loss (See Fig. 5-36). Generally, frequency bin scalloping is a smaller degradation than beamformer loss, L. It is quite similar in nature to the beam scalloping loss discussed in Section 5.9.2.1 and occurs because the transfer characteristics of the individual filters are not perfectly flat across their respective bands (See Fig. 5-36).

- As a demonstration of frequency bin scalloping consider the transfer characteristics of a typical band of filters such as given in Figure 5-36. Ideally, although not always in practice, the crossover points are of the order of a dB down from the normalized maxima (0 dB). Thus, a signal received at some frequency other than the center frequency of any filter will, at worst, be degraded or reduced by one dB. In practice, the frequency bin scalloping loss is usually somewhat higher than this.

- Assuming a threat probability that is constant with frequency, frequency bin scalloping loss can be defined in a manner analogous to the beam scalloping loss discussed in Section 5.9.2.1. Referring to Figure 5-36, the frequency bin scalloping loss is equivalent to the shaded area given there and can be described by

$$\text{Loss} = 10 \log (A/A_f) ,$$

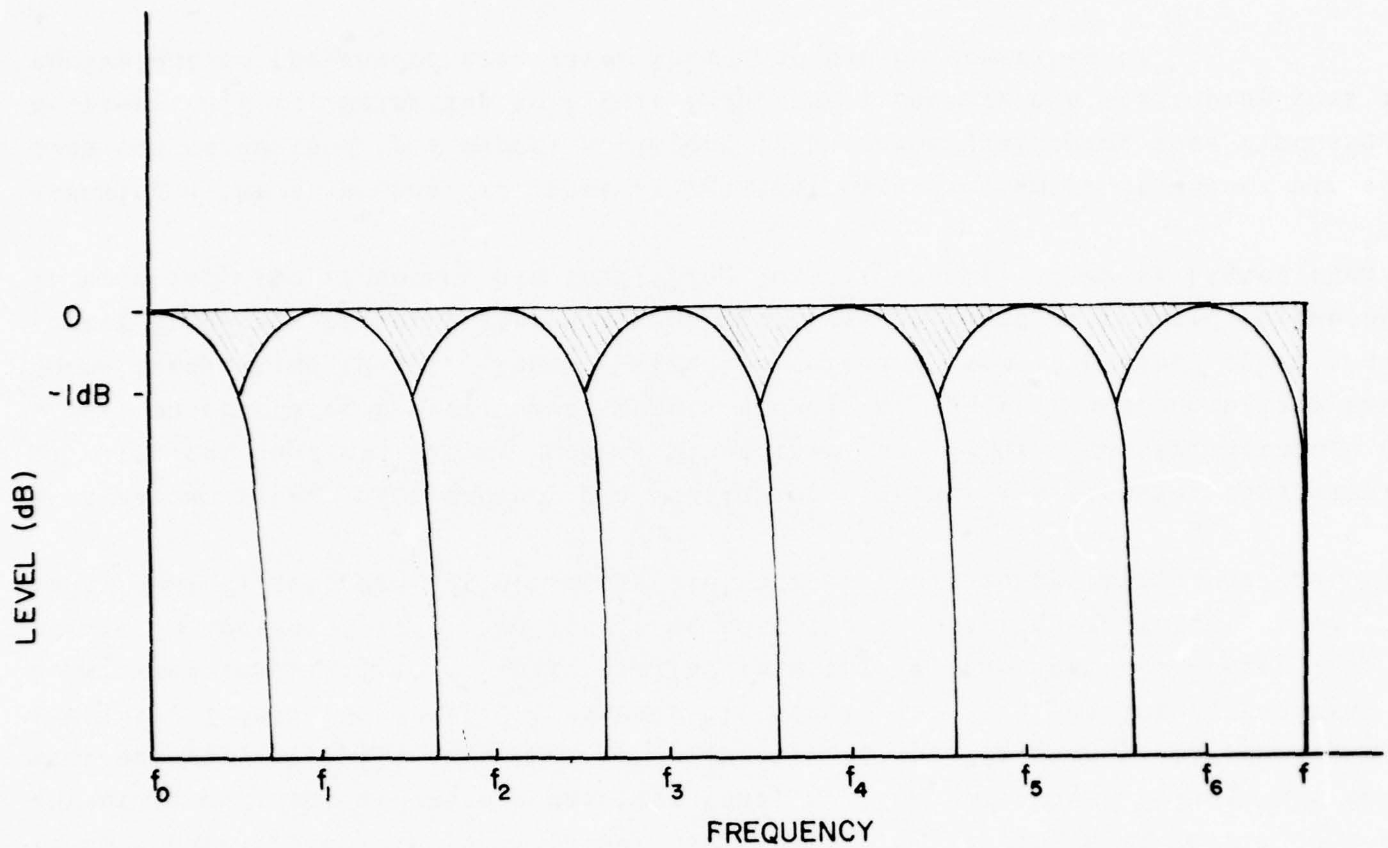

FILTER CHARACTERISTICS

FIGURE 5-36

where A is the rectangular area of unit height and width equal to the total bandwidth B (B=f-fo) and A_f is the total area under the filter characteristics. Thus, we see that frequency bin scalloping loss depends on the filter spacing(s) and on their overlap.

5.9.2.5 Operator Loss

- An operator's capacity for searching a display and recognizing the presence of targets is quite limited. The information bandwidth of a human radar operator, for example, is only about 10 Hz or 20 bits/sec. If the operator is tired, bored or just unmotivated, his information bandwidth will be even less.

- Many experiments have been conducted in order to evaluate an operator's performance under different conditions. For example, tests have been conducted comparing his performance in the laboratory while observing stable synthetic signals in white noise to his performance in the field. Other tests have documented his performance while observing data presented in different ways (i.e. multiscans) on a CRT and on other displays. Still other tests have compared his performance under alerted versus unalerted conditions. Alerted conditions are those under which the operator is notified that a signal is present or that a threshold has been exceeded in one of the threat windows.

- In general, an operator detracts from the ideal performance of a sonar system. That is, even under the best operating conditions an unalerted operator will introduce a loss which is normally of the order of 7 dB. It is interesting to note that this loss is about the same for unalerted radar and sonar operators alike. If the operator is alerted, however, then the loss is not quite as great but rather about a dB or so less than for the unalerted case.

5.9.2.6 Other Losses

- In the foregoing sections on errors and losses we have covered only the more pronounced phenomena that detract from ideal system performance. There are, of course, other effects such as plumbing losses (i.e., transmission line losses, connector losses, etc.), losses due to a lack of signal coherence across the array and even some lesser known losses.

- Plumbing losses are generally no worse than about 2 dB. Losses due to a lack of signal coherence across the array, however, could be quite significant. Even if a signal arriving at the array has a perfectly plane wavefront, any motion or distortion of the array will introduce a coherence loss. The exact amount of coherence loss is difficult to estimate and is a function of the array length, towspeed and the particular mode of instability which the array happens to be in. The problem is entirely analogous to the instability of a flag fluttering in the breeze and is the subject of current research.

5.10 Constraints Imposed By Related Technologies

5.10.1 Telemetry System Constraints

5.10.1.1 Introduction

- In general, the telemetry system or, more exactly, the cable telemetry system conveys power from the towship (or shore based source) to the hydrophones in the array and also returns hydrophone and nonacoustic sensor data. In the sense that these functions require a real system whose size and capacity are limited, the cable telemetry system imposes a constraint on the overall system performance.
  If we consider some of the cable telemetry systems currently proposed or in use whose lengths are of the order of a mile, we can immediately appreciate how the data acquired by the array can be degraded before it reaches the beamformer.

- A cable telemetry system is intended to meet certain functional requirements many of which are listed in Table 5-1. Depending upon how well a selected cable telemetry system meets these requirements, in turn determines the degree to which it degrades the overall system performance.

5.10.1.2 Typical Systems

- In view of the number of sensors or sensor groups used in modern sonar arrays, cable telemetry systems seldom consist merely of a bundle of paired wires each conveying data from a sensor group to the beamformer. Rather, they are generally required to transmit encoded, multiplexed and/or modulated data along a common carrier. Some of the more frequently used techniques are given in the several tables that follow .

5.10.1.2.1 Encoding

- Encoding is the process of sampling an analog signal and arranging or coding the resulting digital samples so as to maintain as much information as possible. For example, delta modulation is a process for encoding analog signals where the output of the delta modulator is a series of digital ones and zeroes (i.e, 1 bit quantization). The rate at which ones appear at the output is directly proportional to the rate of increase of the amplitude of the input analog signal. Integrating the train of ones and zeros over the proper time interval will reproduce the original analog signal. Other encoding methods are given in Table 5-2. When no encoding is used, the analog sensor signals are transmitted directly through the cable telemetry system. Uniform or linear pulse code modulation (PCM) is the uniform time sampling of the analog signal and yields a stream of digital sample groups where the coding of the ones and zeros within each group represents the amplitude of the analog signal at discrete time intervals. Differential PCM (DPCM) is the quantization of the change from the preceding sample amplitude value to the current sample value into two or more discrete quanta or levels. Companded PCM (CPCM) and companded delta modulation (CDM) employ non-uniform mapping of analog amplitude samples into bits of quantized data.

- The particular encoding technique selected is subject to the subsequent temporal processing method (i.e. spectral analysis, averaging, etc.) to be used. Digital transmission, however, provides a minimum of cross-talk and signal degradation when compared to analog transmission. If we compared digital encoding techniques we would see that delta modulation requires simpler circuitry than PCM. For a given binary bit rate transmitted through the telemetry system, however, PCM provides a wider dynamic range than delta modulation. DPCM provides a better slope-overload performance

TABLE 5-1

Functional Requirements of a Cable Telemetry System

To provide transmission from the ship or shorebased source of

(a) Electrical power

(b) command signals.

To provide transmission from the array to the ship or shorebased facility of

(a) Hydrophone data

(b) Non-acoustic sensor and other data.

To minimize any degradation of the signal-to-noise power density ratio at its output (this degradation is usually specified at some value less than 1 dB).

To control spurious cross-products or cross-talk in its output below some specified level.

To control channel-to-channel gain and phase variations within certain specified values.

To provide an adequate dynamic range and frequency band pass which are generally specified in advance.

To provide a certain specified degree of availability or reliability under a broad range of environmental conditions (i.e., static pressure, cable stress, shock, fatique, etc.)

(i.e. for very steep increases in the analog input voltage) than delta modulation but at the cost of more complex circuitry. Companded encoding techniques, on the other hand, generally provide better signal-to-distortion ratios than uniform encoding schemes.

5.10.1.2.2 Multiplexing

- Multiplexing refers to the means of combining all hydrophone group outputs on a common communications carrier such as coax cable without mutual interference. For example, time-division multiplexing(TDM)separates the encoded signals from each sensor on the common carrier in time. Other multiplexing techniques are frequency-division multiplexing (FDM) and code-division multiplexing (CDM). The case of no multiplexing in Table 5-2 refers to the use of multiple pairs of twisted wire for the transmission of hydrophone signals. Each hydrophone group uses one pair of wires. This is particularly constraining for a tow cable telemetry system since the number of wires per unit cross-sectional area in the tow cable must, of necessity, be high in order to minimize the cable diameter. Thus, since the tow cable constitutes a bottle neck of sorts, a hybrid approach might be to use twisted pairs for each hydrophone group for transmission through the array, and then use A/D conversion and TDM for transmission up the cable to the ship. FDM would also be a possibility but oscillator and filter costs are generally quite high. CDM is generally only considered when the number of hydrophones is small (i.e. of the order of 10).

5.10.1.2.3 Modulation

- Amplitude Modulation(AM) is the procedure whereby an analog signal is impressed on a sinusoidal carrier in order to accomplish frequency translation. Two kinds of AM are double sideband (DSB-AM), where the frequency spectrum is symmetrically

TABLE 5-2

Typical Encoding Techniques

1. None
2. (Linear) Pulse Code Modulation (PCM)
3. Differential Pulse Code Modulation (DPCM)
4. Delta Modulation (DM)
5. Companded Pulse Code Modulation (CPCM)
6. Companded Delta Modulation (CDM)

Typical Multiplexing Techniques

1. None
2. Time-Division Multiplexing (TDM)
3. Frequency-Division Multiplexing (FDM)
4. Code-Division Multiplexing (CDM)

Typical Modulation Techniques

1. None
2. Amplitude Modulation (AM)
3. Frequency Modulation (FM)
4. Phase Modulation (PM)

distributed about the carrier frequency and single sideband (SSB-AM), where only that part of the spectrum above the carrier is retained. Other methods for modulating an analog signal are frequency modulation (FM) and phase modulation (PM). No modulation is necessary if each hydrophone group is provided with a pair of wires. Moreover, no modulation is required if TDM or CDM is used. If FDM is used, however, then some modulation technique is required for transmission through the cable telemetry system. Generally, when used with FDM, AM requires less total frequency spectrum than FM and is also simpler and less expensive. An advantage of FM(orPM) over AM, however, is that cross-talk is suppressed more effectively.

- When some sort of digital encoding is employed, FM becomes frequency shift keying (FSK). That is, when frequency modulation is applied to a square wave (i.e. a digital pulse) the resulting frequency translation is called frequency shift keying or FSK. Also, when digital encoding is employed, phase modulation(PM)becomes phase shift keying (PSK). The spectral representation of some of the waveforms discussed above are given in Figure 5-37.

5.10.1.2.4 Comparison of Telemetry Systems

- Table 5-3 lists a series of potential telemetry multiplexing schemes many of which are already in use with existing towed array sonar systems. It might be recalled from above that TDM requires no modulation but that FDM does. Table 5-3 also lists some potential modulation techniques that can be used with the frequency division multiplexing (FDM) of analog signals. Tables 5-4 and 5-5 provide a somewhat more quantitative comparison of these techniques. Hardwire or twisted pair telemetry is included in these tables but is generally not a serious consideration when one observes

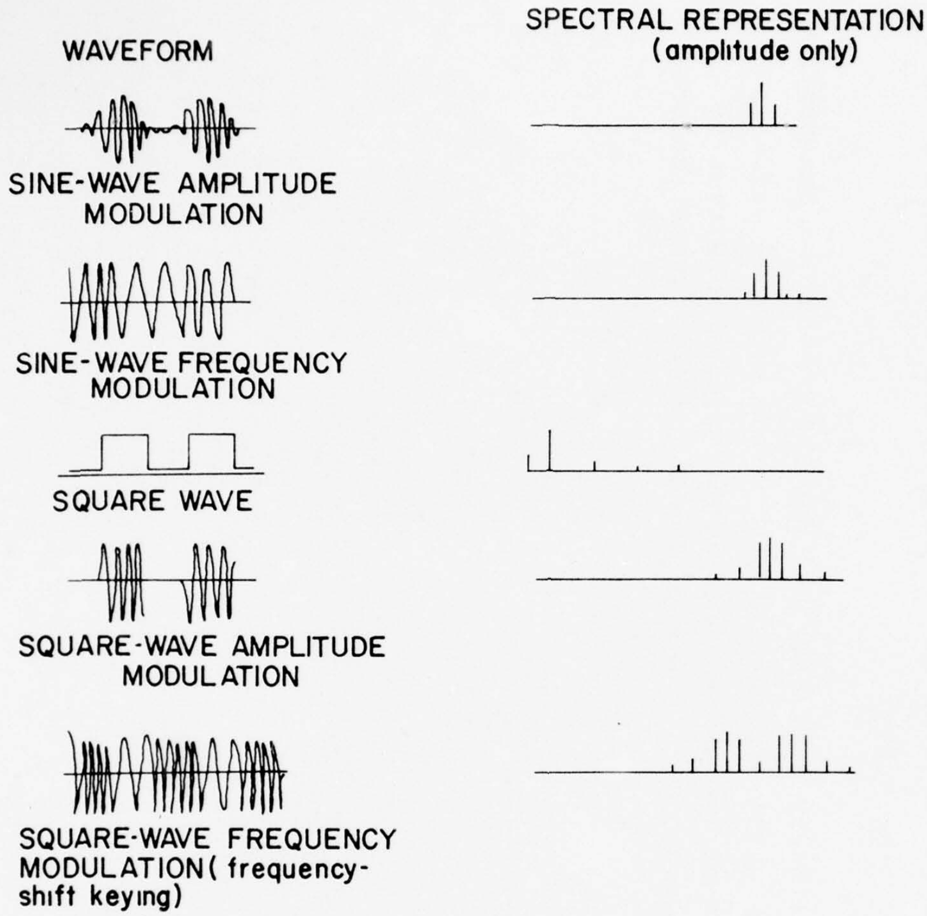

NATURE OF THE FOURIER SPECTRA FOR SOME TYPICAL PERIODIC WAVEFORMS.

FIGURE 5-37

the number of elements in modern sonar arrays and the constraint of the tow cable diameter. Single-sideband amplitude modulation (SSB-AM), which has been used for many years with FDM in commercial telephone systems, is also seldom considered very seriously because of the complex receiver requirements. Finally, pulse position modulation (PPM) is generally not considered as an encoding method because it usually involves a very poor utilization of time-space.

- When a cable telemetry system has finally been selected for overcoming the constraints on the accurate conveyance of large masses of data (i.e. of the order of megabits per second) from an array to a ship or shorebased installation, it should then be possible to construct a list such as in Table 5-6 and give a complete quantitative definition of the final system.

TABLE 5-3

- Telemetry Multiplex Candidates
  - Multiple Twisted Pair Cable
  - Frequency Division Multiplex (FDM)
    - Single Sideband - Amplitude Modulation (SSB-AM)
    - Double Sideband - Amplitude Modulation (DSB-AM)
    - Double Sideband - Amplitude Modulation With Locked Carrier (DSB-AMLC)
    - Phase Quadrature Multiplexing - Amplitude Modulation (PQM-AM)
    - Frequency Modulation (FM)
    - Tiered Frequency Modulation (FM/FM)
  - Time Division Multiplex (TDM)
    - Pulse Position Modulation (PPM)
    - (Linear) Pulse Code Modulation (PCM)
    - Companded Pulse Code Modulation (CPCM)
    - Simple Delta Modulation (DM)
    - Companded Delta Modulation (CDM)

TELEMETRY MULTIPLEX COMBINATIONS

TABLE 5-4

DSB-AM*

- High Power
- High Cost
- Low Commonality
- Restricted To One Octave (Tonals)

DSB-AMLC

- High Power
- Low Commonality
- High Cost
- Moderate Improvement Risk

PQM-AM

- Susceptible To Crosstalk (Error)
- Complex Receiver
- High Cost
- High Development Risk

FM

- Limited Expansion Capability
- Low Commonality
- Noise Susceptibility
- High Cost
- Moderate To High Development Risk

FM/FM

- Low Commonality
- Complex Electronics
- High Cost
- Moderate To High Development Risk

PCM

- Moderately Complex Electronics
- Large Bandwidth
- Medium Cost
- Moderate Development Risk

CPCM

- Moderately Complex Electronics
- Large Bandwidth
- Medium Cost
- Moderate Development Risk

DM*

- High Bandwidth (Clockrate)
- Poor Expansion Capability
- Limited System Accuracy
- Restricted Dynamic Range

CDM*

- Restricted Dynamic Range
- Lower System Accuracy
- Low Cost
- Large Bandwidth
- Low Development Risk

* Systems Presently Used For Towed Array Sonar Systems.

TELEMETRY SYSTEM COMPARISONS

TABLE 5-5

RELATIVE CHARACTERISTIC COMPARISON

	Characteristics / Telemetry Methods	FREQUENCY D.M					TIME D.M				
		DSB-AM	DSB-AMLC	POM-AM	FM	FM-FM	PCM	CPCM	DM	CDM	HARDWIRE
1	SYSTEM ACCURACY	MED 2	MED 2	MED 2	MED 2	MED 2	HIGH 3	HIGH 3	LOW 1.5	MED 2	HIGH 3
2	DYNAMIC RANGE	HIGH 3	HIGH 3	HIGH 3	MED 2	MED 2	MED 2	MED 2	MED 1	MED 2	HIGH 3
3	RELIABILITY	HIGH 3	HIGH 3	MED 2	MED 2	MED 2	MED 2	MED 2	MED 2.5	MED 2.5	HIGH 3
4	COST	HIGH 1	HIGH 1	HIGH 1	HIGH 1	HIGH 1	MED 2	MED 2	LOW 3	LOW 3	LOW 3
5	STANDARDIZATION (Commonality)	LOW 1	LOW 1	LOW 1	LOW 1	LOW 1	HIGH 3	HIGH 3	HIGH 3	HIGH 3	HIGH 3
6	BANDWIDTH/CLOCKRATE	MED 2	MED 2	LOW 3	MED 2	MED 2.5	MED 2	MED 2	HIGH 1	MED 2	LOW 3
7	POWER(Current)	HIGH 1	HIGH 1	HIGH 1	MED 2	MED 2	MED 2	MED 2	LOW 3	MED 3	LOW 3
8	RECEIVERS/TRANSMITTERS (Number/Complexity)	HIGH 1	HIGH 1	HIGH 1	HIGH 1	HIGH 1	MED 2.5	MED 2.5	LOW 3	MED 2.5	LOW 3
9	EXPANSION CAPABILITY	LOW 1	MED 2	MED 2.5	LOW 1	MED 2	HIGH 3	HIGH 3	LOW 1	MED 2.5	LOW 1
10	SIZE (Weight)	LARGE 1	LARGE 1	MED 2	MED 1.5	MED 1.5	MED 2.5	MED 2.5	SMALL 3	SMALL 3	LARGE 0
11	NOISE SUSCEPTIBILITY (RFI)(Distortion)	HIGH 1	MED 2	HIGH 1.5	HIGH 1.5	HIGH 1.5	LOW 3	LOW 3	LOW 2	LOW 3	MED 2
12	FLEXIBILITY	LOW 1	LOW 1	LOW 1	MED 2	MED 2.5	HIGH 3	HIGH 3	MED 2	MED 2.5	LOW 1
	RELATIVE SCORE:	18	20	21	19	21	30	30	26	31	28

Relative Merit
Poor Good Better
0 1 2 3

QUANTITATIVE TELEMETRY SYSTEM COMPARISON

TABLE 5-6

PHYSICAL CHARACTERISTICS

Cable Length
Array Length
Number of Telemetry Channels (Sensors) To Topside
Max Pressure (Depth)

ELECTRONIC CHARACTERISTICS

Hydrophone Preamp Bandpass
Hydrophone Preamp Gain Control Variability(From Topside)
Type of Analog to Digital Conversion (Encoding)
Sampling Rate For All Sensors
Number of Bits Of Quantization Per Sample
Data Rate Through Cable
Maximum Permissible Bit Error Rate
Maximum Channel-To-Channel Gain Variation
Maximum Channel-To-Channel Phase Variation
MTBF
Prime Power For Entire Cable Telemetry Subsystem

CHARACTERISTICS OF THE CABLE TELEMETRY SYSTEM

5.10.2 Ocean Engineering Constraints

- The options presented in the preceding section for handling or telemetering large quantities of data are applicable to fixed, towed and even drifting systems alike. The same is not true, however, for ocean engineering approaches to the installation and deployment of these systems. In fact, due to the diversity of ocean engineering problems associated with these different system types, it is not practical to present a simple and concise description at this point. Rather, we shall discuss the ocean engineering constraints associated with each of them separately in the next chapter.

- Ocean engineering constraints on the performance of an array of hydrophones are both electrical and mechanical in nature. Some general constraints that are expected to be met by all three types of systems are:

  Survival of the array and cable at specified tensions,

  Maintenance of a straight array,

  Minimization of structure induced noise (i.e. strum, etc.),

  Survival of the array and cable at specified depths and temperatures, etc.,

  Survival of the array and cable under specified installation or handling conditions,

  Maintenance of strict electrical characteristics (i.e., cable conductor resistance, inductance, etc.), and more.

THIS PAGE LEFT BLANK INTENTIONALLY.

Bibliography*

Chapter 3.0

Sections 3.1, 3.2 and 3.3

Hansen, R.C., "Microwave Scanning Antennas", Vol. I, Academic Press, New York, 1964.

Silver, S., "Microwave Antenna Theory and Design", MIT Rad. Lab. Series, Boston Technical Publishers, Inc., Lexington, Mass., 1964.

Thourel, L., "The Antenna", Wiley, New York, 1960.

Urick, R.J. "Principles of Underwater Sound for Engineers", McGraw-Hill, Inc., 1967.

Winder, A.A. and C.J. Loda, "Introduction to Acoustical Space-Time Information Processing", ONR Report ACR-63, AD 298 744, 1963.

Chapter 4.0

Section 4.1

Albers, V.M. "Underwater Acoustics Handbook-II", The Pennsylvania State University Press, University Park, 1965.

Urick, R.J., "Principles of Underwater Sound for Engineers", McGraw-Hill, Inc., 1967.

* This list is a partial bibliography consisting only of the major references for a given section. Other sources, including a variety of unpublished reports and analyses, have not been listed.

Section 4.2

Hansen, R.C., "Microwave Scanning Antennas", Vol. II, Academic Press, New York, 1966.

"Introduction to Anti-Submarine Warfare", Document Number 65-211U, TRACOR, Inc., Austin, Texas, 1965.

Silver, S., "Microwave Antenna Theory and Design", MIT Rad. Lab. Series, Boston Technical Publishers, Inc., Lexington, Mass., 1964.

Skolnik, M.I., "Introduction to Radar Systems", McGraw-Hill, Inc., 1962.

Urick, R.J., "Principles of Underwater Sound for Engineers", McGraw-Hill, Inc., 1967.

Section 4.3

Schelkunoff, S.A., "A Mathematical Theory of Linear Arrays", Bell Systems Technical Journal, 22, 80-107, 1943.

Section 4.4

Elliot, R.S., "Beamwidth and Directivity of Large Scanning Arrays", The Microwave Journal, December 1963.

Hansen, R.C., "Microwave Scanning Antennas", Vol. II, Academic Press, New York, 1966.

Silver, S., "Microwave Antenna Theory and Design", MIT Rad. Lab. Series, Boston Technical Publishers, Inc., Lexington, Mass., 1964.

Section 4.5

Doolittle, R.D., "Sector Coverage Using Multibeam Linear Arrays", J. Acoust. Soc. Am., 43, No. 4, 1968.

"Surveillance Towed Array Sensor (SURTASS) Engineering Report (U)", Document Number 24474-W793-RE-00, TRW, Inc., McLean, Virginia, 1974.

Section 4.6

Albers, V.M., "Underwater Acoustics Handbook-II," The Pennsylvania State University Press, University Park, 1965.

Elliot, R.S., "Beamwidth and Directivity of Large Scanning Arrays", The Microwave Journal, December, 1963.

Hansen, R.C., "Microwave Scanning Antennas", Vol. I, Academic Press, New York, 1964.

Hansen, R.C., "Microwave Scanning Antennas", Vol. II, Academic Press, New York, 1966.

Skolnik, M.I., "Introduction to Radar Systems", McGraw-Hill, Inc., 1962.

Stegen, R.J., "Excitation Coefficients and Beamwidths of Tschebyscheff Arrays", Proc. IRE, 41, November, 1953.

Taylor, T.T., "Design of Line-Source Antennas for Narrow Beamwidth and Low Sidelobes", IRE Trans. Antennas Propagation 3, 1955.

Urick, R.J., "Principles of Underwater Sound for Engineers", McGraw-Hill, Inc., 1967.

Section 4.7

Hansen, R.C., "Microwave Scanning Antennas", Vol. I, Academic Press, New York, 1964.

Skolnik, M.I., "Introduction to Radar Systems", McGraw-Hill, Inc., 1962.

Section 4.8

Hansen, R.C., "Microwave Scanning Antennas", Vol. I, Academic Press, New York, 1964.

Pritchard, R.L., "Maximum Directivity Index of a Linear Point Array", J. Acoust. Soc. Am., 26, 1954.

Tai, C.T., "The Optimum Directivity of Uniformly Spaced Broadside Arrays of Dipoles", IEEE Trans. Antennas Propagation 12, July, 1964.

Section 4.9

Hansen, R.C., "Microwave Scanning Antennas", Vol. I, Academic Press, New York, 1964.

Pritchard, R.L. "Maximum Directivity Index of a Linear Point Array", J. Acoust. Soc. Am., 26, 1954.

Section 4.10

Hansen, R.C., "Microwave Scanning Antennas", Vol. II, Academic Press, New York, 1966.

Stegen, R.J., "The Gain-Beamwidth Product of an Antenna", IEEE Trans. Antennas Propagation, 505-506, July, 1964.

Section 4.11

Lo, Y.T. and S.W. Lee, "A Study of Space-Tapered Arrays", IEEE Trans. Ant. and Prop., Vol. AP-14, 22-30, 1966.

McNicholas, J.V. and M.R. Serbyn, "Minimum Redundancy Space Tapered Arrays(U)", U.S. Navy J. of Underwater Acoust., Vol. 26, No. 1, January,1976.

Moffet, A.T., "Minimum-Redundancy Linear Arrays", IEEE Trans. Ant. and Prop., Vol. AP-16, 172-175, 1968.

Section 4.12

Hansen, R.C., "Microwave Scanning Antennas", Vol. II, Academic Press, New York, 1966.

"Introduction to Anti-Submarine Warfare", Document Number 65-211U, TRACOR, Inc., Austin, Texas, 1965.

Skolnik, M.I., "Introduction to Radar Systems", McGraw-Hill, Inc., 1962.

Stegen, R.J., "The Gain-Beamwidth Product of an Antenna", IEEE Trans. Antennas Propagation, 505-506, July, 1964.

Chapter 5.0

Section 5.1

Albers, V.M., "Underwater Acoustics Handbook-II", The Pennsylvania State University Press, University Park, 1965.

Bakewell, H.P., "Longitudinal Space Time Correlation Function in Turbulent Airflow", J. Acoust. Soc. Am., 35, No. 6, 1963.

Bedenbender, J.W., Johnston, R.C. and E.P. Neitzel, "Electro-acoustic Characteristics of Marine Seismic Streamers", Second Annual Offshore Technology Conference, Paper Number OTC 1241, April, 1970.

Skudrzyk, E.J. and G.P. Haddle, "Noise Production in a Turbulent Boundary Layer by Smooth and Rough Surfaces", J. Acoust. Soc. Am., 32, No. 1, 1960.

Urick, R.J., "Principles of Underwater Sound for Engineers", McGraw-Hill, Inc., 1967.

Section 5.2 Unpublished References

Section 5.3

Sears, R.W., "Design of Hydrophone Arrays for Multipath Environments", IEEE Engineering in the Ocean Environment Conference, 1971.

Section 5.4

Skolnik, M.I., "Introduction to Radar Systems", McGraw-Hill, Inc., 1962.

"Surveillance Towed Array Sensor (SURTASS) Engineering Report(U)", Document Number 24474-W793-RE-00, TRW, Inc., McLean, Virginia, 1974.

Sections 5.5, 5.6 and 5.7

Berman, H.G. and A. Berman, "Effect of Correlated Phase Fluctuation on Array Performance", J. Acoust. Soc. Am., 34, No. 5, 1962.

Cox, H., "Line Array Performance When the Signal Coherence Is Spatially Dependent", J. Acoust. Soc. Am., 54, No. 6, 1973.

Kleinberg, L.I., "Effect of Amplitude and Phase Fluctuations on Array Gain", Project Jezebel 25th Interim Report (U), Vol. I, September, 1968.

Urick, R.J., "Principles of Underwater Sound for Engineers", McGraw-Hill, Inc., 1967.

Section 5.8

Silver, S., "Microwave Antenna Theory and Design", MIT Rad. Lab. Series, Boston Technical Publishers, Inc., Lexington, Mass., 1964.

"Surveillance Towed Array Sensor (SURTASS) Engineering Report (U)", Document Number 24474-W793-RE-00, TRW, Inc., McLean, Virginia, 1974.

Sections 5.9 and 5.10 Unpublished References

THIS PAGE LEFT BLANK INTENTIONALLY.

SUBJECT INDEX

THIS PAGE LEFT BLANK INTENTIONALLY.